

CHALMERS



Validation of POLCA7 Cross Section Model

Master's Thesis

RASHED SARWAR

Department of Applied Physics
Division of Nuclear Engineering
CHALMERS UNIVERSITY OF TECHNOLOGY
Gothenburg, Sweden 2013
CTH-NT-282

ISSN 1653-4662

CTH-NT-282

Validation of POLCA7 Cross Section Model

Master's Degree Thesis
Master's Program in Nuclear Engineering
CHALMERS UNIVERSITY OF TECHNOLOGY

RASHED SARWAR

Department of Applied Physics
Division of Nuclear Engineering
CHALMERS UNIVERSITY OF TECHNOLOGY

Gothenburg, Sweden 2013

Validation of POLCA7 Cross Section Model
Master's Degree Thesis
RASHED SARWAR

©RASHED SARWAR, 2013

Master's thesis
CTH-NT-282
ISSN 1653-4662
Department of Applied Physics
Division of Nuclear Engineering
Chalmers University of Technology
SE-412 96 Gothenburg
Sweden
E-mail: sarwarr@student.chalmers.se

Cover:
Westinghouse Electric Company PWR Fuel Assembly
Thermal Systems: Fuel Assemblies In Nuclear Reactors
<http://me1065.wikidot.com/fuel-assemblies-in-nuclear-reactors>

Master's thesis in Master Program in Nuclear Engineering
RASHED SARWAR
Department of Applied Physics
Division of Nuclear Engineering
Chalmers University of Technology

Abstract

POLCA7, developed by Westinghouse Electric Company, is a three-dimensional code for simulating the neutronic, thermal, and hydraulic behavior of a reactor core by solving the coupled two-group neutron diffusion - thermal hydraulic problem with state-of-the-art methods involving the Analytical Nodal Method. The performance of the macro-micro cross section model of POLCA7 is very crucial for providing appropriate nodal parameters required by the core simulator's neutron flux solver in order to carry out desired core physics calculations. Therefore, the objective of this thesis is to validate the most important components of the cross section model such as the isotopic history model, the xenon feedback model, spectrum interaction models and the tabulation of microscopic cross section data as function of the fuel exposure, coolant density and coolant density history.

For the purpose of quantifying the accuracy of these cross section model components, the thesis has been divided into three broad numerical studies, starting with a set of simplistic two-dimensional single-node test problems involving shutdown cooling that has been evaluated against reference solutions prepared by solving the neutron transport equation (i.e. PHOENIX4). Following this, similar comparison for a set of two-dimensional 2x2 mini-cores involving one shuffling was conducted while the final evaluation involved a set of three-dimensional 2x2 mini-cores.

Based on the numerical results obtained from the three different phases, it is concluded that the current cross section model of POLCA7, in combination with the standard three-dimensional tabulation of microscopic cross section data performs well with an acceptable accuracy for the considered depletion history, i.e. for the most severe history cases the error in reactivity is below 200 pcm in single-node simulations. However, the performance of the spectrum interaction models did not perform as expected since they fail to account for the leakage induced spectrum changes resulting in an oscillation with a peak-to-peak amplitude of 400 pcm for the most severe history cases.

Acknowledgments

Foremost, I would like to express my sincere gratitude to my advisor Petri Forslund Guimarães for the continuous support of my masters thesis study, for his patience, motivation, enthusiasm, and immense knowledge. His guidance helped me during the entire time of research and writing the thesis. I could not have imagined having a better advisor and mentor for my thesis.

Besides my advisor, I would also like to thank my examiner Prof. Christophe Demazière for his encouragement and insightful suggestions.

My sincere thanks also goes to Dr. Augusto Hernandez Solis from Chalmers, Waldemar Lipiec and Kalev Tammemäe from Westinghouse Electric Sweden for offering me their time and patience to give me advice on different issues that I encountered during my thesis work.

I would also like to extend my gratitude towards my fellow thesis workers at Westinghouse Electric Sweden: Oscar Puebla Carcia, Karin H. Rosenqvist, Niclas C. Halldin, and Alborz Azadrad, for the stimulating discussions and the tireless weekends we were working together before deadlines, and for all the fun conversations we have had over lunch. Also I thank my friends from Chalmers University of Technology.

This thesis work has been produced during my scholarship period at Chalmers University of Technology, thanks to a Swedish Institute scholarship.

Last but not the least, I would like to thank my family: my parents, sister and wife for giving me support throughout my life. I am blessed to have you all in my life.

Rashed Sarwar, Gothenburg 2013.

List of Abbreviation

- 2D** Two-dimensional
- 3D** Three-dimensional
- LWR** Light Water Reactor
- SDC** Shutdown Cooling
- BOL** Beginning-Of-Life condition (i.e. zero burn-up)
- BOC** Beginning-Of-Cycle condition (i.e. zero burn-up if a given cycle)
- EOL** End-Of-Cycle condition
- SA** Single Assembly
- QA** Quadruple Assembly
- BA** Burnable Absorber
- QQQ** Cross section base table interpolation order for burn-up, coolant density history and coolant density: Quadratic / Quadratic / Quadratic
- QLL** Cross section base table interpolation order for burn-up, coolant density history and coolant density: Quadratic / Linear / Linear
- ISI** Instantaneous Spectrum Interaction Model
- SIH** Spectrum Interaction History Model
- CD-file** Cell Data File which contains tables for different parameters used in POLCA7
- ptXS** Cell Data File with point values/2D tables for microscopic cross sections
- NOHIST** Cases with isotopic history model bypassed
- XENOLD** Cases using old Xenon Model (i.e. pure macroscopic correction)
- NOSIDISO** Cases with no treatment of side isotopics in the intra-nodal cross section model
- NOSPEC** Cases with spectrum interaction models (i.e. instantaneous and historical) bypassed
- NOXECORR** Cases with no xenon correction applied to macroscopic cross sections
- BASE** Cases with all corrections deactivated
- NOHYDR** All thermal hydraulics feedback disabled in POLCA7 simulation
- NEU3** Standard neutronics calculation option for solving the two-group diffusion equation using the Analytic Nodal Method
- P7_DEP** Cases using internal base depletion steps of POLCA7
- PHX_DEP** Cases using the depletion steps employed in lattice depletion calculations
- NOM_DEP** Cases applying user defined depletion steps of size 1 MWd/kgHM

List of Basic Tools

POLCA7 POLCA7 is a three-dimensional code for simulating the neutronic, thermal and hydraulic behavior of a reactor core by solving the coupled two-group neutron diffusion - thermal hydraulic problem involving the Analytical Nodal Method.

CROSS Nodal simulation tool which combines all the necessary routines and modules of POLCA7 to simulate (spatially homogeneous) single-assembly depletion and branch cases similar to those (spatially heterogeneous) cases employed to generate cell data for POLCA7 with a lattice code such as PHOENIX4.

PHOENIX4 Two-dimensional lattice physics code solving the multi-group transport equation for a specific fuel assembly segment (Ref. [9]).

CoreLink Lattice code post-processor which prepares nodal cross section data for the nodal simulator POLCA7 for a specific fuel assembly segment (Ref. [6]).

Contents

1	Introduction	1
2	POLCA7 cross section model	3
2.1	Xenon cross section correction	4
2.2	Instantaneous spectrum interaction cross section correction	4
2.3	Spectrum history cross section correction	5
2.4	Nodal cross section data	5
2.5	Definition of some basic reactor parameters	6
3	Objective and Methodology	7
3.1	Methodology for 2D Single-Node Studies	8
3.1.1	General procedure for creating a reference solution	8
3.1.2	Calculation options of POLCA7	9
3.2	Methodology for 2D Mini-Core Studies	10
3.2.1	General procedure for creating a reference solution	10
3.2.2	Calculation options of POLCA7	11
3.3	Methodology for 3D Mini-Core Studies	11
3.3.1	General procedure for creating a reference solution	11
3.3.2	Calculation options of POLCA7	11
3.4	Identifying relevant isotopes	12
4	Specification of the testing scenarios	13
4.1	2D Single-Node Studies	13
4.2	2D Mini-Core Studies	14
4.3	3D Mini-Core Studies	15
4.3.1	Void Profiles	15
5	Part A: 2D Single-Node Studies	17
5.1	Validation of reactivity prediction capability	17
5.1.1	Non-SDC cases	17
5.1.2	SDC cases	22
5.1.3	Mixed operation cases	25
5.2	Validation of microscopic cross section representation	27
5.2.1	Actinides	27
5.2.2	Fission products	30
5.3	Reactivity effect of various depletion step sizes	32

6	Part B: 2D Mini-Core Studies	35
6.1	Clean Configuration 1	35
6.2	Configurations 2 & 4 with assembly-wise homogeneous void distribution	36
6.2.1	Configuration 2	36
6.2.2	Configuration 4	40
6.3	Configurations 3 & 5 with assembly-wise heterogeneous void distribution	41
6.3.1	Configuration 3	41
6.3.2	Configuration 5	44
7	Part C: 3D Mini-Core Studies	45
7.1	Reflective boundary conditions	45
7.1.1	Clean Configuration	45
7.1.2	Configuration 3 with assembly-wise homogeneous void distribution	46
7.1.3	Configurations 2, 4 & 5 with axially heterogeneous void distribution	47
7.2	Black boundary conditions	56
7.2.1	Clean Configuration 1	56
7.2.2	Configuration 3 with assembly-wise homogeneous void distribution	59
7.2.3	Configuration 2, 4 & 5 with axially heterogeneous of void distribution	61
8	Conclusion	65
A	2D Single-Node Studies	68
B	2D Mini-Core Studies	81
C	3D Mini-Core Studies	84

1

Introduction

THE macro-micro cross section model of POLCA7 is very crucial in providing appropriate nodal parameters required by the neutron flux solver employed in the nodal core simulator¹ to carry out desired core physics calculations. Since in real life the core state normally deviates from those imposed in lattice physics for the generation of nodal cross section data (i.e. so-called “cell data”), it is imperative that the cross section representation model and its components (i.e. base and additive correction terms) are as accurate as possible and representative of the real life situation.

Over the years, the cross section model of POLCA7 has been subject to many revisions and upgrades with the aim of improving its performance. However, recent experiences of using POLCA7 in core predictions have revealed an undesired cycle-wise reactivity drop behavior when compared to an earlier but more simplistic implementation of the cross section model consistent with version 3.0.6 of POLCA7 [3].

In this thesis work, a quantitative evaluation of the most significant improvements made to the cross section model since version 3.0.6 is presented. The evaluation is carried out at different reference and non-reference coolant conditions, involving various scenarios. Based on the testing methodology, the test bed may be divided into three broad areas of investigation:

1. The first evaluation is carried out at different reference and non-reference coolant, fuel temperature and power conditions involving various shutdown cooling scenarios. The test bed utilized for this purpose is comprised of a set of simplistic and **two-dimensional single-node problems** using the tool CROSS to evaluate the level to which the prediction capability of POLCA7 has been improved since version 3.0.6. The single-node tool CROSS combines all necessary subroutines and modules of POLCA7 in order to simulate single-assembly depletion and branch cases, similar to those employed in lattice physics calculations but by considering an equivalent homogeneous medium instead of the heterogeneous one of the transport solution. The evaluation is based on comparing CROSS results against a set of pre-built reference PHOENIX4 results which were prepared using identical state parameters.

¹The nodal core simulator of POLCA7 is a three-dimensional code for simulating the neutronic, thermal, and hydraulic behavior of a reactor core by solving the coupled two-group neutron diffusion - thermal hydraulic problem with state-of-the-art methods involving the Analytical Nodal Method [1], [2].

2. The second evaluation is carried out using a set of **two-dimensional mini-cores with 2x2 fuel assemblies** involving one and two cycle (one shuffling). The evaluation is based on comparing POLCA7 results against reference PHOENIX4 results produced in quadruple assembly configuration using identical state parameters. One of the main objectives of this evaluation is to quantify the effectiveness of the spectrum interaction model.
3. The final set of evaluation involves a set of **three-dimensional mini-cores with 2x2 fuel assemblies** involving one and two cycle (one shuffling) with different axial void conditions. The reference solutions will be prepared in POLCA7, but using a very strict approach in a fine mesh configuration so as to ensure the validity of the reference solutions itself (see Section 3.3). The main objective is to quantify the interpolation/extrapolation error and quantify the effect of axial leakage.

This report is organized as follows. In Section 2, a brief overview of the currently implemented so-called best-estimate cross section model of POLCA7 is given. Section 3 describes the objective in more details, as well as specifying some design parameters and the methodology employed for building the different test scenarios and the corresponding reference solutions. Section 4 specifies the test cases that have been evaluated. From Section 5 through 7, numerical results from the three different investigation groups are provided in order to demonstrate the significance of the improved cross section model in terms of its reactivity, microscopic cross section, macroscopic cross section and node power density. Finally, in Section 8 some concluding remarks are given.

2

POLCA7 cross section model

THE steady state cross section model of POLCA7 is based on a Taylor series expansion around a so-called ‘base’ conditions defined at a physical state where all state parameters except for the fuel exposure, coolant density history and momentaneous coolant density are fixed at their nominal reference values. Therefore, the cross section model takes the following generic form for all types of cell data (i.e. macroscopic and microscopic cross sections, discontinuity factors, pin power form factors, etc.) [4]:

$$\begin{aligned} \Sigma_\alpha = & \Sigma_\alpha^{base}(E, \rho_h, \rho) + \frac{\partial \Sigma_\alpha}{\partial CR} \Delta CR(E, \rho_h, \rho) + \frac{\partial \Sigma_\alpha}{\partial SG} \Delta SG(E, \rho_h, \rho) + \\ & \frac{\partial \Sigma_\alpha}{\partial \sqrt{T_f}} \left(\sqrt{T_f} - \sqrt{T_f^{base}} \right) + \frac{\partial \Sigma_\alpha}{\partial C_B} \left(C_b - C_b^{base} \right) + \Sigma_\alpha^{Xe} + \\ & \sum_i \sigma_i (N_i - N_i^{base}) + \Delta \Sigma_\alpha^{Spat} + \Delta \Sigma_\alpha^S + \Delta \Sigma_\alpha^{Sh} + \Delta \Sigma_\alpha^{Het} \end{aligned} \quad (2.1)$$

The base cross sections and most additive correction terms (i.e. due to perturbations such as control rod, spacer grid, fuel Doppler temperature, soluble boron and xenon concentration, isotopic history, burn-up induced spatial variation, instantaneous spectrum interaction, spectrum interaction history and heterogeneity of water density and soluble boron) are represented as three-dimensional (3D) tables dependent on the fuel exposure, the coolant density history and the momentaneous coolant density. These additive deviation terms are computed by varying the relevant state parameters individually or in unison relative to the base condition. The additive terms come into play when the real life simulations are performed at conditions different from the base condition eventually leading to a buildup of an isotope inventory different to the one inherent in base data. Therefore, the cross section model of POLCA7 includes an isotopic history correction term (i.e. represented by the 7th term in Equation 2.1) to account for such off-base nuclide inventories. These long-term isotopic number densities are normally tracked during ordinary power operation and during outage periods (i.e. the shutdown cooling effect). Since the half-life of iodine and xenon are much shorter in comparison having a scale of 7-9 hours, they are treated separately in POLCA7.

The microscopic cross sections for both actinides and fission products are given the following representation in POLCA7:

$$\sigma_i = \sigma_i^{base}(E, \rho_h, \rho) + \sigma_i^{CR} + \frac{\partial \sigma_i}{\partial N_{Xe}} \left(N_{Xe} - N_{Xe}^{base} \right) \quad (2.2)$$

where additional correction terms due to combined impact of control rod presence and xenon are included. In addition, correction terms to account for the Doppler effect are included for certain actinides that have large resonances (i.e. epithermal absorption for U-238, Pu-240 and Pu-242) [5].

The following heavy nuclides are treated by POLCA7: U-235, U-236, U-238, Np-239, Pu-239, Pu-240, Pu-241, Pu-242, Am-241 and Am-242. Furthermore, a large number of fission products, along with a burnable absorber pseudo (BA) isotope, are also tracked [5]. The base number densities are computed internally in POLCA7 for all isotopes (except for Xe-135, see Section 2.1) prior to the power-void iteration using a flux solution consistent with corresponding lattice depletion calculations employing a homogeneous medium instead of a heterogeneous one.

In the following subsections, the most important components of the cross section model addressed in this thesis are discussed in more detail.

2.1 Xenon cross section correction

The macroscopic cross section correction term due to varying xenon concentration (i.e. Σ_α^{Xe} in Equation 2.1) is given by Equation 2.3. The xenon sensitivity coefficients in cell data are tabulated as functions of burn-up, coolant density history and instantaneous coolant density[4]:

$$\Sigma_\alpha^{Xe} = \left(\frac{\partial \Sigma_\alpha}{\partial N_{Xe}} + \frac{\partial \Sigma_\alpha^{CR}}{\partial N_{Xe}} \right) (N_{Xe} - N_{Xe}^{base}) \quad (2.3)$$

The base number density of xenon is taken directly from the lattice code output (i.e. cell data file) as the base cross sections are very sensitive to underlying xenon state inherent in them.

The **old xenon model** which was available in version 3.0.6 neglects the xenon spectrum effect and corrects only for the effect of xenon on the macroscopic cross absorption section [4]:

$$\Sigma_{a2}^{Xe} = \sigma_{a2}^{Xe} (N_{Xe} - N_{Xe}^{base}) \quad (2.4)$$

2.2 Instantaneous spectrum interaction cross section correction

Cross section changes due to instantaneous variations in the flux spectrum due to leakage are accounted for by applying the instantaneous spectrum interaction (ISI) model (i.e. Σ_α^S in Equation 2.1) [4]. It is computed in POLCA7 itself in an iterative manner and can be represented by Equation 2.5 [9]:

$$\Sigma_\alpha^S = \frac{\partial \Sigma_\alpha}{\partial S} \Delta S; \text{ where, } \Delta S = \left(\frac{\Phi_2}{\Phi_1} \right) \cdot \left(\frac{\Sigma_{a2}}{\Sigma_r} \right)^{noleak} - 1 \quad (2.5)$$

where (Φ_2/Φ_1) is the spectrum index taken from the leakage affected situation while (Σ_{a2}/Σ_r) represents the leakage-free infinite-medium spectrum index. The sensitivity coefficients (i.e. $\partial \Sigma_\alpha / \partial S$) are computed in POLCA7 assuming that any cross section change due to variation in spectrum is independent of phenomenon that induces this variation. This allows the spectrum interaction sensitivity coefficients to be computed from the average cross sections corresponding to any leakage-free situations that yield different spectra. Hence, in POLCA7 these coefficients are estimated based on the pre-tabulated cross section dependence on *coolant density* to represent the leakage-affected and the leakage-free states, respectively.

2.3 Spectrum history cross section correction

The impact of flux spectrum variations during depletion is not fully accounted for by the history tracking model of POLCA7. Consequently, a spectrum history model is employed to capture any residual history effect on the cross sections. The spectrum history correction (i.e. $\Sigma_\alpha^{S_h}$ in Equation 2.1) takes the following form [4]:

$$\Sigma_\alpha^{S_h} = \frac{\partial \Sigma_\alpha}{\partial S_h}(S_h - S_h^{base}) = \frac{\partial \Sigma_\alpha}{\partial S_h}(S_h - 1) \quad (2.6)$$

where the spectrum history is defined as:

$$S_h = \frac{\frac{1}{E} \int_0^E dE' \frac{\Phi_2(E')}{\Phi_1(E')}}{\frac{1}{E} \int_0^E dE' \frac{\Phi_2^{base}(E')}{\Phi_1^{base}(E')}} \text{ and per definition, } S_h^{base} = 1 \quad (2.7)$$

The numerator on the right-hand-side of Equation 2.7 corresponds to the spectrum history of the actual conditions (i.e. generated by accumulation of the spectrum history at the leakage affected state) while the denominator represents the base state (i.e. generated by interpolation in pre-tabulated spectrum history tables representing the non-leakage state at which cell data were prepared by the lattice code). The spectrum history sensitivity coefficients, $\partial \Sigma_\alpha / \partial S_h$, are computed by using pre-tabulated cross section data at two different *coolant density history* conditions to represent the leakage-affected and the leakage-free state, respectively.

2.4 Nodal cross section data

The various nodal cross section data required by the nodal core simulator are computed utilizing a lattice transport code. The lattice code solves the multi-group Boltzmann transport equation over a spatial domain constituting a single fuel assembly segment with reflective boundaries. By utilizing the acquired detailed flux distribution combined with depletion calculations, data from the employed basic cross section library are transformed from a micro-region representation to a macro-region representation (i.e. spatial homogenization, Equation 2.8) and from a micro-group representation to a macro-group representation (i.e. energy condensation, Equation 2.9) using the following general expressions:

$$\Sigma_{\alpha,I,G} = \frac{\sum_i \Sigma_{\alpha,i,G} \Phi_{i,g} V_i}{\sum_i \Phi_{i,G} V_i} \quad (2.8)$$

$$\Sigma_{\alpha,i,G} = \frac{\sum_g \Sigma_{\alpha,i,g} \Phi_{i,g}}{\sum_g \Phi_{i,g}} \quad (2.9)$$

where the index i represents the various spatial regions and index g the neutron energy groups, whereas I and G represent the corresponding macro-region and macro-group indices, respectively. This set of nodal data is pre-tabulated as a function of various state parameters aiming at describing the core conditions anticipated during real reactor operation [6].

2.5 Definition of some basic reactor parameters

Below are the definitions of some basic reactor parameters that are relevant to this report [7]:

$$\text{Infinite-medium multip. factor} = K_{\infty} = \frac{\nu\Sigma_{f1} + \nu\Sigma_{f2} \cdot \Sigma_r / \Sigma_{a2}}{\Sigma_{a1} + \Sigma_r} \quad (2.10)$$

$$\text{Infinite-medium Spectrum Index} = \frac{\Phi_2}{\Phi_1} = \frac{\Sigma_r}{\Sigma_{a2}} \quad (2.11)$$

$$\text{Relative node power density for node } n = P_n = \kappa_n(\Sigma_{f1}\Phi_{1n} + \Sigma_{f2}\Phi_{2n}) \cdot \frac{f_{norm}}{Q_{rel}\pi_v} \quad (2.12)$$

In the expression for the relative power density, Q_{rel} represents the relative core power, π_v is the nominal volumetric power density and f_{norm} is a normalization factor chosen such that the volume-weighted core average value of the node power density equals unity.

3

Objective and Methodology

BASED on the discussion given in Ref. [8] with the title “Specification of simulation cases for studying the observed cycle-wise drop in POLCA7 core eigenvalue predictions”, the major upgrades of the cross section model going from version 3.0.6 to 4.15.0 are listed below:

1. Actinide microscopic cross section tables extended from two-dimensional tables (i.e. fuel exposure and instantaneous coolant density) to three-dimensional tables (i.e. fuel exposure, instantaneous coolant density, coolant density history).
2. Fission product microscopic cross section tables from point values to three-dimensional tables (i.e. fuel exposure, instantaneous coolant density, coolant density history).
3. Depletion step synchronization between the main depletion calculation and the corresponding base depletion calculation, where for the latter calculation a set of hard-coded depletion steps is used.
4. Treatment of xenon and its impact on nodal cross section data including the xenon spectrum effect, i.e. xenon feedback model.
5. Inclusion of instantaneous spectrum interaction (ISI) and spectrum interaction history (SIH) models.
6. Impact of using extrapolated cross section table at high void conditions (i.e. extrapolation over coolant density and coolant density history).
7. Quadratic interpolation scheme set as default for cross section table interpolation (i.e. burn-up, coolant density and coolant density history).

Additionally, there has been reporting of issues in POLCA7 related to drop in reactivity at intra and inter cycle [3]. Investigation will be carried out to validate these observations and identify possible cause.

Single-node studies (Part A of the thesis) will address items 1-4 as well as validation of SDC calculations, where as 2D mini-core studies (Part B of the thesis) will look into items 1, 2, 4, 5 and investigate the reported intra and inter cycle drop in reactivity. Finally, 3D mini-core studies (Part C of the thesis) will address item 6 and 7 while at the same time quantify the contamination of results due to the use of black boundary conditions (i.e. representing axial leakage of neutrons with albedo set to zero at the top and bottom edge of the core).

3.1 Methodology for 2D Single-Node Studies

The objective here is to prepare some reference solutions with very specific state parameters using PHOENIX4 [9] and then execute CROSS at the same state parameters. Since PHOENIX4 is solving the transport equation directly, it is accepted that the solutions from PHOENIX4 are accurate and therefore taken as reference solutions. Upon determining the magnitude of deviation between the corresponding PHOENIX4 and CROSS simulations, it will be possible to judge the accuracy of the cross section model of POLCA7.

3.1.1 General procedure for creating a reference solution

In order to set up appropriate lattice physics calculation cases to cover anticipated realistic histories obtained during real reactor core operation, standard PHOENIX4 [9] input files were modified manually to obtain the following types of run cases utilized:

1. **SDC Depletion Cases:** Lattice depletion calculations at different coolant density conditions (i.e. consistent with 0, 20, 40 and 60% coolant void history) at four different power levels corresponding to 50, 75, 100 and 125% rated power combined with a 14 day long SDC time imposed at the burn-up points 8, 16, 24 and 32 MWd/kgHM. Additionally, cases with varying fuel temperature and SDC time were also considered.
2. **SDC Restart Cases:** Lattice restart calculations to the same conditions as computed in the above mentioned **SDC Depletion Cases**. These restart cases were performed to be fully consistent with the cell data generation procedure which were also based on a similar restart/depletion calculation scheme [10], [11].

The depletion steps employed in the lattice depletion and restart calculations are specified in Table 3.1. Note that only nuclear data from restart cases were used for building the reference solutions in CoreLink [6] with dependencies on fuel burn-up, coolant density and coolant density history.

Table 3.1: Fuel exposure steps employed for the various types of lattice physics calculations.

Fuel exposure [MWd/tHM] DEPLETION CASES	Fuel exposure [MWd/tHM] RESTART CASES
0	X
1	1
350	350
500	500
E≥1000; Δ=500	E≥1000; Δ=500
E≥20000; Δ=1000	E≥8000; Δ=1000
E≥24000; Δ=2000	E≥24000; Δ=2000
E≥60000; Δ=4000	E≥60000; Δ=4000

At BOL, all restart cases were performed at 1 MWd/tHM in order to obtain lattice code nuclear data at xenon equilibrium conditions. This is due to PHOENIX4-specific methodology for computing the equilibrium xenon number density which requires a small burn-up step to obtain an equilibrium xenon condition [9]. Using this same principle, the restart cases after each SDC were also performed after a small fuel exposure step of 1 MWd/tHM.

3.1.2 Calculation options of POLCA7

In order to investigate the importance of the various improvements made to the cross section model since the release of POLCA7 version 3.0.6, the following calculation options [12] were considered in this analysis:

- **NOHIST:** Isotopic history model is bypassed. This option also automatically activates the NOBA (i.e. explicit BA isotope contribution to nuclide history correction to the node average absorption cross section is bypassed) and NOSIDISO (i.e. node side isotopic treatment in intra-node cross section model is deactivated) options in the model. This option is used to assess the importance of having an isotopic history correction term in the cross section model of POLCA7.
- **XENOLD:** The old xenon model based on a macroscopic xenon number density correction term consistent with Equation 2.4 is activated. This option is used to quantify reactivity impact of the xenon feedback model and its ability to handle the xenon spectrum effects, see Equation 2.3.
- **NOSIDISO:** Side isotopic treatment in the intra-nodal cross section model is deactivated.
- **NOSPEC:** Spectrum interaction models (i.e. instantaneous spectrum interaction and spectrum interaction history) were deactivated, see Section 2.2 and 2.3.

The generation of necessary cell data tables (CD-file) to be used by CROSS was carried out using a standard operational matrix [10] and is consistent with Table 3.1. This CD-file is referred to as *standard CD-file*. Additionally, a customized cell data file (referred to as *ptXS* henceforth) was created accommodating the following conditions consistent with POLCA7 version 3.0.6 [8]:

1. Point values for fission product microscopic cross sections were imposed with the used values chosen from the 3D table at BOL with $\rho = \rho_{his} = 40\%$ coolant void.
2. 2D tables were imposed for the actinide microscopic cross sections as function of fuel exposure and coolant density (i.e. $\sigma = \sigma(E, \rho)$). This was done by removing all coolant density history entries from the 3D table except for the entry representing 40% coolant void.
3. Point values for the microscopic cross sections of U-236, Pu-242, Am-241 and Am-242 were imposed with the used values chosen from the 3D table at BOL with $\rho = \rho_{his} = 40\%$ coolant void.

Table 3.2 presents an overview of the different sets of depletion steps applied in the simulations performed by CROSS. The objective is to identify the influence of using different depletion step sizes on reactivity and microscopic cross sections alike. Three different sets of depletion steps have been used in this analysis, namely, *P7_DEP* representing the internal base depletion steps of POLCA7, *PHX_DEP* representing the steps used by PHOENIX4 during depletion calculation (see Table 3.1) and *NOM_DEP* representing user defined depletion steps of size 1 MWd/kgHM. The numerical results presented in the report are based on the internal POLCA7 base depletion steps (*P7_DEP*), unless stated otherwise.

During the burn-up intervals of 8-20 and 60-80 MWd/kgHM, interpolated values will be used in POLCA7 as the CROSS simulations run at smaller depletion steps compared to the entry values of the cell data tables as well as the depletion steps of the reference solution (compare Table 3.1 vs. Table 3.2). As a result, numerical noise has been observed in form of fluctuations at

Table 3.2: Fuel exposure steps [MWd/tHM] employed for the various types of nodal calculations.

P7_DEP [MWd/t]	PHX_DEP [MWd/t]	NOM_DEP [MWd/t]
0	0	0
1	1	1
E≥100; Δ=100	350	1000
E≥500; Δ=250	500	2000
E≥1000; Δ=500	E≥1000; Δ=500	E≥3000; Δ=100
	E≥20000; Δ=1000	
	E≥24000; Δ=2000	
	E≥60000; Δ=4000	

these non-tabulated burn-up entry points. Hence, to avoid contamination of the plots/statistics presented in this analysis, these interpolated burn-up points were excluded from the study even though POLCA7 is running at these intervals. In other words, only the burn-up points that are common to both PHOENIX4 and CROSS were evaluated.

3.2 Methodology for 2D Mini-Core Studies

The basic idea and the process of evaluation is the same as in the single node studies, except that for this set of evaluation, POLCA7 was used directly instead of CROSS. Additionally, a 2x2 mini-core configuration was realized in both PHOENIX4 and POLCA7. Fuel depleted in single-assembly configuration was used for the construction of mini-cores to represent core shuffling.

3.2.1 General procedure for creating a reference solution

In order to set up appropriate lattice physics calculation cases to cover anticipated realistic histories obtained during real reactor core operation, standard PHOENIX4 input files were modified manually to obtain the following types of run cases utilized to test the cross section model:

1. **Single Assembly Depletion Case:** Lattice depletion calculation of a single-assembly (SA) configuration with reflective boundaries at reference coolant density (i.e. corresponding to 40 coolant void history), power and fuel temperature conditions. In these cases, the standard depletion steps employed in cell data generation technique were utilized [11]. The objective of this calculation is to extract the required “COMPOSITION+” cards [9] which are needed to build the relevant quadruple-assemblies (QA) configurations to be analyzed.
2. **Quadruple Assembly Depletion Case:** Lattice depletion calculations considering different 2x2 mini-core configurations as specified in Section 4. In these QA depletion calculations, very fine depletion steps were employed to obtain agreement with an equivalent SA depletion case defined for calibration purposes.

The reference solutions were computed using the infinite-medium spectrum by deactivating the B1-critical buckling search in all calculations because having a critical buckling search

activated for the QA geometries results in an inconsistency due to a limitation in PHOENIX4¹.

3.2.2 Calculation options of POLCA7

The calculation options mentioned in Section 3.1.2 were considered along with a new option called BASE² in order to investigate the importance of the various improvements made to the cross section model since the release of POLCA7 version 3.0.6.

Note that any thermal hydraulics feedback was disabled in POLCA7 using the NOHYDR option. Furthermore, the standard neutronics option NEU3 was used in all calculations. The generation of necessary cell data tables to be used by POLCA7 was carried out using a standard operational matrix [10]. Additionally, a customized cell data file (*ptXS CD-file*) was generated following the same procedure as mentioned in Section 3.1.2. Both CD-files were generated using infinite-medium spectrum (i.e. no B1 search) to maintain consistency with the reference solution.

3.3 Methodology for 3D Mini-Core Studies

Since PHOENIX4 is only able to perform lattice calculations on two-dimensional configuration, a traditional PHOENIX4 vs. POLCA7 evaluation is not possible in this study. Hence, in order to set up appropriate reference core physics calculation cases, a fine-mesh simulation using 100 nodes per channel was conducted in POLCA7 using a specially constructed cell data file (CD-file) using a modified standard operational matrix of PHOENIX4 to include the coolant void conditions mentioned in Section 3.3.1.

3.3.1 General procedure for creating a reference solution

All reference solutions were computed with instantaneous spectrum interaction, spectrum history models, axial homogenization (i.e. calculation of axial discontinuity factors) and the internal burn-up model (i.e. model for within-node variation of cross sections) deactivated. Additionally, these solutions were to be computed using hundred nodes per assembly. Finally, the following entries were incorporated in the reference CD-file:

1. **Coolant Density:** 0, 10, 20, 30, 40, 50, 60, 70 and 80%.
2. **Coolant Density History:** 0, 10, 20, 30, 40, 50, 60, 70 and 80%.

3.3.2 Calculation options of POLCA7

The calculation options of XENOLD and NOHIST mentioned in Section 3.1.2 were considered for this evaluation along with the following interpolation schemes:

1. **QQQ:** Quadratic interpolation scheme is utilized while carrying out cross section base table interpolation over burn-up, instantaneous coolant density and coolant density history. Note that a linear extrapolation is forced for coolant density and coolant density history regardless of the interpolation scheme employed in the calculation.

¹STI-22004, “Quadruple assembly calculation on a single-assembly configuration mis-predicts microscopic cross sections at depleted conditions”. STI stands for Software Technology Issue.

²All correction terms in the macroscopic cross section representation were neglected, i.e. only base cross sections from the cell data file were used in the simulations. This was achieved by the combined activation of the following calculation options: NOHIST, NOSPEC and NOXECORR.

2. **QLL**: Quadratic interpolation scheme is utilized while carrying out cross section base table interpolation over burn-up, while linear interpolation scheme is used for instantaneous coolant density and coolant density history.

Since the test cases were prepared with ten axial nodes per channel, the reference cross section results (having hundred axial nodes) had to be converted accordingly in order to maintain consistency. This was achieved by condensing the cross section results from the reference solution in accordance to the convention defined in Equation 2.8. The condensation of the relative node power density was carried out by computing the arithmetic average over every 10 nodes.

The generation of necessary cell data tables to be used by POLCA7 was carried out using a standard operational matrix [10] which only contains histories for 0, 20, 40 and 60% coolant void conditions. Additionally, a customized cell data file (*ptXS CD-file*) was created according to the procedure mentioned in Section 3.1.2. Note that any thermal hydraulics feedback was disabled in POLCA7 using the NOHYDR option. Furthermore, the standard neutronics option NEU3 was used in all calculations. All simulations were conducted twice and then with black boundary condition (i.e. albedo set to zero) at the top/bottom edge of the core.

3.4 Identifying relevant isotopes

In order to identify the isotopes with microscopic cross sections of substantial worth when computing the corresponding macroscopic cross section, a so-called “isotopic worth”, $ISO_{\alpha,i,b}$, is defined for each cross section type α , for isotope i at each evaluated burn-up point b according to the Equation 3.1. Note that this isotopic worth is, in this context, evaluated based on PHOENIX4 reference results.

$$ISO_{\alpha,i,b} = \frac{\sigma_{\alpha,i,b} \cdot ND_{\alpha,i,b}}{\Sigma_{\alpha,b}} \cdot 100 \quad (3.1)$$

Table 3.3 contains the maximum $ISO_{\alpha,i,b}$ at any given fuel exposure for actinides and fission products having a worth of at least 5% and 0.75% respectively. These cut-off values were chosen based on engineering judgment.

Table 3.3: Maximum Isotope worth in percentage [0 to 80 MWd/kgHM].

Actinides	mSA1	mSA2	mSF1	mSF2	Fission Products	mSA1	mSA2
U235	32.4	56.3	70.4	100.0	Pm147	0.87	
U238	57.4	55.3	69.8		Xe135		3.25
Pu239		35.5	19.6	69.2	Rh103	2.25	1.31
Pu240	13.6				Sm149		1.50
Pu241		11.7	13.0	27.0	Sm151		0.97
BAeff		25.9			Sm152	1.37	
					Nd143		2.16
					Eu153	1.11	
					Eu154		1.05
					Eu155		1.03

4

Specification of the testing scenarios

4.1 2D Single-Node Studies

IN this section, the detailed state conditions (i.e. power level, coolant density and fuel temperature) evaluated in the different SDC simulation cases are specified. The objective of these SDC cases is to simulate realistic histories obtained during reactor core operation and subsequent outage intervals. The detailed sequence of such histories is presented in Table III, while Table IV identifies the different combinations of state parameter (SP) values.

Table 4.1: Specification of cases for the evaluated SDC scenarios.

HISTORY ID	EXPOSURE RANGE (MWd/kgHM)				
	0-8 SP - SDC	8-16 SP - SDC	16-24 SP - SDC	24-32 SP - SDC	32-50 SP - SDC
1*	A-14	A-14	A-14	A-14	A-14
2*	B-14	B-14	B-14	B-14	B-14
3**	C-14	C-14	C-14	C-14	C-14
4*	D-14	D-14	D-14	D-14	D-14
5*	C-730	C- 0	C- 0	C- 0	C- 0
6	E-14	E-14	E-14	E-14	E-14
7	F-14	F-14	F-14	F-14	F-14
8	G-14	G-14	G-14	G-14	G-14
9	F-14	E-14	C- 0	C- 0	C- 0
10	G-14	C-14	F-14	E-14	E-14

* Reference coolant condition (40% void and 100 % fuel temp)
 ** Hot Full Power (100% power, 40% void, 100% fuel temp)

Table 4.2: Different state conditions used to build the SDC cases.

State Parameter (SP)	Power Level (%)	Fuel Temp (%)	VOID (%)
A*	50%	100% T_f	40 %
B*	75%	100% T_f	40 %
C*	100%	100% T_f	40 %
D*	125%	100% T_f	40 %
E	50%	50% T_f	00 %
F	75%	75% T_f	20 %
G	125%	125% T_f	60 %

These SDC cases cover both constant operating conditions (History 1 through 8) and also cases with varying operating conditions, i.e. so-called “mixed operation conditions” (History 9 and 10). Additionally, Histories 1 through 4 are based on reference void conditions (i.e. 40% void fraction) and fuel temperature. It may also be noted that in order to quantify the absolute contribution from the SDC effect, all histories were also simulated without the implementation of SDC. Such cases are referred to as “non-SDC cases” in this report.

4.2 2D Mini-Core Studies

In this section the various mini-core configurations evaluated with POLCA7 and PHOENIX4 are described in detail. All cores were free of any control rods and loaded with a segment of 10x10 SVEA-96 Optima3 lattice type. The dimension of the core was $(2 \times 15.375)^2 \times 15.000$ cm³. Below a more detailed specification of the considered mini-core configurations is given.

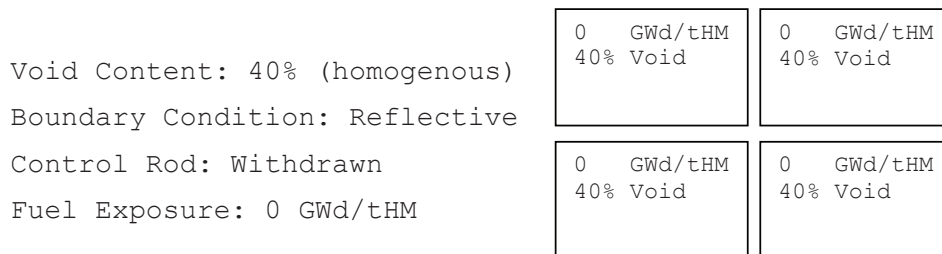


Figure 4.1: Different state conditions used to build Configuration 1.

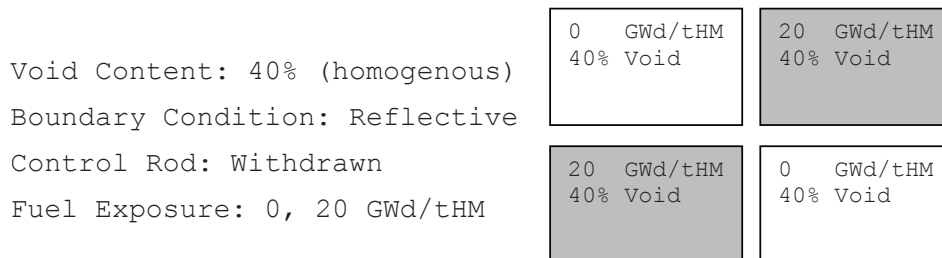


Figure 4.2: Different state conditions used to build Configuration 2.

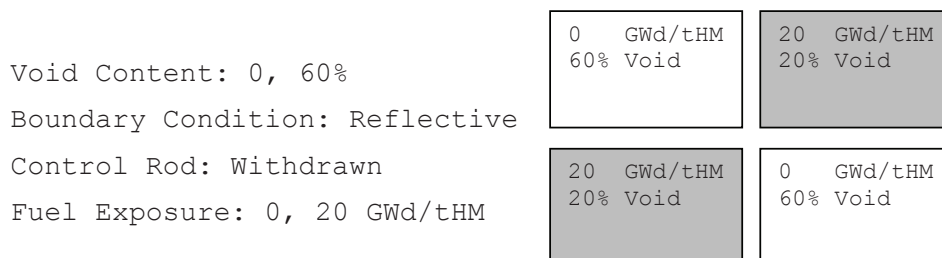


Figure 4.3: Different state conditions used to build Configuration 3.

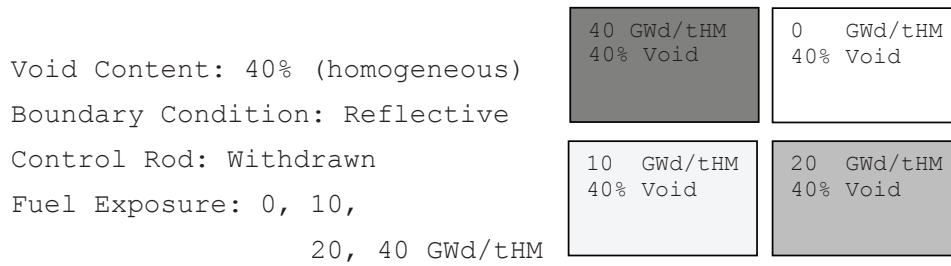


Figure 4.4: Different state conditions used to build Configuration 4.

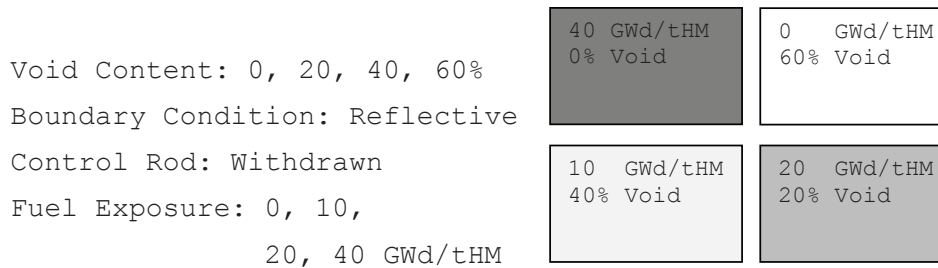


Figure 4.5: Different state conditions used to build Configuration 5.

4.3 3D Mini-Core Studies

In this section the various 3D mini-core configuration evaluated are described. The configuration layout are identical to those used in 2D mini-core studies. All cores were free of any control rods and loaded with a segment of 10x10 SVEA-96 Optima3 lattice type. The dimension of the core was $(2 \times 15.375)^2 \times 100.000 \text{ cm}^3$. The reference cases were created with hundred axial nodes per assembly whereas the test cases contain only ten nodes per assembly. Different axial void profiles (see Section 4.3.1) were used according to specification in the list below.

1. **Configuration 1:** Same as Figure 4.1 with axially homogeneous void profile of 40%.
2. **Configuration 2:** Same as Figure 4.1 with Void Profile 00 (Section 4.3.1) void axially for all assemblies.
3. **Configuration 3:** Same as Figure 4.3 with axially homogeneous void profile of 20, 60%.
4. **Configuration 4:** Same as Figure 4.3 with axial Void Profile 00, 20 (Section 4.3.1).
5. **Configuration 5:** Same as Figure 4.5 with Void Profile 00, 20, 40 (Section 4.3.1).

4.3.1 Void Profiles

Below, the various axial void profiles used in the simulations are listed. To improve readability, the naming of the profile is based on the analogy that, for example, **Profile 10** was used in conjunction with the assembly which is at a burn-up of **10 MWd/kgHM** at the beginning of second cycle.

CHAPTER 4. SPECIFICATION OF THE TESTING SCENARIOS

```

*****
* PROF 00 *   BOC Fuel Exposure: 0 MWd/kgHM   Unit=kg/m3   Scal power = 0
*****
                Avg value = 358.86

Node  Average
10    177.05
9     177.05
8     247.30
7     247.30
6     317.90
5     387.40
4     458.60
3     525.34
2     525.34
1     525.34

II-----I-----I-----I-----II
I          *           :           I
I          *           :           I
I          *           :           I
I          *           :           I
I          *           :           I
I          *           :           I
I          *           :           I
I          *           :           I
I          *           :           I
I          *           :           I
II-----I-----I-----I-----II
0          150        300        450        600

*****
* PROF 10 *   BOC Fuel Exposure: 10 MWd/kgHM   Unit=kg/m3   Scal power = 0
*****
                Avg value = 415.88

Node  Average
10    177.05
9     247.30
8     247.30
7     317.90
6     387.40
5     458.60
4     525.34
3     599.30
2     599.30
1     599.30

II-----I-----I-----I-----II
I          *           :           I
I          *           :           I
I          *           :           I
I          *           :           I
I          *           :           I
I          *           :           I
I          *           :           I
I          *           :           I
I          *           :           I
I          *           :           I
II-----I-----I-----I-----II
0          150        300        450        600

*****
* PROF 20 *   BOC Fuel Exposure: 20 MWd/kgHM   Unit=kg/m3   Scal power = 0
*****
                Avg value = 436.82

Node  Average
10    247.30
9     247.30
8     247.30
7     317.90
6     387.40
5     458.60
4     525.34
3     599.30
2     668.90
1     668.90

II-----I-----I-----I-----II
I          *           :           I
I          *           :           I
I          *           :           I
I          *           :           I
I          *           :           I
I          *           :           I
I          *           :           I
I          *           :           I
I          *           :           I
I          *           :           I
II-----I-----I-----I-----II
0          175        350        525        700

*****
* PROF 40 *   BOC Fuel Exposure: 40 MWd/kgHM   Unit=kg/m3   Scal power = 0
*****
                Avg value = 493.20

Node  Average
10    247.30
9     247.30
8     317.90
7     387.40
6     458.60
5     525.34
4     599.30
3     668.90
2     740.00
1     740.00

II-----I-----I-----I-----II
I          *           :           I
I          *           :           I
I          *           :           I
I          *           :           I
I          *           :           I
I          *           :           I
I          *           :           I
I          *           :           I
I          *           :           I
I          *           :           I
II-----I-----I-----I-----II
0          200        400        600        800

```

5

Part A: 2D Single-Node Studies

IN this section, the results from the numerical study of the single-node simulations will be examined in detail. The section is divided in three parts addressing the validation of reactivity, microscopic cross section and finally the effect of using different depletion steps.

5.1 Validation of reactivity prediction capability

In this section the absolute deviations¹ in predicted reactivity (i.e. k -infinity) at different reference/non-reference fuel temperature and coolant conditions and for different power histories are quantified. Not all histories are presented, but only the ones that lead up to and/or support different conclusions. This section is further divided into three additional parts based on the type of cases being evaluated: Non-SDC cases, SDC cases and Mixed Operation cases.

5.1.1 Non-SDC cases

5.1.1.1 Reference coolant condition

In Figure 5.1 through 5.3, the absolute deviations in predicted reactivity are shown using the different calculation options of POLCA7 discussed in Section 3.1.2. All evaluated histories are at the reference coolant density and fuel temperature condition, but at the following different power levels: 50% rated power in Figure 5.1 (History 1), 100% rated power in Figure 5.2 (History 3) and 125% rated power in Figure 5.3 (History 4). The plot for History 2 (i.e. 75% power) may be found in Appendix A.1.

The reactivity deviation profile demonstrated in Figure 5.2 (i.e. depletion at 100% rated power) is considered here as a baseline result running on the same conditions as employed for cell data generation. Consequently, very small errors are expected for this particular case. However, a slight underestimation of the reactivity by CROSS may be observed at BOL due to an overestimation of the xenon number density during the BA depletion range as predicted by CROSS compared to the reference lattice code solution. This can be attributed to the methodology used in the xenon correction model in POLCA7, which is very sensitive to the time step sizes used in these simulations (i.e. POLCA7 runs on internal base depletion steps whereas the base xenon number density is provided by the lattice code employing different depletion

¹Difference between numerical results computed by CROSS and PHOENIX4, evaluated at given history conditions.

steps). In fact, when running the same case with the NOXECORR option (plot not presented in this report), this deviation in reactivity is close to zero thereby confirming the above conclusion. However, this observed deviation in k -infinity is reduced at higher burn-ups while the BA is burning out until approximately around 10-15 MWd/kgHM. As the fuel exposure increases further beyond 20 MWd/kgHM, there are distinctive jumps in the magnitude of the reactivity deviation. This is due to the fact that at these burn-up points, the internal base depletion steps of POLCA7 (also used in CROSS main depletion calculation in these simulations) deviate from the depletion steps employed in the corresponding PHOENIX4 reference depletion calculation (see Table 3.1 and 3.2), giving rise to larger difference in the xenon number densities.

Changing the power level in the CROSS simulations has a more significant impact on the magnitude of the deviation profiles, as may be observed by comparing Figure 5.1, 5.2 and 5.3 (Table 5.1 also confirms these observations). The observed changes in the reactivity behavior arise from the fact that all histories of the employed CD-file are computed at rated power conditions [6], and that the current cross section model does not include an explicit correction term for such power regulation effects. As power related effects are only handled partly (i.e. through the implicit account of corresponding xenon number density and fuel Doppler temperature deviations if imposed through feedback), the further away the power level prevails from the nominal reference value, the larger deviation in the reactivity is obtained. It may be noted that below rated power, CROSS underestimates the reactivity while the opposite occurs when running the system above rated power. Nonetheless, when using the current cross section model (i.e. the best-estimate so-called “New Model”) along with the standard CD-file (i.e. abbreviated “std” in the plots in contrast to the “ptXS” customized CD-file), this tilt in deviation profile due to off-base power histories is considered small (i.e. less than 100 pcm) and within acceptable bounds.

In the following a more comprehensive and detailed discussion is provided addressing the use of the different calculation options considered in this analysis (as specified in Section 3.1.2) and their impact on numerical results:

New Model: Demonstrates the performance of the current cross section model implemented in POLCA7 version 4.15.0 (i.e. current production version). In general, this model shows best performance for any given history when comparing to corresponding lattice physics results. This is due to the fact that the new model includes correction terms to account for both isotopic history and xenon spectrum effects thereby significantly improving the prediction capability of reactivity at off-base power histories.

NOHIST: Demonstrates the importance of considering the isotopic impact of any off-base depletion history on macroscopic cross sections. By activating this skip option, the change in cross section data due to the build-up of an off-base isotopic inventory is not accounted for. As is evident from the large deviations observed, the isotopic history model in POLCA7 plays a significant role in improving the performance at off-base depletion conditions.

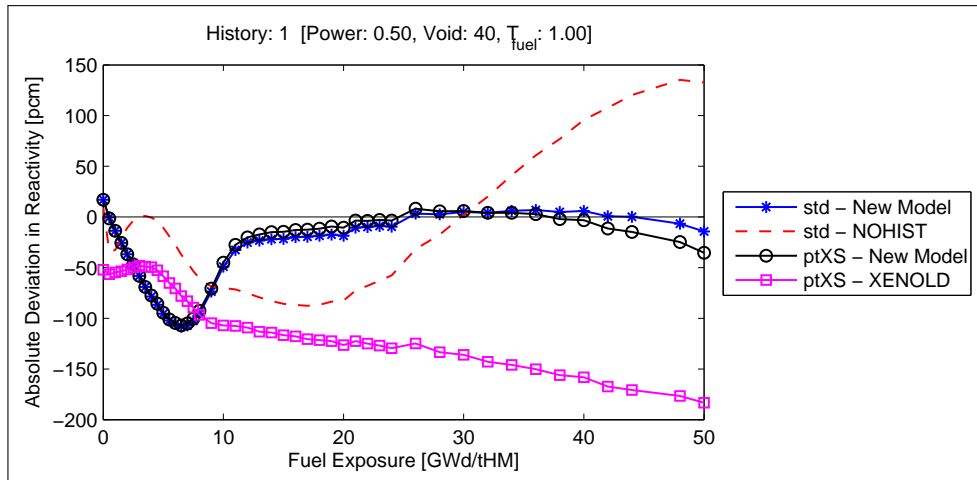


Figure 5.1: Deviation in k-infinity for History 1, CROSS vs. PHOENIX4.

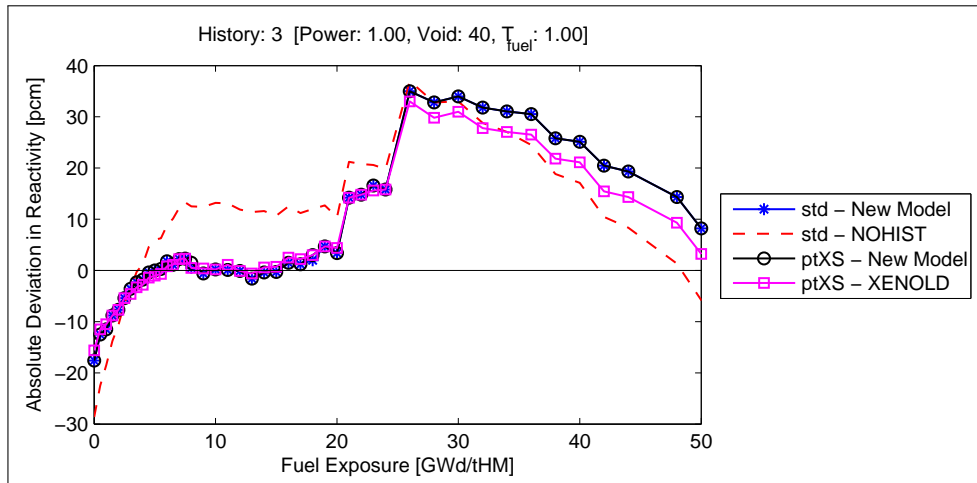


Figure 5.2: Deviation in k-infinity for History 3, CROSS vs. PHOENIX4.

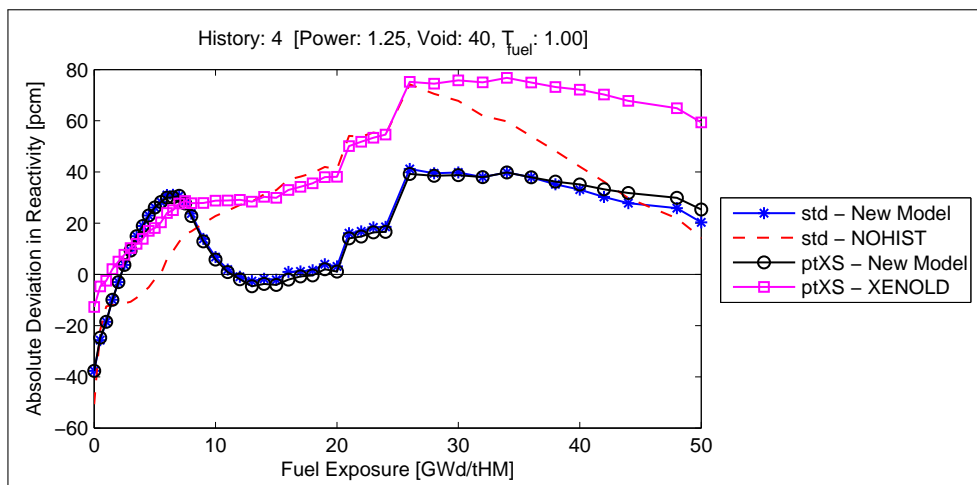


Figure 5.3: Deviation in k-infinity for History 4, CROSS vs. PHOENIX4.

ptXS: Demonstrates the importance of having burn-up, coolant density and coolant density history dependent of microscopic cross section data. At BOL the deviation in reactivity when using point microscopic data in the cell data file is identical to using the standard CD-file. This is because the point values used in this regard are taken from the 3D tables at BOL and reference coolant density conditions (see Section 3.1.2). However, at depleted conditions (above 30 MWd/kgHM) for off-base power histories, the deviation profiles diverge slightly with the ptXS CD-file compared to the cases that use the standard CD-file. Therefore, it may be concluded that having 3D tables for microscopic cross section data for the off-base power histories considered here seems to be of less importance than the isotopic tracking itself.

XENOLD: Demonstrates the importance of accounting for the xenon spectrum effect on cross sections especially during core operation with large power variation. The inclusion of such a model is crucial for the cross section model as XENOLD consistently fails to predict the reactivity at non-reference power histories. This observation is true at both BOL and EOL conditions.

NOSIDISO, NOSPEC: The effects of these calculation options are seen to be very small (as expected) as the analysis in this context is based on single-node simulations at reference coolant conditions with no change in the boundary conditions (i.e. always reflective). Consequently, these model options will not be explored any further in this report.

5.1.1.2 Non-reference coolant condition

In general, the off-base reactivity deviations studied here show similar behavior with burn-up except for a higher magnitude in the errors compared to the cases with the same power history but with the coolant density and fuel temperature kept at their reference values (see the discussion in Section 5.1.1.1). Therefore, due to their similarity with regard to reactivity predictions, only results for History 6 are selected here for a more detailed analysis in terms of Figure 5.4 with the results for the other evaluated history cases given in Appendix A.

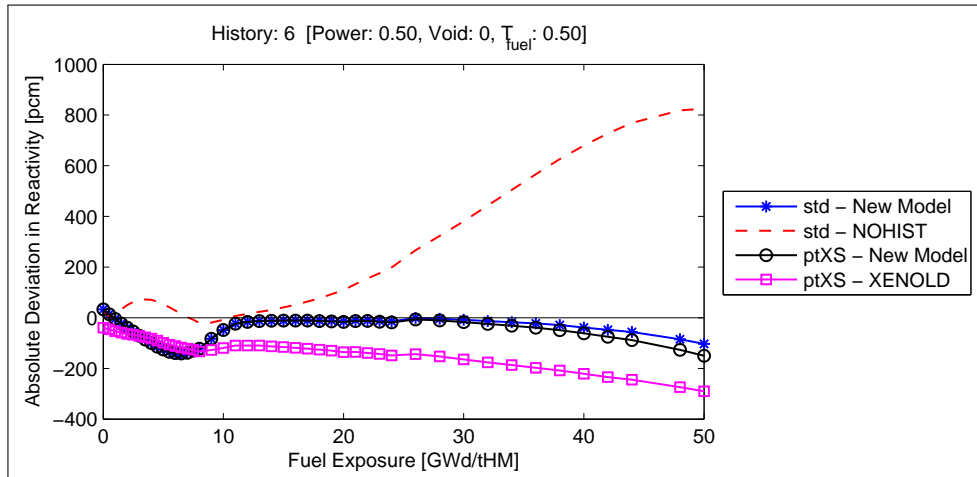


Figure 5.4: Deviation in k-infinity for History 6, CROSS vs. PHOENIX4.

The increased magnitude of the observed k-infinity deviation is mainly due to the fact that the fuel temperature is no longer kept at its reference value and set to a non-entry value ($T_f = 0.5 \cdot T_f^{ref}$ in History 6), i.e. a different value compared to the values used for computing the Doppler coefficients in the CD-file. This suggests that the various Doppler correction terms

applied on nodal cross section data are not sufficient to fully account for the combined effect of both power and fuel temperature variations. In this regard, it is suspected that the assumption of a linear first order Doppler correction model [4] in combination with missing cross-coupling correction terms between off-reference xenon concentration and fuel Doppler temperature (i.e. truncated Taylor series) are the main contributors to the observed k-infinity error with the latter being more significant. Since such an insufficient modeling of fuel Doppler temperature variation will certainly impact the ability to predict a correct heavy nuclide inventory in POLCA7 reflecting the true spectrum history of this case, the reactivity error of CROSS is observed to diverge during BA depletion range and at very high fuel exposure. Furthermore, any change to the flux spectrum due to increased/decreased epithermal resonance absorption will also result in deviations in microscopic cross sections since only the epithermal microscopic absorption cross sections for U-238, Pu-240 and Pu-242 are corrected for the Doppler effect [4].

Table 5.1: Statistics of k-infinity deviation using P7_DEP depletion steps [0-80 MWd/kgHM].

A. STD-CDFILE + NEW MODEL						B. ptXS-CDFILE + NEW MODEL				
Hist	BOLerr	AveErr	StdErr	MinErr	MaxErr	BOLerr	AveErr	StdErr	MinErr	MaxErr
1	16.90	-39.1	40.2	-120.5	16.9	16.90	-42.6	43.3	-137.5	16.9
2	6.60	-7.0	22.8	-61.6	29.9	6.60	-8.4	25.0	-68.6	31.9
3	-17.60	4.2	14.4	-21.5	35.0	-17.60	4.2	14.5	-21.9	35.0
4	-37.70	14.6	16.9	-37.7	41.2	-37.70	15.5	17.3	-37.7	39.8
6	33.00	-81.3	92.3	-350.0	33.0	33.00	-97.7	111.2	-404.0	33.0
7	5.90	-35.1	43.0	-158.4	15.4	5.90	-41.4	50.2	-180.4	14.4
8	-40.90	38.6	24.6	-40.9	73.0	-40.90	42.2	28.1	-40.9	81.4
9	-40.90	0.6	56.9	-134.7	119.3	-40.90	-18.1	66.7	-194.7	117.3
10	-40.90	-104.8	142.9	-378.2	78.1	-40.90	-209.0	253.9	-631.3	77.1

C. ptXS-CDFILE + XENOLD					
Hist	BOLerr	AveErr	StdErr	MinErr	MaxErr
1	-52.10	-122.4	49.7	-199.9	-48.1
2	-21.40	-42.1	23.5	-91.7	-15.7
3	-15.60	2.9	13.5	-22.5	33.0
4	-12.70	38.2	23.5	-12.7	76.8
6	-39.00	-177.6	111.6	-437.0	-39.0
7	-22.10	-76.4	49.5	-198.9	-22.1
8	-15.90	68.6	32.0	-15.9	106.2
9	-15.90	-37.0	84.8	-245.4	71.0
10	-15.90	-255.0	296.2	-736.4	71.0

Table 5.1 shows some k-infinity error statistics with regard to the burn-up dependence for all evaluated non-SDC cases, including the deviation at BOL, mean deviation, standard deviation, minimum and maximum deviation for each non-SDC case (i.e. these statistics are taken over a depletion range of 0 to 80 MWd/kgHM and a sample size of 55). Based on these statistics, it is evident that the new model in combination with the standard CD-file does indeed provide the best set of k-infinity results. However, usage of an off-nominal fuel temperature in these simulations will increase the overall errors in reactivity (i.e. compare the average errors, the corresponding standard deviations and min./max. errors between non-SDC Histories 1-4 and 6-10). Furthermore, somewhat larger errors are obtained using the ptXS CD-file where Histories 1-4 indicates the importance of having burn-up dependent microscopic cross sections whereas Histories 6-10 quantify the impact of having both the burn-up and coolant density dependence for these data. It is observed that having a burn-up dependence of microscopic cross section

data seems to be of less importance (less than 20-30 pcm difference in results) than having the coolant density dependence (up to 250 pcm difference in k-infinity error for History 10), a conclusion in accordance with results provided in Ref. [13]. Finally, by comparing the results for the new model with those of the XENOLD option, one may conclude that xenon spectrum correction model plays an important role especially for handling off-reference power and fuel temperature conditions.

5.1.2 SDC cases

5.1.2.1 Reference coolant condition

The deviation profiles and accuracy of the SDC cases are similar to the non-SDC cases presented in Section 5.1.1.1, except for the predicted k-infinity behavior at SDC intervals² at 8, 16, 24 and 32 MWd/kgHM. The deviation profiles at 50% (Figure 5.5) and 100% rated power (Figure 5.6) are shown below.

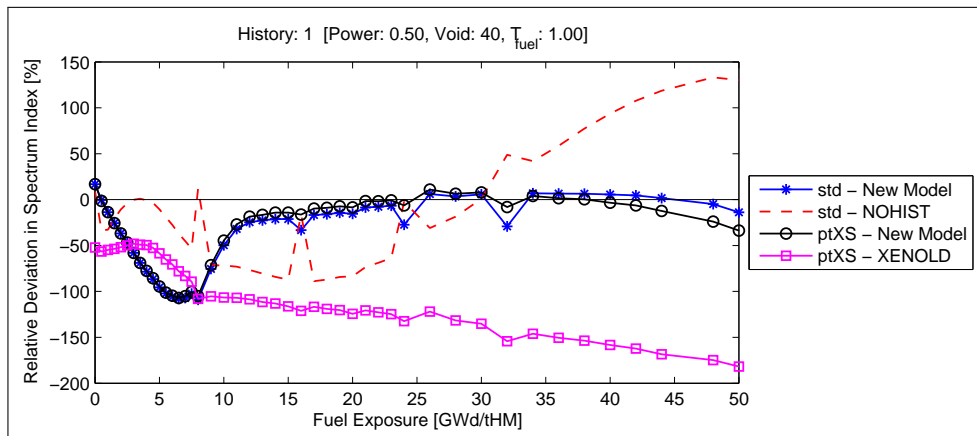


Figure 5.5: Deviation in k-infinity for History 1 with SDC, CROSS vs. PHOENIX4.

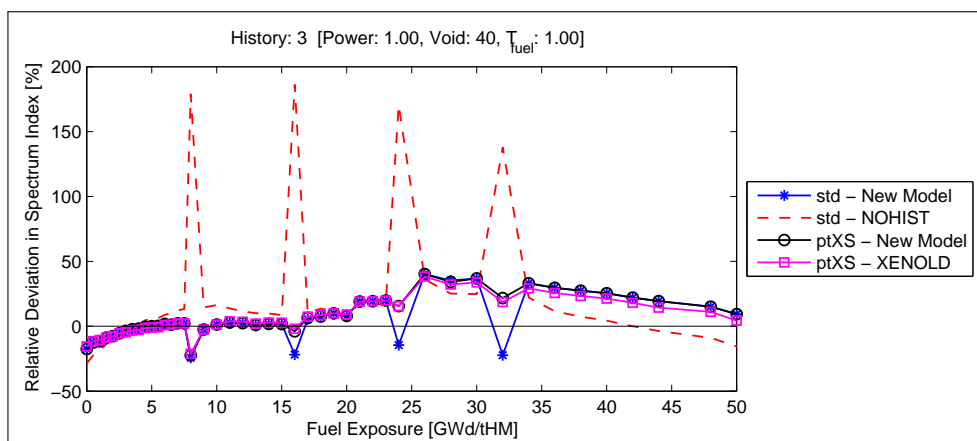


Figure 5.6: Deviation in k-infinity for History 3 with SDC, CROSS vs. PHOENIX4.

When using the NOHIST option (i.e. no account for SDC is made in CROSS), the reactivity at the end of the SDC intervals is overestimated in CROSS about 150-200 pcm at 100%

²The time duration of the SDC imposed at a particular burn-up point.

power history. However, for all other calculation options evaluated, CROSS underestimates the reactivity locally at the end of each SDC intervals by a small amount. In other words, there is a small “dip” in reactivity due to SDC. The magnitude of these dips increases as both the power level and the fuel exposure increase (NOHIST constitutes an exception in this regard at high burn-up). Finally, it should be noted that the use of 3D tables for the microscopic cross section data in the standard CD-file increases slightly ($\approx 20\text{-}30$ pcm) the magnitude of this dip compared to the ptXS CD-file.

As may be indicated by Figure 5.7, the dips in the reactivity error profiles can be attributed to the fact that the spectrum index (defined here as Φ_2/Φ_1) used to compute the energy-collapsed two-group cross sections is different from the actual spectrum at the point of restart after a SDC interval. Consequently, this difference in the spectrum is not fully accounted for in the nodal cross section data provided to the nodal simulator (see also the discussion in Section 5.2), thereby resulting in the dips in the reactivity deviation profiles.

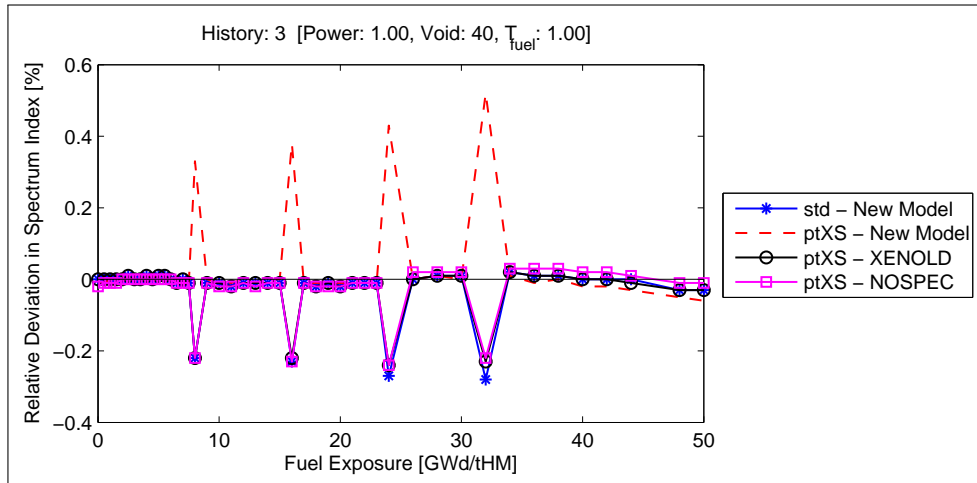


Figure 5.7: Deviation in spectrum index for History 3 with SDC, CROSS vs. PHOENIX4.

It may also be noted that by using point values for fission product microscopic cross sections in the CD-file (ptXS), the dip in spectrum index at higher fuel exposure is observed to be a little smaller indicating that a 3D table representation for microscopic cross sections seems to be slightly less accurate compared to point values. However, one should also consider the fact that this could be an indication that the tracking of some important isotopes is neglected in POLCA7 in the context of shutdown cooling compared to PHOENIX4 and that the ptXS based cross section more effectively cancels this deficiency.

In Figure 5.8, the deviation profiles for History 5 are plotted. This history case is similar to History 3 but with only one SDC conducted at 8 MWd/kgHM for 730 days (representing fuel discarded to the fuel pool for approximately 2 years). Compared to the results obtained for the baseline case running on the same conditions as employed for cell data generation without any SDC (Figure 5.2), similar performance with all options (except for NOHIST, see below) is obtained for History 5 with a slightly larger error at the end of the SDC interval when using the ptXS CD-file and the old treatment of xenon (i.e. XENOLD option). Superior accuracy (i.e. error below 20-30 pcm) is obtained by using the standard CD-file in combination with the current cross section model confirming the ability of POLCA7 to handle reactor shutdown properly. Finally, the importance of modeling SDC is clearly demonstrated by the NOHIST results

where errors up to 200-250 pcm are obtained for a fuel outage around two years, also indicating a reactivity worth of SDC rather insensitive to the outage time (compare Figure 5.6 with 5.8). Once again, these observed errors can be attributed to the difference in spectrum, as seen from Figure 5.9 showing a comparison of the spectrum index deviation profile for History 5. Disregarding the isotopic history model (i.e. NOHIST), it can be seen that the predicted spectrum index is slightly harder in CROSS compared to PHOENIX4 at the end of the SDC interval. Nonetheless, this error margin is very small and within the bounds of the base case (Figure 5.6).

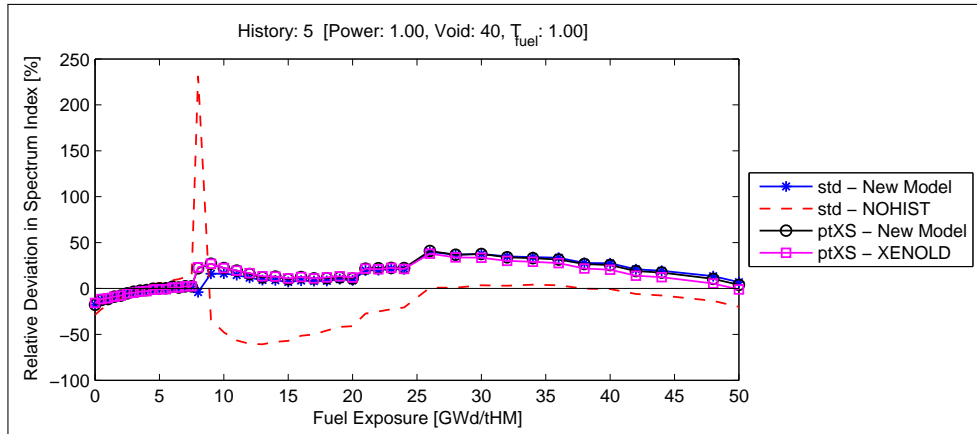


Figure 5.8: Deviation in k-infinity for History 5 with SDC, CROSS vs. PHOENIX4.

5.1.2.2 Non-reference coolant conditions

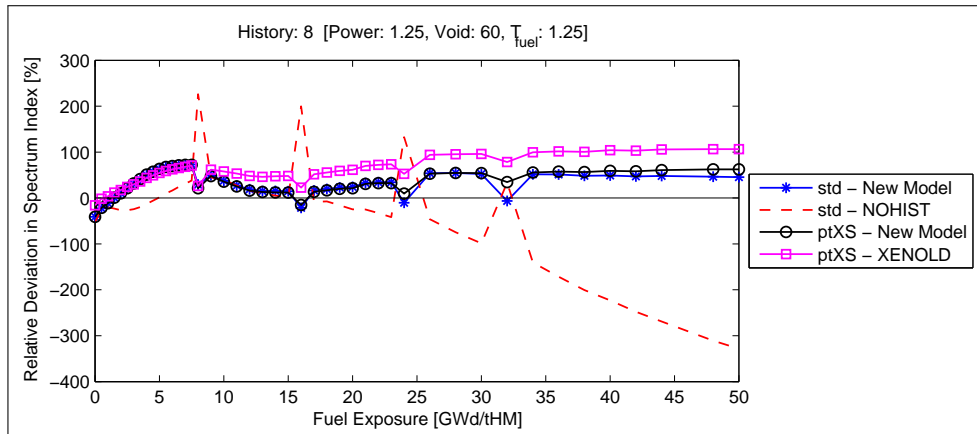


Figure 5.9: Deviation in k-infinity for History 8 with SDC, CROSS vs. PHOENIX4.

For the cases having SDC in combination with off-reference power and fuel temperature histories, the reactivity deviation profiles show similar behavior obtained for the reference fuel temperature and coolant condition, i.e. the trends in Figure 5.9 (History 8) are similar to those in Figure 5.3 (History 4) shown in Section 5.1.1.1. However, all obtained errors here have higher magnitude in accordance with the results given in Section 5.1.1.2. Consequently, the same conclusions as given in Section 5.1.1.2 apply here. Similar figures for History 6 and 7 are presented in Appendix A.3 and A.5.

5.1.3 Mixed operation cases

In general, the reactivity deviation profiles for the mixed depletion histories (i.e. History 9 and 10 in Table 4.1) have many similarities with their individual counterparts discussed in Sections 5.1.1.2 (i.e. results without SDC). In particular, for each burn-up interval having the same operational condition as the corresponding case employing this condition over the whole considered burn-up range, similar trends in the k-infinity error can be observed, as shown in Figure 5.10 and 5.11 for all considered calculation options except for NOHIST. For example, for History 10 in Figure 5.11 a positive tilt in the reactivity in the burn-up range 0-8 MWd/kgHM similar to History 8 (Appendix A.6) is obtained whereas a rather constant error in the range 8-16 MWd/kgHM similar to History 3 (Figure 5.2) and in the range 16-24 MWd/kgHM similar to History 7 (Appendix A.4) can be recognized, etc.. However, rather large discontinuous steps are seen in the deviation profiles at the burn-up points of state parameter change, especially for History 9 where individual jumps up to 200 pcm can be observed. These large steps in the k-infinity error profiles are believed to be caused by the fact that large isotopic cross section corrections are involved in these simulations and because the microscopic cross sections used for the computation of these isotopic corrections are not adjusted accordingly for the inherently strong spectrum shifts occurring after each so-called “steady depletion state” interval.

Note that the results of using the NOHIST option for History 10 shows an error up to 1600 pcm at 50 MWd/kgHM which never recovers at high burn-ups (i.e. asymptotically approaches zero), again confirming the importance of applying an isotopic cross section history model to handle off-base depletion conditions.

It may also be noted that the use of the standard CD-file improves the prediction capability over the ptXS CD-file option, now also by a larger margin than shown before (at most around 300 pcm at 50 MWd/kgHM for History 10) thereby demonstrating the importance of having a 3D table representation for microscopic cross sections data.

For the corresponding SDC cases considering mixed operation conditions, as shown in Figure 5.12 for History 9, no additional dips due to SDC can be recognized in the reactivity predictions after each SDC interval. It appears that the downward shift in the reactivity deviation profile discussed above dominates the effect of SDC at the end of each SDC interval. A similar plot for History 10 is to be found in Appendix A.7.

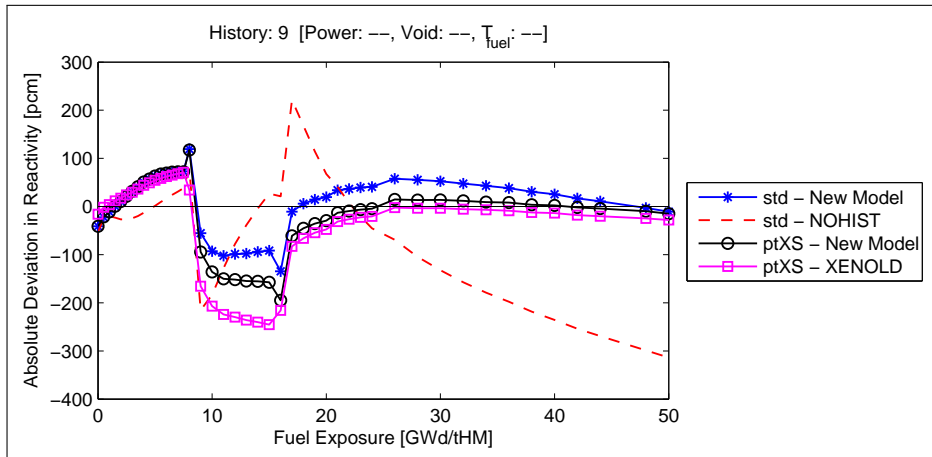


Figure 5.10: Deviation in k-infinity for History 9 without SDC, CROSS vs. PHOENIX4.

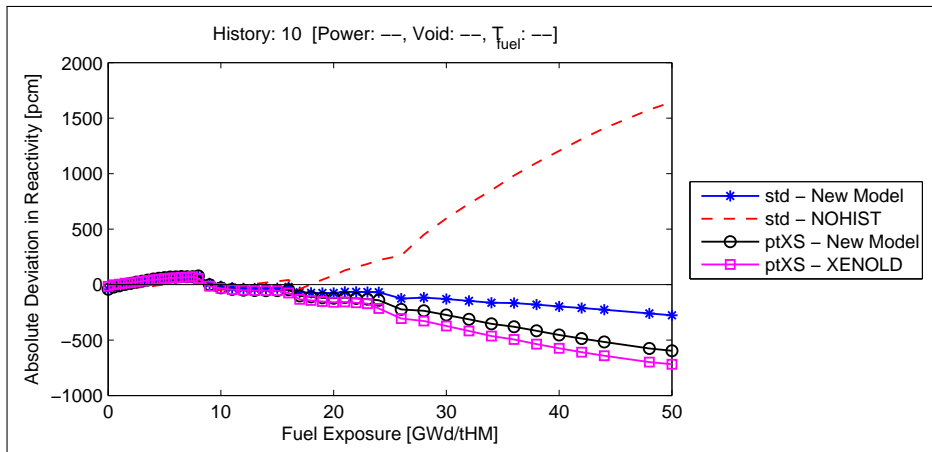


Figure 5.11: Deviation in k-infinity for History 10 without SDC, CROSS vs. PHOENIX4.

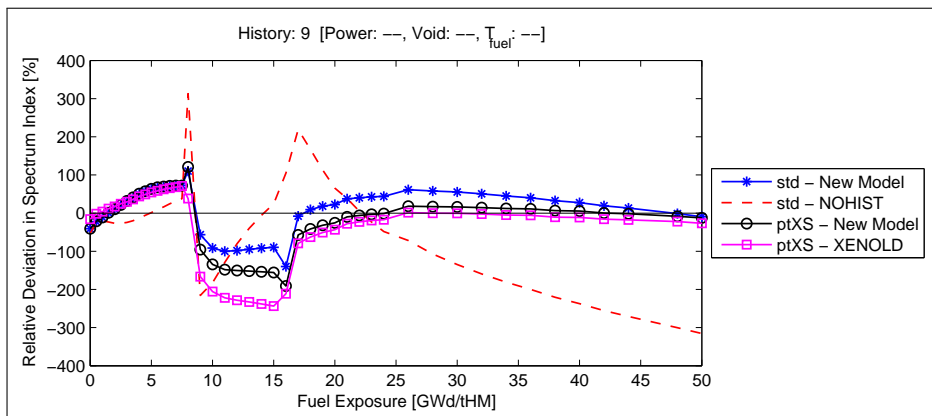


Figure 5.12: Deviation in k-infinity for History 9 with SDC, CROSS vs. PHOENIX4.

5.2 Validation of microscopic cross section representation

In this section, an analysis quantifying the relative deviations in predicted microscopic cross sections for the isotopes identified in Section 3.4 is conducted. Due to the vast amount of results available, the discussion presented here is limited to those power histories having a non-reference fuel temperature imposed (History 6, 9 and 10). However, it needs to be noted that the deviation profiles for Histories 1-4 (i.e. cases with reference fuel temperature) are rather similar to Histories 6-8 (i.e. cases with non-reference fuel temperature), although smaller in magnitude. Evaluation of History 3 and 5 are also included in this discussion in order to identify a base line and to demonstrate the effectiveness of the current cross section model for long SDC intervals.

All calculations in this analysis are performed using the standard CD-file and the current best-estimate cross section model, and only the SDC cases are considered in this regard. In general, it may be seen that the cross sections are underestimated at power levels lower than the rated conditions (e.g., Figure 5.13, 5.14, etc) while the opposite is true for higher powers (e.g., Figure 5.15 and 5.21).

5.2.1 Actinides

Figure 5.13 shows the deviation in the microscopic fission cross sections (both the epithermal and thermal groups) for History 6, i.e. depletion at 50% power and fuel temperature, while Figure 5.14 shows the same for the absorption cross sections for History 6 while Figure 5.15 shows History 8, i.e. depletion at 125% rated power and fuel temperature. Already at BOL, cross section errors around 0.5% are observed (mostly for the thermal group), which are subsequently magnified with burn-up (except for the epithermal fission cross section of U-238). Given that U-235 is one of the prime fissile materials of LWRs, the thermal fission cross section of U-235 seems to have rather large errors (up to 1.5% in absolute sense) compared to the other evaluated cross sections. The behavior of the epithermal absorption cross section of Pu-240 (Figure 5.14) constitutes an important exception in that it displays a rather different profile with an error of +0.5% at BOL that decreases with burn-up changing sign before stabilizing at -1.5% suggesting that the combined effect of off-reference xenon concentration and fuel Doppler temperature is not fully accounted for in the microscopic cross section representation. However, even though the error in the microscopic cross section shows large deviation at high burn-up points, the reactivity (being a global, integrated parameter) is predicted very well, indicating that some error cancellation occurs when computing the k-infinity.

For History 3 in Figure 5.16 (i.e. depletion at reference condition), a step-wise increase in the thermal fission cross sections of U-235, Pu-241 and Pu-239 can be recognized after each SDC interval. This is a consequence of the time-step issue of the xenon correction that is applied to the microscopic thermal cross sections as discussed in Section 5.1.1.1. Since the microscopic xenon correction is only applied in the thermal group, only cross sections in this group are seen to be affected. Nonetheless, the magnitude of this deviation is very small at the reference condition.

The effect of SDC in Figure 5.16 can be clearly seen in terms of pronounced peaks at the end of each SDC interval which is enhanced with increasing power conditions mainly due to changes in spectrum that are not accounted for at the microscopic level. This deviation is mostly present in the thermal group due to stronger decrease in thermal flux compared to the smaller increase epithermal flux giving a spectrum at the end of each SDC interval that is too hard relative to the reference solution (see Figure 5.7). Overall, these peak errors are considered to be rather small (below 0.3%) giving k-infinity errors in the order of 20-30 pcm (see Figure 5.6).

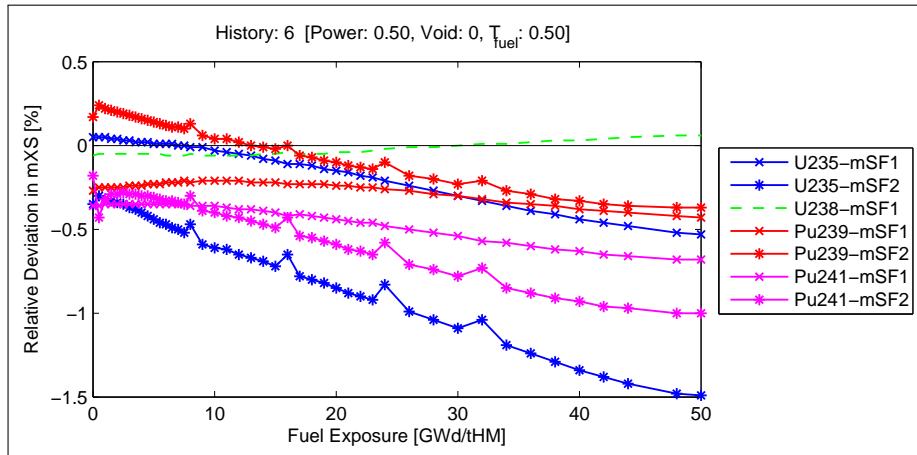


Figure 5.13: Deviation in microscopic fission cross section for History 6 with SDC, CROSS vs. PHOENIX4.

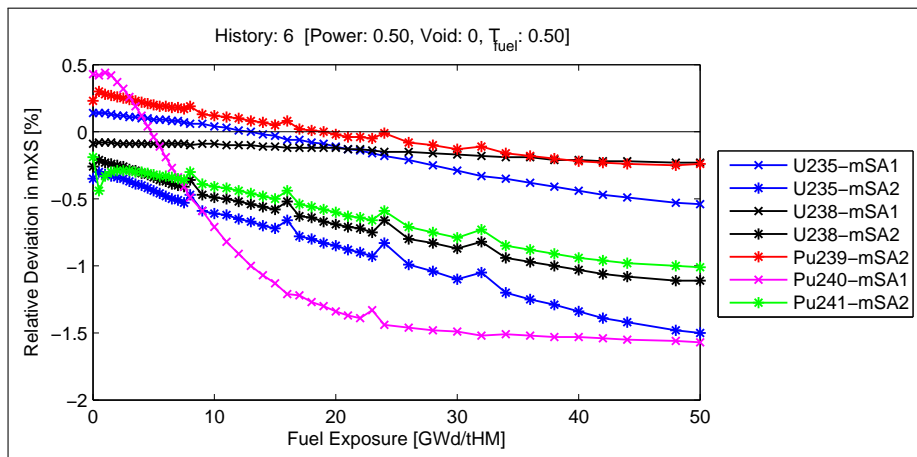


Figure 5.14: Deviation in microscopic absorption cross section for History 6 with SDC, CROSS vs. PHOENIX4.

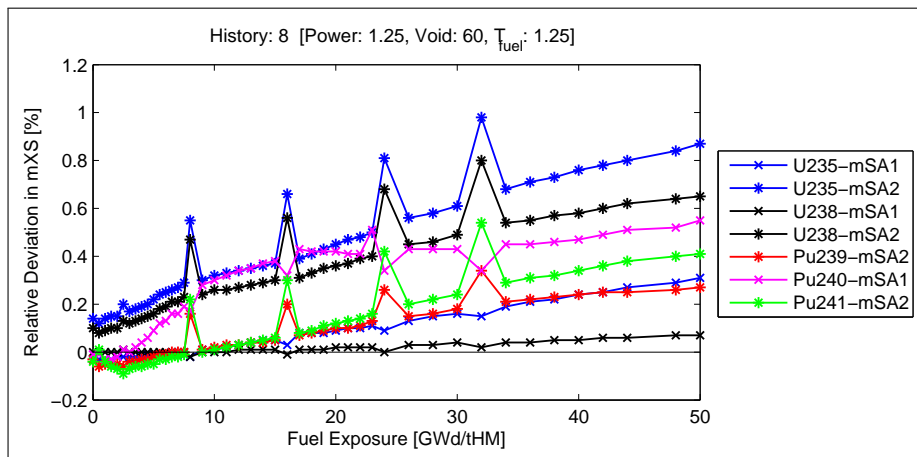


Figure 5.15: Deviation in microscopic absorption cross section for History 8 with SDC.

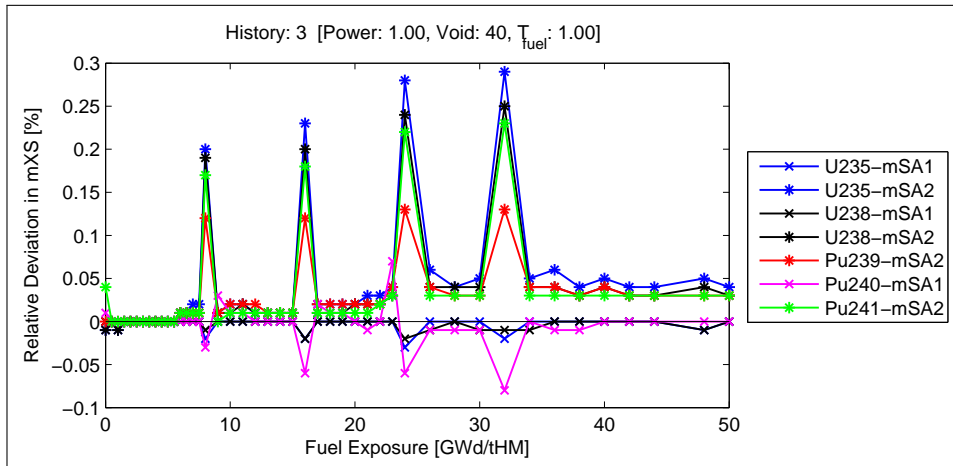


Figure 5.16: Deviation in microscopic absorption cross section for History 3 with SDC.

Considering the history case with 730 days of shutdown (History 5 in Figure 5.17), the overall deviations in microscopic fission cross sections after the SDC are seen to be very small and stay well below the deviations obtained for the history case at the reference condition (Figure 5.16). In other words, no inferior accuracy in the microscopic fission cross sections with shutdown time may be observed confirming the ability of POLCA7 to handle the effects of SDC. The same conclusion may be made regarding fission cross section as well (Appendix A.22).

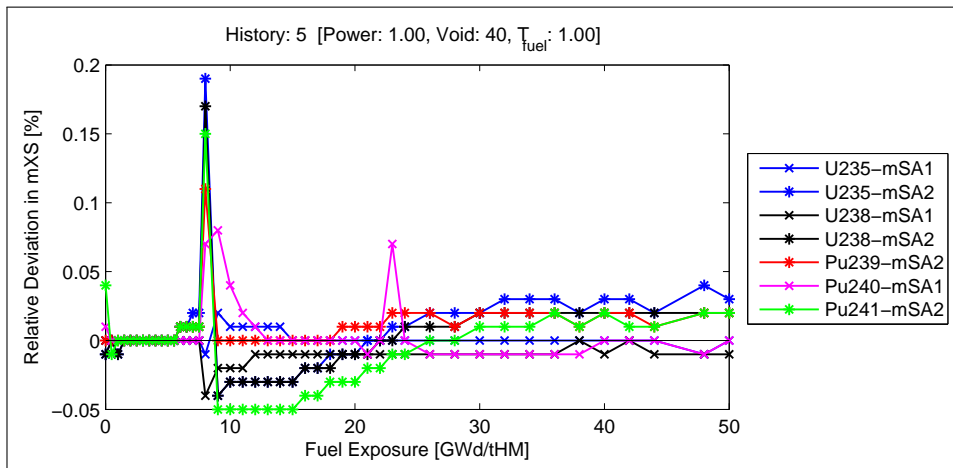


Figure 5.17: Deviation in microscopic absorption cross section for History 5 with SDC.

Finally, Figure 5.18, A.36 and 5.19 show the cross section deviation profile for the cases with mixed operation conditions. In accordance with the results shown for reactivity predictions, these errors are obtained due to the combined effect of the individual histories mainly caused by the lack of appropriate spectrum correction terms due to Doppler and xenon in the microscopic cross section representation. Again, epithermal absorption cross section of Pu-240 excels with an increase in the deviation after each power level and fuel temperature adjustment confirming the conclusion drawn before, that the microscopic cross section representation lacks some higher order terms accounting fully for operation at these mixed power and fuel temperature conditions.

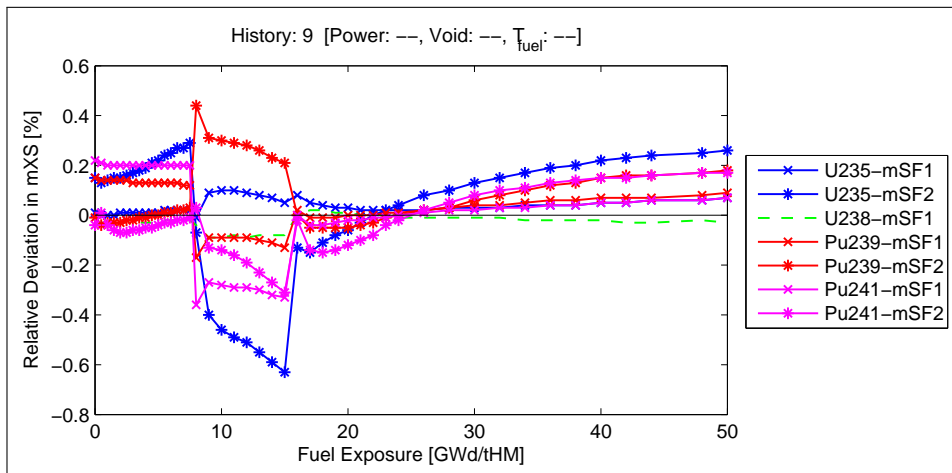


Figure 5.18: Deviation in microscopic fission cross section for History 9 with SDC.

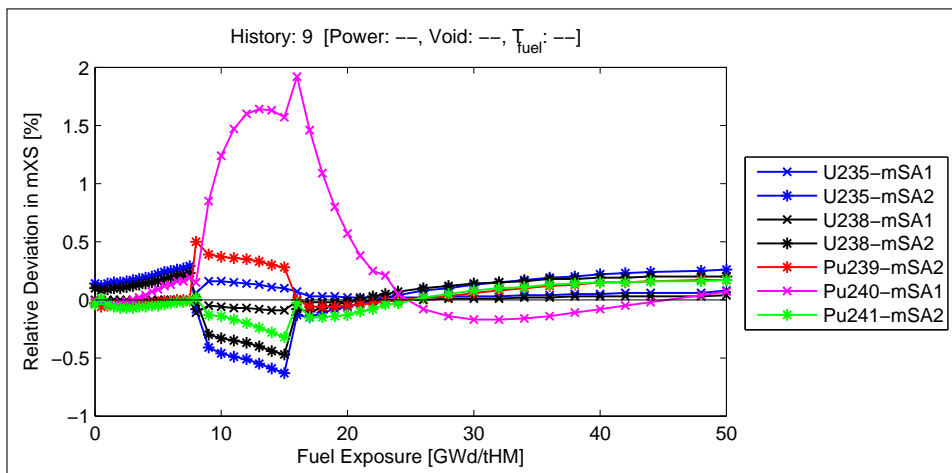


Figure 5.19: Deviation in microscopic absorption cross section for History 9 with SDC.

5.2.2 Fission products

The epithermal microscopic absorption cross section for fission products show similar deviation profiles to those that are seen for actinides in the previous section (i.e. CROSS over estimates cross section at BOL (for all concerned isotopes except Eu-153) while underestimating at higher fuel exposure level at operating conditions below rated levels, while the opposite is true for operating conditions above rated levels). Nonetheless, since these deviations in epithermal cross section are negligible in most cases, they have been placed in Appendix A.

Figure 5.20 shows the deviations in the thermal microscopic absorption cross section of most important fission products for History 6 (i.e. depletion at 50% power and fuel temperature). In general, the error trends are seen to be very similar to the observations made in Section 5.2.1 for the actinides. However, the thermal absorption cross section of Xe-135 constitute an exception in this regard where the cross section is underestimated by 4% at BOL to asymptotically approach a value around -0.5% at higher burn-ups (with no BA remaining). In contrast, very small errors are obtained for History 3 (i.e. depletion at reference conditions) in Appendix A.18, as expected.

Comparing History 8 (i.e. depletion at 125% power and fuel temperature) in Figure 5.21

with History 6 in Figure 5.20, an opposite effect is observed for the Xe-135 at BOL where the cross section is overestimated by 1.5% approaching a rather stable value of +0.5% in due time. Overall, these results suggests that some additional cross section terms are needed for some important fission products (e.g. Sm-151) to handle the simultaneous effect of xenon and fuel temperature variations. This conclusion is further confirmed by corresponding results obtained with the fuel temperature set to the reference value, see Appendix A.18, where some of these cross section errors are seen to be reduced significantly.

Finally, it is interesting to see that only Sm-149 is sensitive to SDC showing pronounced peaks at the end of each SDC interval. Furthermore, the magnitude of these spikes is seen to increase with power (i.e. compare Figure 5.20 with 5.21) which is consistent with the results obtained for k-infinity. Note that the deviation profiles of mixed scenarios have been placed in Appendix A as no additional conclusions can be drawn from these cases compared to Section 5.2.1.

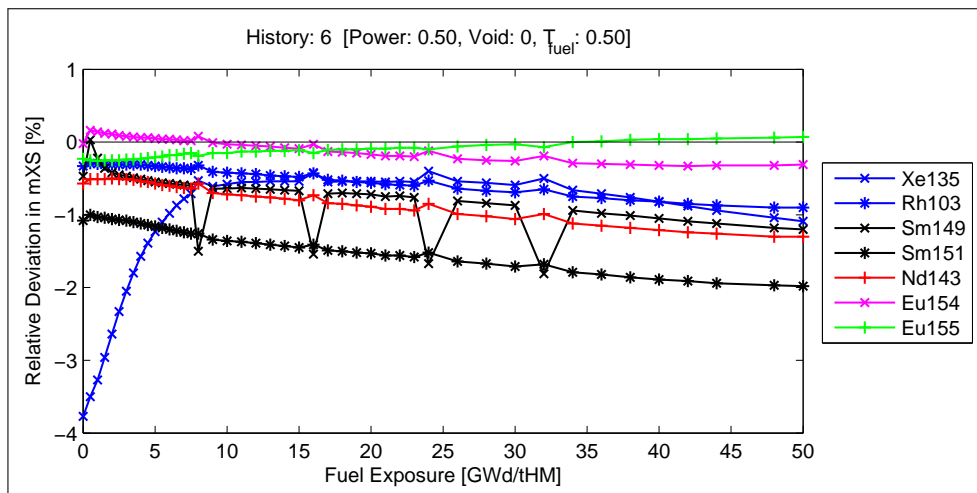


Figure 5.20: Deviation in microscopic absorption cross section for History 6 with SDC.

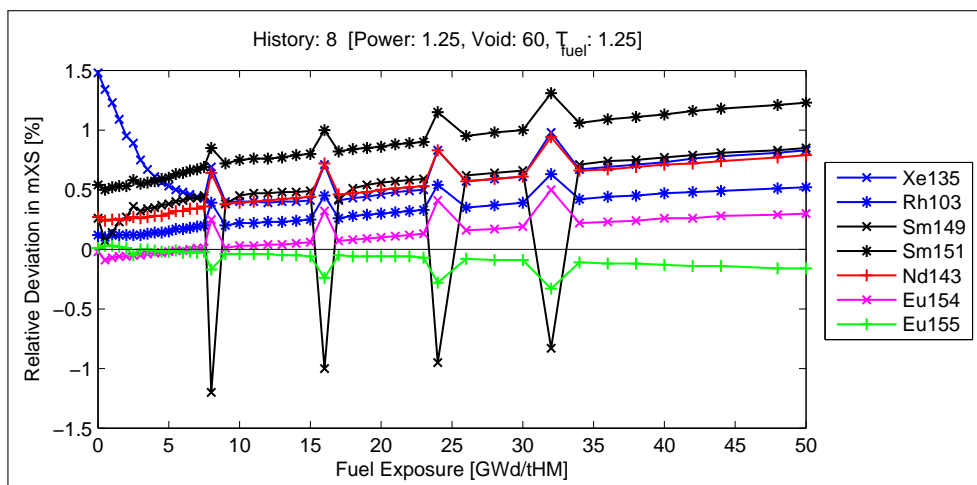


Figure 5.21: Deviation in microscopic absorption cross section for History 8 with SDC.

5.3 Reactivity effect of various depletion step sizes

Using depletion steps in the main depletion calculation that differ from the ones used internally in the base depletion calculation of POLCA7 will lead to errors, especially when an explicit straight-Euler time-integration method is applied. Figure 5.22 and 5.23 show the magnitude of the k-infinity deviation to expect due to this asynchronous depletion step effect for History 1 and 3, respectively. The step sizes used in this analysis have been defined in Table 3.2.

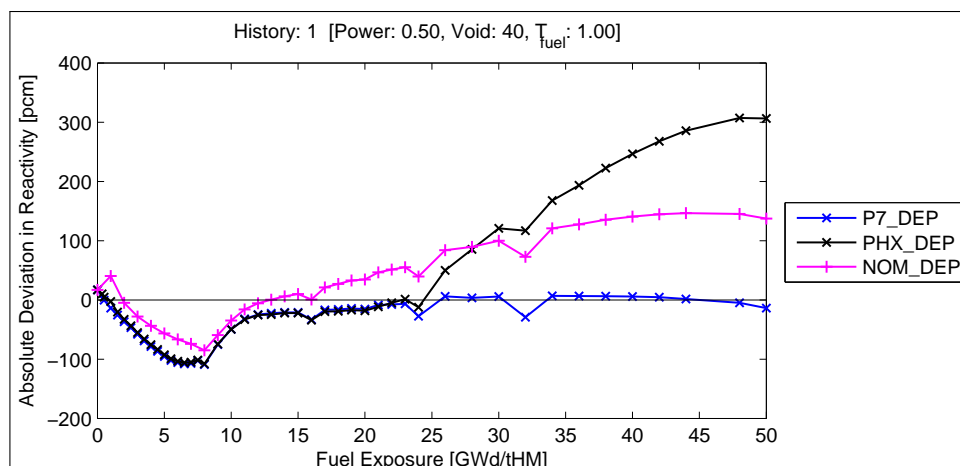


Figure 5.22: Deviation in microscopic absorption cross section for History 6 with SDC.

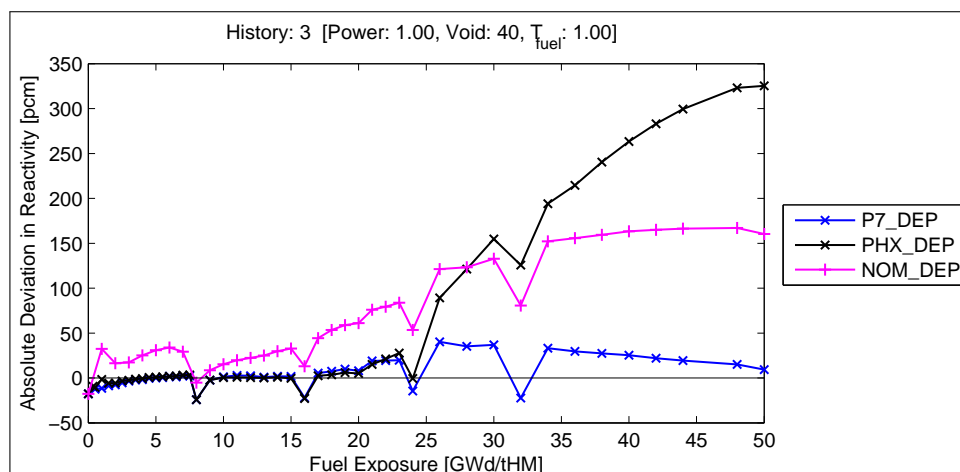


Figure 5.23: Deviation in microscopic absorption cross section for History 8 with SDC.

As expected, using the internal depletion step size of POLCA7 (P7_DEP) produces the best results throughout the entire depletion range due to synchronization between the main depletion calculation and the corresponding internal hard-coded depletion calculation.

Furthermore, up to fuel exposures around 20 MWd/kgHM, the depletion step size of PHOENIX4 and POLCA7 are the same (see Table 3.1 and 3.2), hence both PHX_DEP and P7_DEP have the same k-infinity errors. However, once these step sizes start to diverge, a growing deviation of up to 300 pcm is observed for PHX_DEP.

Using a set of nominal step sizes, as anticipated in real simulations (i.e. 1 MWd/kgHM steps throughout the burn-up range), actually performs well with an error bound around 150 pcm considered acceptable for a explicit time-integration method. In order to reduce these errors further, it will be necessary to implement a predictor-corrector based implicit time-integration method for both the main and base depletion schemes.

No impact of depletion step size can be observed in the magnitude of the reactivity dips at the end of each SDC interval.

Table 5.2: Statistics of reactivity deviation using PHX_DEP depletion steps [0-80 MWd/kgHM].

Hist	STD-CDFILE + NEW MODEL					ptXS-CDFILE + XENOLD				
	BOLerr	AveErr	StdErr	MinErr	MaxErr	BOLerr	AveErr	StdErr	MinErr	MaxErr
1	16.90	57.9	139.4	-106.1	313.3	-52.10	-122.4	49.7	-199.9	-48.1
2	6.60	88.4	128.5	-32.5	319.6	-21.40	-42.1	23.5	-91.7	-15.7
3	-17.60	98.4	130.9	-17.6	329.4	-15.60	2.9	13.5	-22.5	33.0
4	-37.70	107.8	134.5	-37.7	342.4	-12.70	38.2	23.5	-12.7	76.8
6	33.00	45.9	172.0	-260.0	401.2	-39.00	-46.8	120.2	-327.0	214.2
7	5.90	78.0	146.7	-64.7	369.6	-22.10	41.7	126.9	-60.4	299.6
8	-40.90	110.9	111.1	-40.9	318.6	-15.90	148.5	137.6	-15.9	392.6
9	-40.90	92.9	130.0	-134.7	305.2	-15.90	61.8	163.7	-245.4	308.5
10	-40.90	36.4	108.0	-240.2	258.3	-15.90	-105.1	123.2	-416.2	72.0

Table 5.3: Statistics of reactivity deviation using NOM_DEP depletion steps [0-80 MWd/kgHM].

Hist	STD-CDFILE + NEW MODEL					ptXS-CDFILE + XENOLD				
	BOLerr	AveErr	StdErr	MinErr	MaxErr	BOLerr	AveErr	StdErr	MinErr	MaxErr
1	16.90	36.3	68.2	-77.5	141.2	-52.10	-56.8	33.3	-144.5	-3.6
2	6.60	64.3	54.4	-19.6	149.0	-21.40	28.3	38.7	-43.6	90.6
3	-17.60	73.2	53.5	-17.6	157.4	-15.60	76.4	54.8	-15.6	162.3
4	-37.70	81.9	56.0	-37.7	167.9	-12.70	113.9	68.0	-12.7	215.9
6	33.00	15.2	125.3	-325.0	176.6	-39.00	-96.4	98.3	-406.0	-7.9
7	5.90	48.8	77.4	-127.4	164.3	-22.10	3.9	58.5	-159.4	88.3
8	-40.90	89.7	45.0	-40.9	144.9	-15.90	131.7	63.4	-15.9	218.9
9	-40.90	65.5	79.2	-94.7	155.3	-15.90	26.4	109.6	-207.9	130.2
10	-40.90	-38.7	105.1	-345.2	108.4	-15.90	-208.6	228.7	-550.2	112.4

This page was left blank intentionally.

6

Part B: 2D Mini-Core Studies

In this section the obtained deviations (i.e. POLCA7 vs. PHOENIX4) in k-effective and relative node power density for the different mini-core configurations discussed in Section 4.2 are presented. This section is divided into three sub-sections based on the type of configuration considered in the analysis: clean¹ configuration, configurations with a homogeneous void distribution and configurations with a heterogeneous void distribution.

6.1 Clean Configuration 1

Configuration 1, having a homogeneous void distribution (i.e. 40% void fraction) with all fresh assemblies running at reference power and fuel temperature, is the most trivial configuration. The only purpose for considering this configuration is to ensure that the evaluation framework is working properly.

The reactivity deviation profiles² for this clean configuration are plotted in Figure 6.1³. At the BOC zero xenon condition, all calculations employing the current xenon feedback model (see Section 2.1) show excellent agreement with the PHOENIX4 reference results, i.e. an error less than 10 pcm was obtained. As expected, all the different correction model options perform almost identically due to the fact that these simulations are running at the base condition. However, note that the BASE option shows a large BOC0 deviation since it contains no xenon correction terms to account for the zero xenon state at 0 MWd/kgHM. By disregarding the xenon spectrum effect represented by the XENOLD option, an error of -231 pcm was obtained which is consistent with the errors reported in Ref. [14] quantifying the reactivity worth of the

¹Clean in the sense that it represents the infinite-medium core condition allowing for a direct comparison of a QA calculation with a corresponding SA calculation.

²All cases running with the standard CD-file have a legend starting with “Std CD” and a marker “*” while cases running with the CD-file employing point microscopic cross sections are represented by “ptXS CD” along with a box marker. The additional tag (e.g. New, XENOLD, etc.) indicates which calculation option (see Section 3.1.2) was employed for that particular case. All figures include a table that illustrates some basic statistics (i.e. mean deviations, max./min. deviations, standard deviations and BOC deviations) over the depletion range 0-40 MWd/kgHM (i.e. sample size was 37). The “LGD-x” column headers in the table stand for “legend” with the number representing the corresponding legends in the figure counting from top to bottom (e.g. LGD-4 represents “Std CD + NOSPEC”).

³Title of the figure is defined as follows: configuration number for identification purpose; assembly wise void fraction in percentage; and assembly wise fuel exposure at BOC.

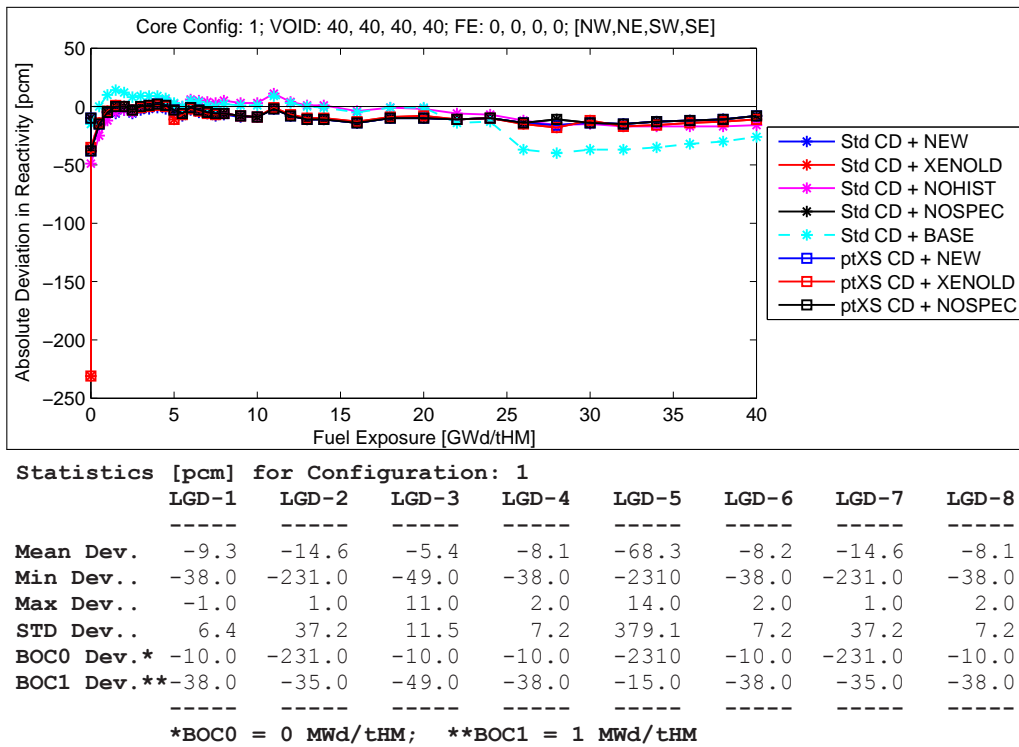


Figure 6.1: Deviation in k-effective for Configuration 1, POLCA7 vs. PHOENIX4.

xenon spectrum effect.

6.2 Configurations 2 & 4 with assembly-wise homogeneous void distribution

6.2.1 Configuration 2

The reactivity deviation profiles for the different model options running on Configuration 2 (see Figure 4.2) are shown in Figure 6.2. Similar to Configuration 1, the current xenon feedback model has a superior performance at BOC (+118 pcm vs. -63 pcm for XENOLD) considering the fact that the equilibrium xenon state at 1 MWd/kgHM is contaminated with an error of 75 pcm due to deficiencies in other models (i.e. the use of XENOLD results in a rather large jump in the reactivity deviation profile from -65 to 75 pcm compared to the other evaluated model options when going from a zero xenon state to an equilibrium xenon state).

The use of the ptXS CD-file results in an over-prediction of the reactivity at BOC compared to cases using the standard CD-file (i.e. compare BOC0 and BOC1 deviations of LDG-1 with LGD-6, LGD-2 with LGD-7 and LGD-4 with LGD-8) by a magnitude of around $40 \approx 50$ pcm. This error occurs purely due to the lack of a burn-up dependence in microscopic cross section data as the coolant density is set to its reference value and does not come into play in this case. However, after some irradiation, the error for both CD-files shows similar behavior with burn-up since the simulations are running at the reference coolant density condition (i.e. at 40% void, an entry value present in both CD-files, see Section 3.1.2).

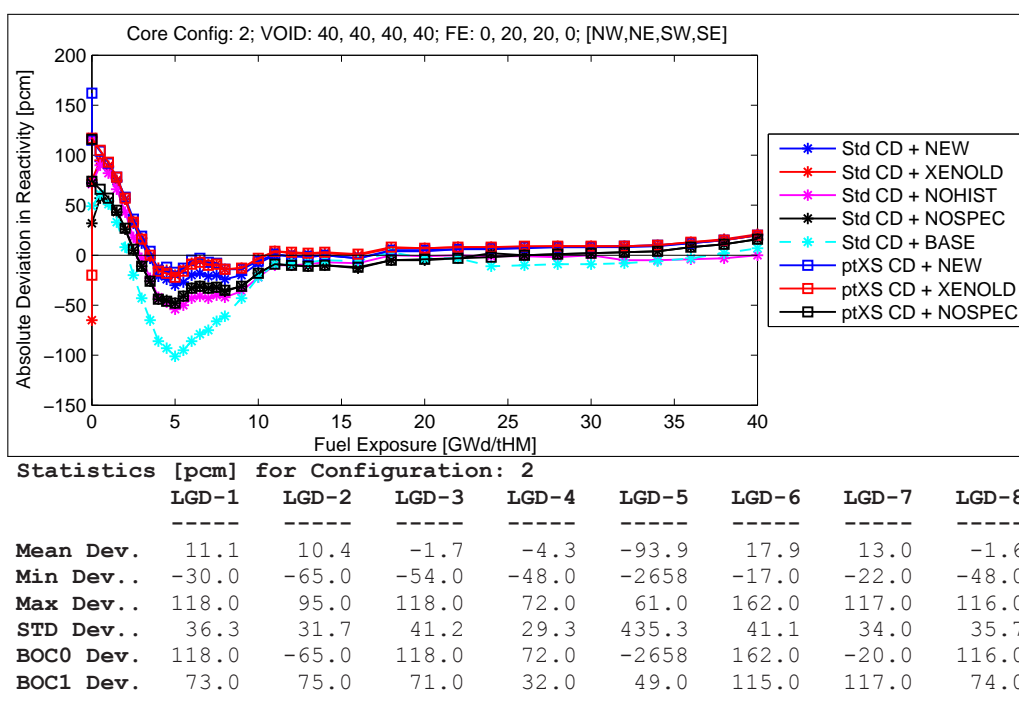
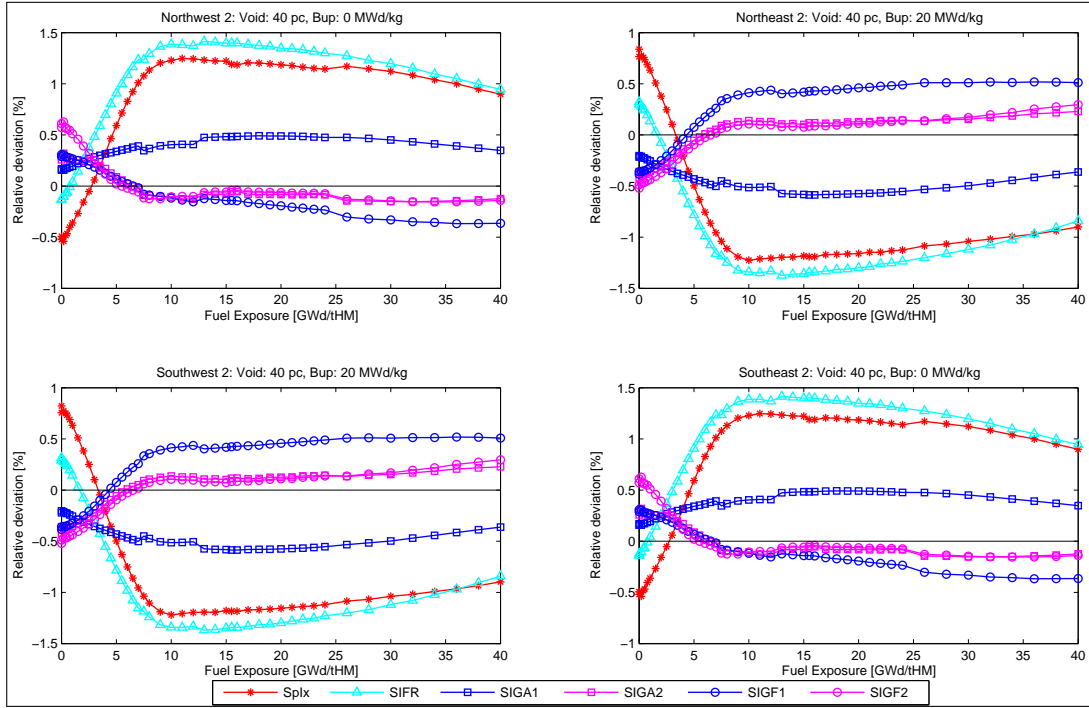


Figure 6.2: Deviation in k-effective for Configuration 2, POLCA7 vs. PHOENIX4.

One of the most prominent features of the reactivity deviation profiles is the rather strong drop in the reactivity error (approx. 130 - 150 pcm over the depletion range 0 - 5 MWd/kgHM, see in the table associated with Figure 6.2). After approximately 10 MWd/kgHM, a healing effect of the reactivity error is observed where the POLCA7 solution asymptotically approaches the PHOENIX4 reference solution. It may also be noted that the deviation at BOC for the cases using the NOSPEC calculation option (i.e. with the instantaneous spectrum interaction (ISI) and spectrum interaction history (SIH) models bypassed) is smaller compared to the current best-estimate model indicating that the ISI model does not perform as expected, i.e. the ISI correction gives a positive insertion of reactivity when the opposite is expected in order to compensate for leakage induced spectrum changes. The contribution from the spectrum interaction history model was seen to be very small (i.e. 3-5 pcm) for all fuel exposures. In this regard, it was further identified that the span of the coolant density history entries around which the sensitivity coefficients of the SIH model are prepared was chosen to be very small thereby inducing very small sensitivity coefficients and making them prone to catastrophic cancellation. This implies that the current implementation of computing these coefficients is not numerically robust.

It was also observed in an auxiliary investigation that both Φ_1 and Φ_2 have a strong spatial curvature due to the prevailing flux mismatch between the fresh and depleted assemblies. Therefore, a net leakage of epithermal/thermal neutrons from the fresh assemblies to the depleted ones is expected, also confirmed by the POLCA7 predicted net currents. Consequently, due to this leakage effect and according to PHOENIX4 reference calculations, the cross sections for the fresh (depleted) assemblies should get a negative (positive) contribution compared to the cross sections of the SA calculation. However, the magnitude of the correction provided by the current ISI model (i.e. Σ_{a1}^S , see in Equation 2.5) shows an opposite effect. As such, the cross sections are overestimated (underestimated) for the fresh (depleted) assemblies at BOC compared



BOC Error [%] in different reactor parameters for Configuration: 2

	NW	NE	SW	SE
SpIx...	-0.49	0.84	0.82	-0.49
SIGR...	-0.13	0.32	0.32	-0.14
SIGA1...	0.17	-0.22	-0.22	0.17
SIGA2...	0.26	-0.42	-0.42	0.26
SIGF1...	0.31	-0.39	-0.39	0.31
SIGF2...	0.61	-0.52	-0.52	0.61

Figure 6.3: Assembly wise deviation in Σ_α and spectrum index for Configuration 2, using current cross section model with standard CD-file.

to the SA condition (see Figure 6.3⁴) before “ramping” down (up) as the fuel is irradiated. The worth of this erroneous correction for the fresh (depleted) assemblies is 52 pcm (62 pcm) at 1 MWd/tHM (i.e. 0 MWd/tHM was not evaluated since it contains other corrections due to zero xenon state), therefore having a total core-wise worth of 57 pcm. A more detailed discussion about the observed behavior of the spectrum interaction model will be given in Section 6.3.1 in conjunction with the evaluation of configurations having a heterogeneous void distribution.

The assembly-wise relative node power density profiles shown in Figure 6.4 is what one would expect for a symmetric core with a checkerboard loading of fresh and depleted assemblies (i.e. assemblies with the same composition have similar power profiles). Due to presence of BA in the fresh assemblies, the power of these fresh assemblies is initially lower compared to the irradiated ones. As the BA is depleted out, the fresh assemblies will provide more power in due time.

The assembly-wise relative node power density deviation profiles for the different calculation options considered in this analysis are plotted in Figure 6.5⁴. Since the deviation profiles for

⁴Each sub-plot represents the individual assemblies in the mini-core (i.e. northwest, northeast, southwest and southeast). The tile of each sub-plot identifies the assembly; assembly wise void fraction (in percentage) and assembly wise fuel exposure at BOC.

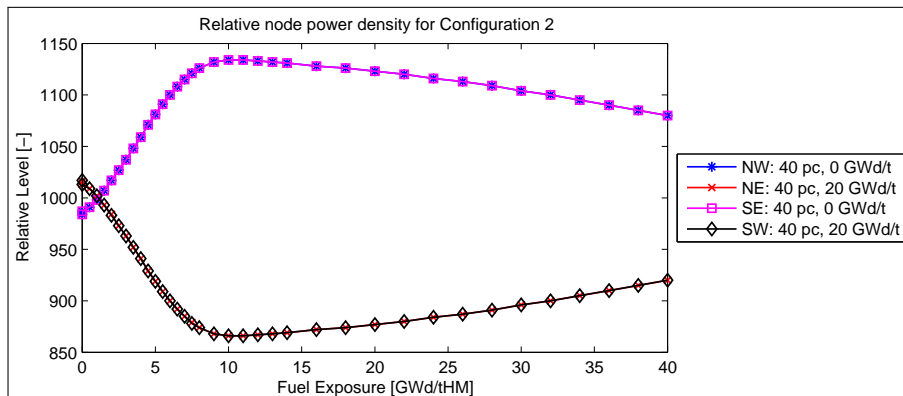


Figure 6.4: Relative node power density profile for Configuration 2.

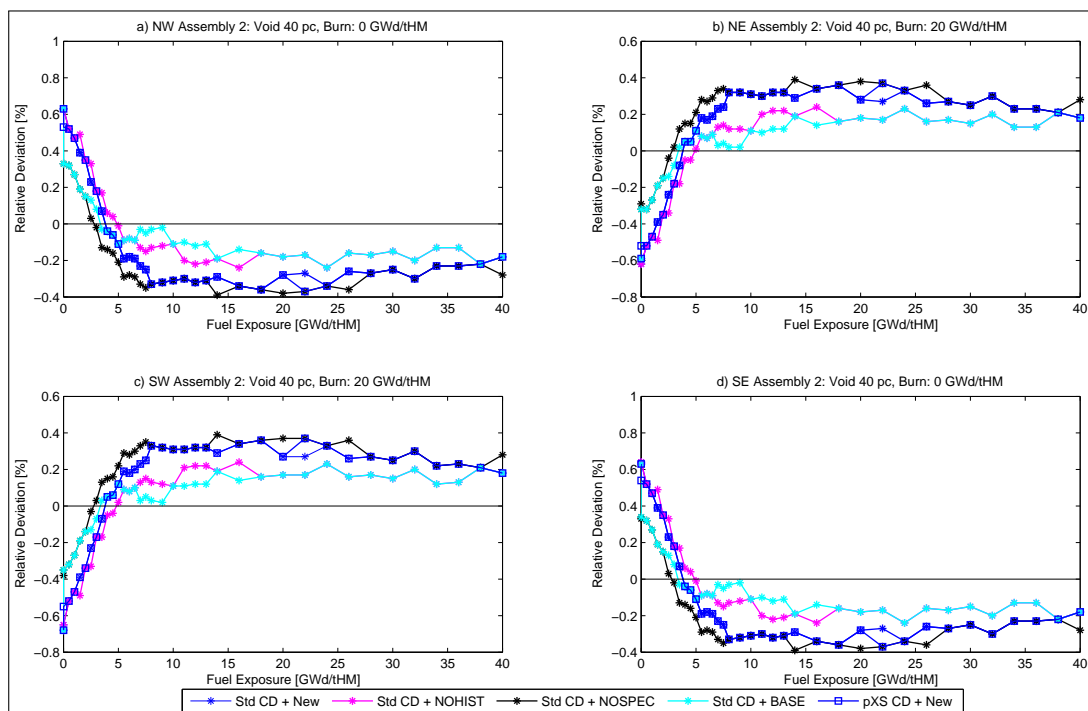


Figure 6.5: Assembly wise deviation in relative node power density for Configuration 2.

both xenon models were identical (except at BOC), only results for the current xenon feedback model are shown. Given the definition of the relative node power density (i.e. see Equation 2.12, which states that the relative node power density is a function of the node total fission rate) and due to the combined effect of a too hard spectrum and a too large epithermal fission cross section, as recognized from Figure 6.3, the power output from the fresh (depleted) assemblies is seen to be overestimated (underestimated) at BOC. Furthermore, notice that deactivating the spectrum interaction models generally translates to a lower magnitude of observed deviations at BOC, which is in accordance with the conclusions made in the previous paragraphs regarding the performance of the spectrum interaction model implemented in POLCA7. It can also be observed from Figure 6.5 that, even though the reactivity predicted by POLCA7 asymptotically approaches the PHOENIX4 reference solution after 10 MWd/kgHM, some errors in the node-wise power distribution still prevail at high fuel exposures implying that some error cancellation occurs when computing the reactivity.

6.2.2 Configuration 4

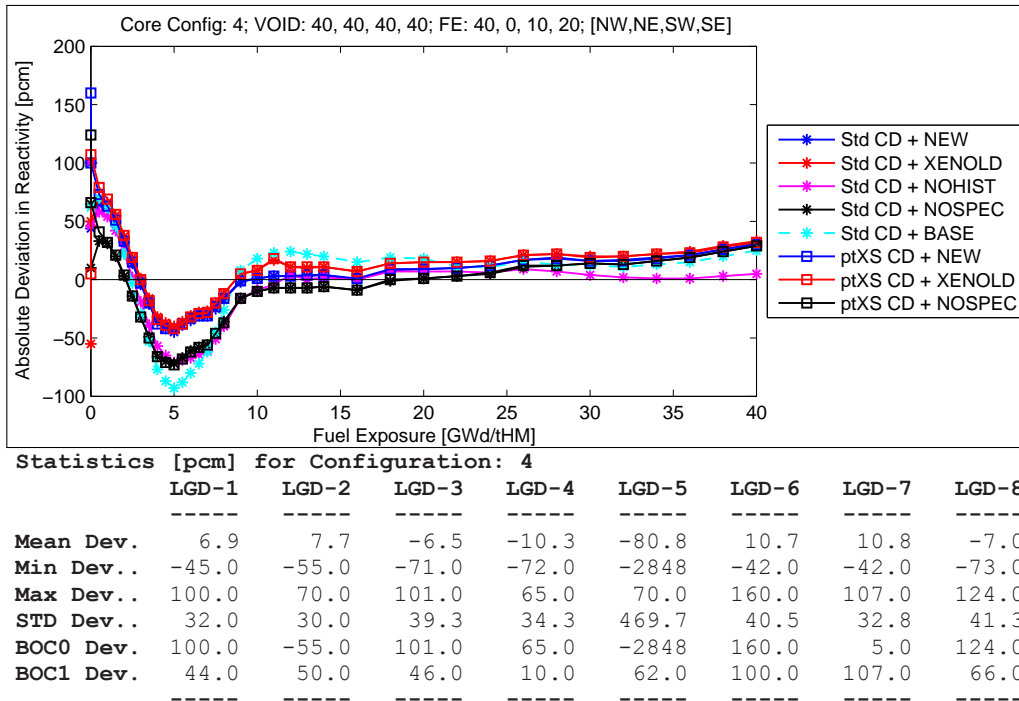


Figure 6.6: Deviation in k-effective for Configuration 4, POLCA7 vs. PHOENIX4.

In Figure 6.6 the reactivity deviation profiles for Configuration 4 (i.e. see Figure 4.4) are presented. As may be seen, the k-effective errors show no significant sensitivity to the type of CD-file being used except for BOC conditions, which is in accordance with the conclusions drawn in Sections 6.1 and 6.2.1. However, it is seen that the magnitude of the reactivity drop is little smaller for this configuration compared to Configuration 2 (see Figure 6.2 in Section 6.2.1). This is most probably due to the fact that there is less BA in this configuration, diminishing somewhat the effect on reactivity of the complex interplay between spectrum variations (i.e. spectrum softening in the fresh bundle) and BA depletion (i.e. Configuration 4 consists only of one fresh assembly with BA in contrast to the two fresh assemblies in Configuration 2).

Again it can be seen that the BOC k-effective predictions improve when the spectrum interaction models are deactivated, hence supporting the conclusions made in Section 6.2.1. The possible reason for such a behavior will be discussed in Section 6.3.1 in more detail.

It may also be noticed that since an asymmetric core loading is utilized in this configuration, the relative node power density from individual assemblies differs from each other as seen in Appendix B.1. Again the relative node power density deviation profile gets worse at BOC when using the ISI model (compare NEW to BASE at 1 MWd/tHM in Appendix B.2). Furthermore, it can again be seen that even though the reactivities predicted by POLCA7 and PHOENIX4 approach each other asymptotically (see in Figure 6.6), there are still inherent errors in the nodal power distribution.

6.3 Configurations 3 & 5 with assembly-wise heterogeneous void distribution

6.3.1 Configuration 3

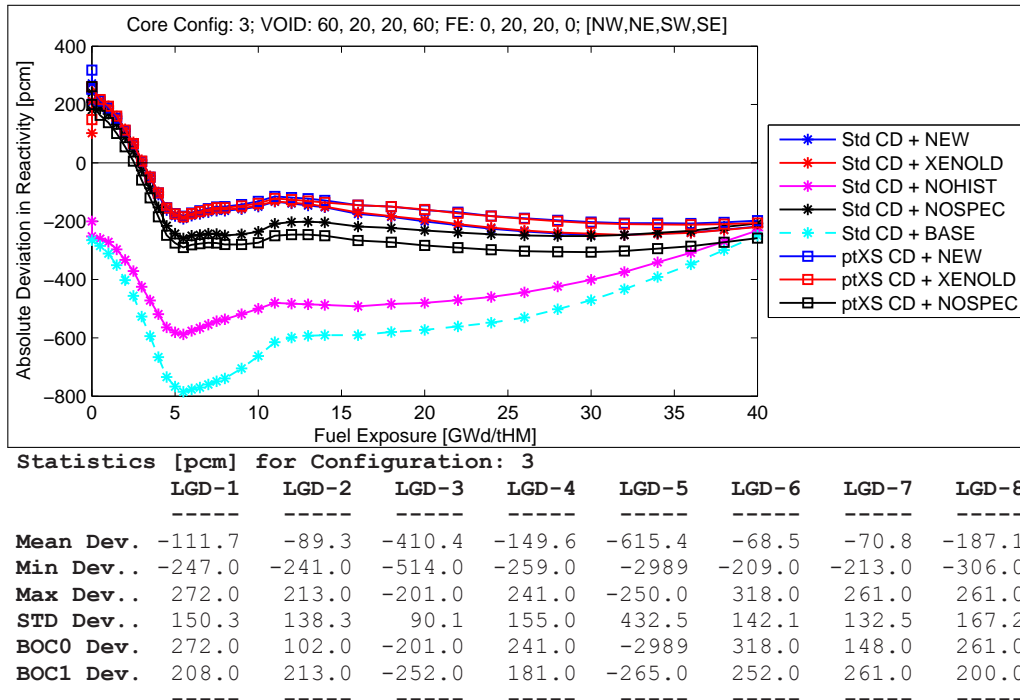


Figure 6.7: Deviation in k-effective for Configuration 3, POLCA7 vs. PHOENIX4.

Configuration 3 is similar to Configuration 2 except for the different void conditions set for the different assemblies (i.e. fresh assemblies have a higher void fraction of 60% while the depleted assemblies have a lower void fraction of 20%, compare Figure 4.2 and 4.3 in Section 4.2). The general trend of the reactivity deviation profiles remains the same compared to Configuration 2 (compare Figure 6.7 with Figure 6.2) even though the magnitude of the k-effective errors becomes larger. The reason for these larger errors in reactivity may be attributed to the fact that these simulations are subject to stronger leakage through the introduction of a heterogeneous void distribution in the core which further amplifies the errors in the spectrum interaction model.

Likewise as seen in Configuration 2, the reactivity is being overestimated at BOC resulting in the burn-up dependent oscillation in the reactivity deviation profiles. Again it is noticed that using the ISI model results in somewhat larger overestimation of k-effective at BOC (compare LGD-1 with LGD-4 in the table associated with Figure 6.2). The worth of these corrections by the ISI model for the fresh (depleted) assemblies is 170 pcm (127 pcm), hence having a core-wise worth of 148.5 pcm at 1 MWd/tHM. In addition, the SIH model adds a large negative correction to the cross sections of the depleted fuel assemblies with a worth of -135 pcm at BOC (i.e. per definition, no SIH correction for the fresh assemblies occurs), with a core-wise worth of -67.5 pcm, as also illustrated by Figure 6.10 containing results for Configuration 5. Based on these observations and the conclusions drawn in Section 6.2, one can make the statement that given the rather ad-hoc formulation of the different spectrum interaction sensitivity coefficients (see Section 2.2 and 2.3) computed internally by POLCA7 based on coolant density tabulation of

cross sections without consideration of explicit leakage conditions, the current implementation of the ISI and SIH models is unable to properly compensate for leakage-induced spectral changes.

Note that there is a change in the coolant density history condition between the first and second cycle, i.e. going from a 40% void history to either a 20% or 60% void history. Considering the history state at BOC of cycle 2, due to the fact that the base depletion calculation assumes a constant coolant density and a prehistory corresponding to the prevailing coolant density, i.e. 20% or 60% void history, cross sections are corrected for the contribution of a 40% void history in cycle one, i.e. $\Delta N = N(40\%) - N_{base}(60\%)$. Consequently, by ignoring this history effect by applying the NOHIST option results in a large underestimation of the reactivity throughout the second cycle as seen from Figure 6.7.

The effect of using the ptXS CD-file becomes more prominent at high burn-ups for this configuration having a heterogeneous coolant density (i.e. void) distribution as microscopic cross section data do not have table entries for the coolant density and coolant density history. As before, at BOC k-effective errors of the same magnitude as obtained for Configuration 2 and 4 are observed due to the lack of a burn-up entry in microscopic cross section data. However, after some irradiation, the errors tend to diverge between the standard and customized CD-file (applying equivalent model options) with a maximum difference around few hundreds of pcm recognized thereby supporting the conclusion drawn in Part A and [2] stating that having a burn-up dependence of microscopic cross section data is of less importance than having a coolant density dependence. This observation is especially prominent when the NOSPEC option is activated thereby eliminating part of the error cancellation caused by the combined use of ISI and isotopic history models, something that may also be seen from Figure 6.9 by looking at the relative nodal power density deviation profiles for the standard CD-file. Hence, if ISI model is deactivated, there is nothing to compensate for the limitations of the ptXS CD-file and the wrong accumulation of isotopic number densities. Otherwise, these power density profiles including their errors behave as expected based on the results obtained for Configuration 2.

The power profile for the different assemblies seen in Figure 6.8 is what one would expect: the fresh (depleted) assemblies with higher (lower) void condition produces less (more) power compared to the already depleted (fresh) assemblies.

The relative nodal power density deviation profiles in Figure 6.9 for different cases are in accordance to the conclusions made in the previous section. Additionally, it can be seen that the history model is able to compensate the cross sections to account for the build-up of off base isotope inventory due to off nominal power level (i.e. deviation in the node-wise power density for the case running on NOSPEC (i.e. history model is active) holds constant after 5 MWd/kgHM). However, the isotopic history model cannot alone determine the power correctly (i.e. the case running on NOSPEC underestimates (down shifted) the power for the fresh core at BOC) and neither can the ISI model do the job by itself (i.e. the case running on NOHIST overestimates (up shifted) the power for the fresh core at BOC), which is in accordance to conclusions made in the previous paragraphs.

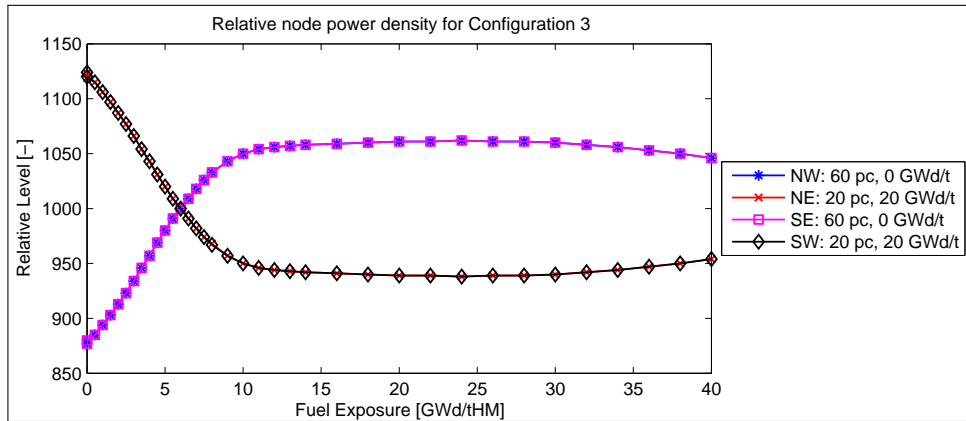


Figure 6.8: Relative node power density profile for Configuration 3.

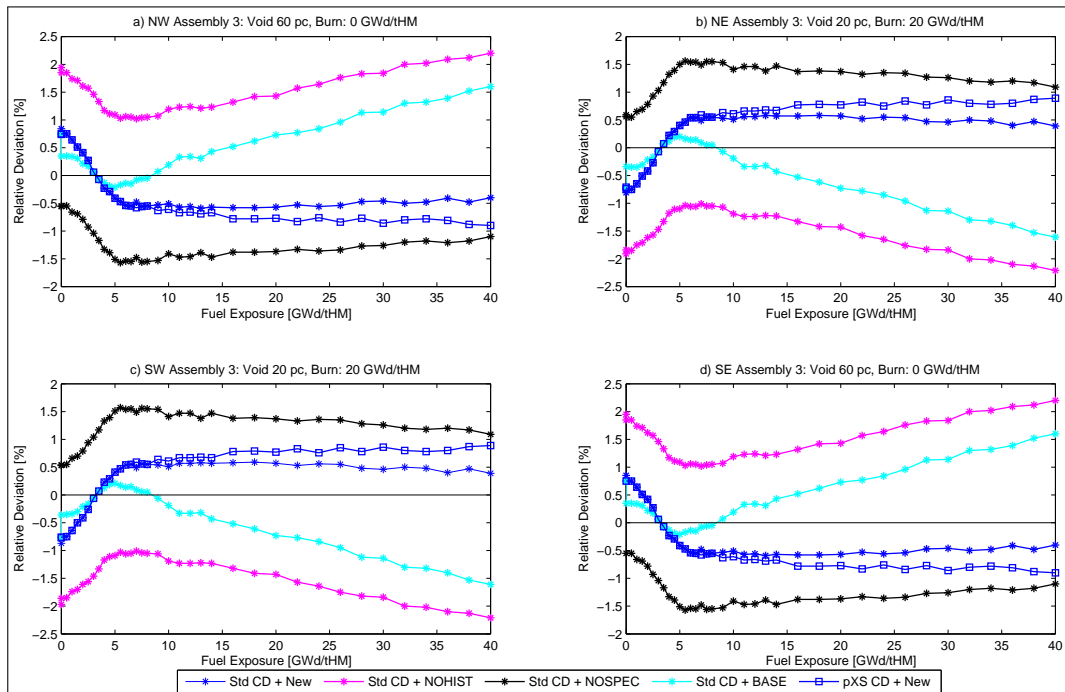


Figure 6.9: Assembly wise deviation in relative node power density for Configuration 3.

6.3.2 Configuration 5

According to Figure 6.10 and compared to Configuration 4 (see Section 6.2.2), similar conclusions can be drawn for Configuration 5 regarding the reactivity and its error behavior. However, the oscillation in the k-effective error is seen to be even larger for this core with a heterogeneous coolant density distribution compared to a corresponding configuration with a homogeneous void distribution due to the increased leakage. Appendix B.4 shows the relative nodal power density deviation profiles which show the combined effect of the behaviors presented in Sections 6.2.2 and 6.3.1.

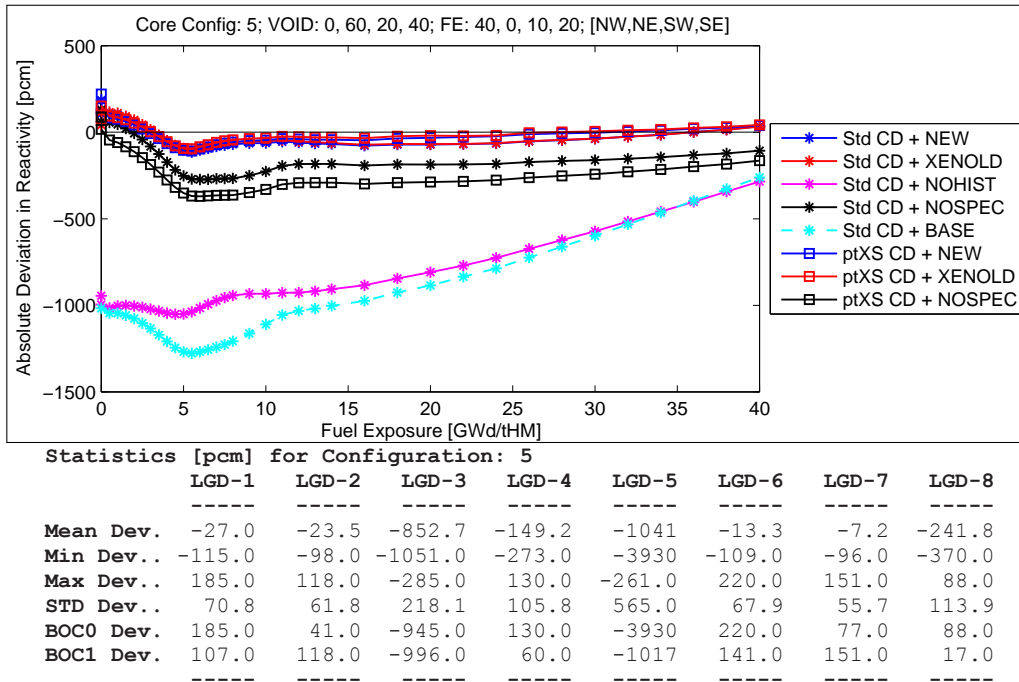


Figure 6.10: Deviation in k-effective for Configuration 5, POLCA7 vs. PHOENIX4.

7

Part C: 3D Mini-Core Studies

IN this section the deviations in k-effective and relative node power density for the different mini-core configurations specified in Section 4.3 using reflective boundary conditions at the top and the bottom edge of the core are presented. The discussion will be limited to the configurations which provide new/support previous conclusions.

7.1 Reflective boundary conditions

7.1.1 Clean Configuration

Configuration 1, having a homogeneous void distribution (i.e. 40% void fraction) with all fresh assemblies running at reference power and fuel temperature condition, is the most trivial¹ configuration for calibration purpose.

The reactivity deviation profiles² are plotted in Figure 7.1³. It can be observed that there is no deviation between the reference and the test solution, except when the old xenon model is used (i.e. XENOLD) which results in the underestimation of the reactivity at BOC by a magnitude of 221 pcm. Additionally, the different interpolation schemes (compare cases running on QQQ and QLL) produce identical results since all these simulations are running on the entry points of the CD-file (i.e. 0, 20, 40 and 60% void fractions are included in the standard CD-file tabulation, see Section 3.1.2). For the same reasons, negligible differences are observed by using different CD-files in these simulations. The macroscopic cross sections and relative node power density are predicted with excellent accuracy when using the current cross section model (not presented in this report).

¹Trivial in the sense that it represents the infinite-medium core condition allowing for a direct comparison of a QA calculation with a corresponding SA calculation.

²All cases running with the standard CD-file have a legend starting with “Std CD” and a marker “*” while cases running with the CD-file employing point microscopic cross sections are represented by “ptXS CD” along with a box marker. The first additional tag (e.g. New, XENOLD, etc.) indicates which calculation option was employed for that particular case while the second tag indicates the type of interpolation scheme used (see Section 3.1.2). All figures include a table that illustrates some basic statistics (i.e. mean deviations, max./min. deviations, standard deviations and BOC deviations) over the depletion range 0-40 MWd/kgHM (i.e. sample size was 37). The “LGD-x” column headers in the table stand for “legend” with the number representing the corresponding legends in the figure counting from top to bottom (e.g. LGD-4 represents “Std CD + XENOLD QLL”).

³Title of the figure is defined as follows: configuration number for identification purpose; and assembly wise

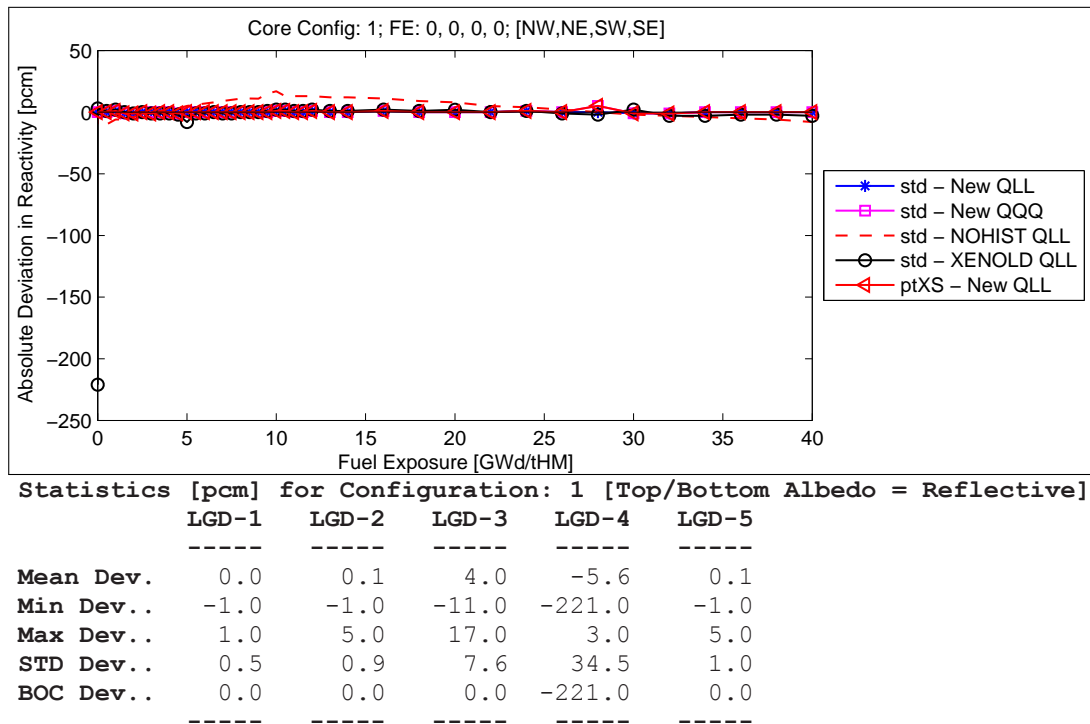


Figure 7.1: Deviation in k-infinity for Configuration 1 (reflective axial boundary conditions).

7.1.2 Configuration 3 with assembly-wise homogeneous void distribution

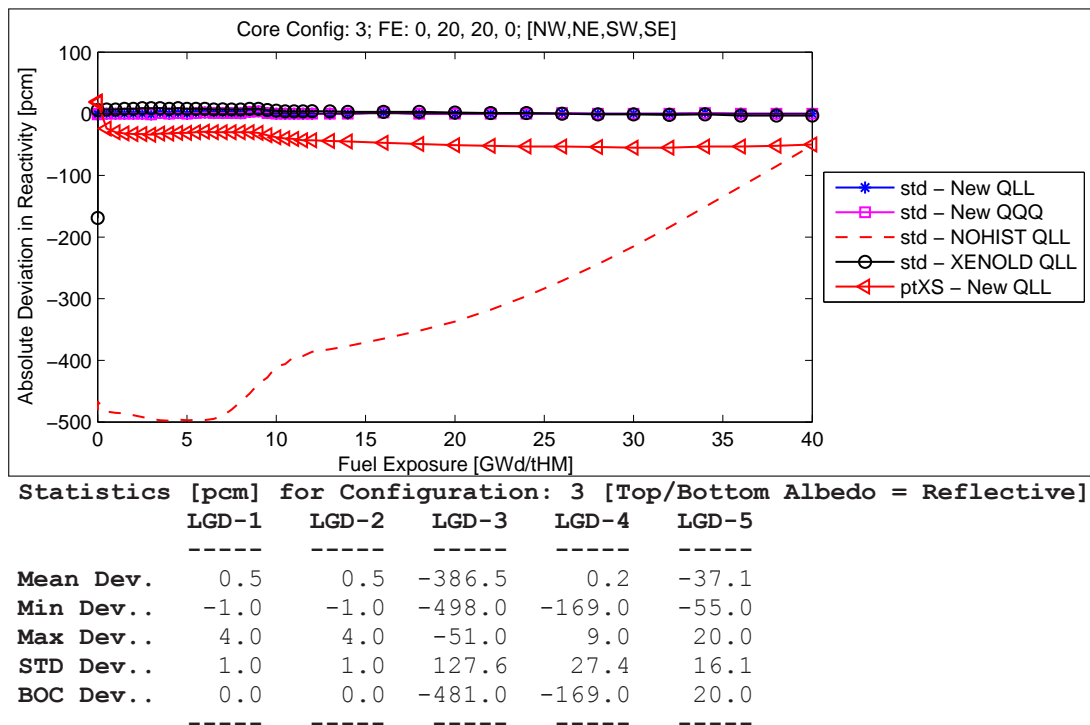


Figure 7.2: Deviation in k-infinity for Configuration 3 (reflective axial boundary conditions).

fuel exposure at BOC.

Configuration 3 constitutes of assemblies with two different fuel compositions (i.e. different burn-up at BOC, cycle two) are utilized in a checkerboard setup (see Section 4.3) using reflective axial boundary conditions and assembly-wise different void conditions (but axially homogeneous) of 20 and 60% for the fresh and depleted assemblies, respectively. The reactivity deviation profiles for the different cases are plotted in Figure 7.2 which shows no deviation between the reference and the test solutions when using the current cross section model with the standard CD-file. Since the test core is running on entry points of the CD-file, the use of different interpolation schemes is of no consequence.

The case utilizing NOHIST calculation option (i.e. isotopic depletion model bypassed) results in an underestimation of reactivity throughout the entire depletion range, having a worth at 386 pcm in average (see the table associated with Figure 7.2). This is in accordance with Ref. [8] which demonstrates the importance of having an isotopic history model following core shuffling with different void conditions. This is due to the fact that there is a change in the coolant density history condition between the first and second cycle, i.e. going from a 40% void history (axially homogeneous) to either a 20% or 60% void history. Considering the history state at BOC of cycle 2, due to the fact that the base depletion calculation assumes a constant coolant density and a prehistory corresponding to the prevailing coolant density, i.e. 20% or 60% void history, cross sections are corrected for the contribution of a 40% void history in cycle one, i.e. $\Delta N = N(40\%) - N_{base}(60\%)$.

The use of the XENOLD option results in the underestimation of the reactivity at BOC by 169 pcm, which is also in accordance to previous findings. The macroscopic cross sections, spectrum index and the relative nodal power density are predicted with excellent accuracy using the current cross section model (results not presented in this report).

7.1.3 Configurations 2, 4 & 5 with axially heterogeneous void distribution

Configurations 2, 4 and 5 constitute cases with axial void profiles (see Section 4.3.1) for each individual assembly. Configuration 2 is a setup using fresh assemblies only, while Configuration 4 and 5 are loaded with fuels having different burn-ups (see Section 4.3). The reactivity deviation profiles for these configurations using reflective boundary condition at the top and bottom edge of the core are plotted in Figure 7.3, 7.9 and 7.13, respectively.

7.1.3.1 Configuration 2

As can be seen from the table associated with Figure 7.3, the BOC reactivity (i.e. zero xenon state) is best predicted by the current xenon model (compare LGD-1 vs. LGD-4)). The most prominent behavior of the reactivity deviation profiles is the observed oscillation during BA depletion, which has a peak-to-peak amplitude of 540 pcm for the case using the current cross section model (see min./max. deviation in the table associated with Figure 7.3). This is due to the fact that the coolant density table entry values employed in the PHOENIX4 lattice physics calculations while preparing the cell data files cover up to the range of 60% void fraction (see Section 3.1.2) whereas the upper parts of the core reach a void of 80%. Consequently, extrapolated cross section data is used by POLCA7 in this core region. The magnitude of this extrapolation error for Σ_{a1} , Σ_{a2} , Σ_{f1} and Σ_{f2} using the current cross section model with the standard CD-file can be seen in Figure 7.4⁴, 7.5⁴, 7.6⁴ and 7.7⁴ respectively. Nodes 9 and 10 are at 80% void

⁴Each sub-plot represents the individual assemblies in the mini-core (i.e. northwest, northeast, southwest and southeast). The tile of each sub-plot contains the configuration number for identification purpose; identification tag for the assembly location; and assembly wise fuel exposure at BOC.

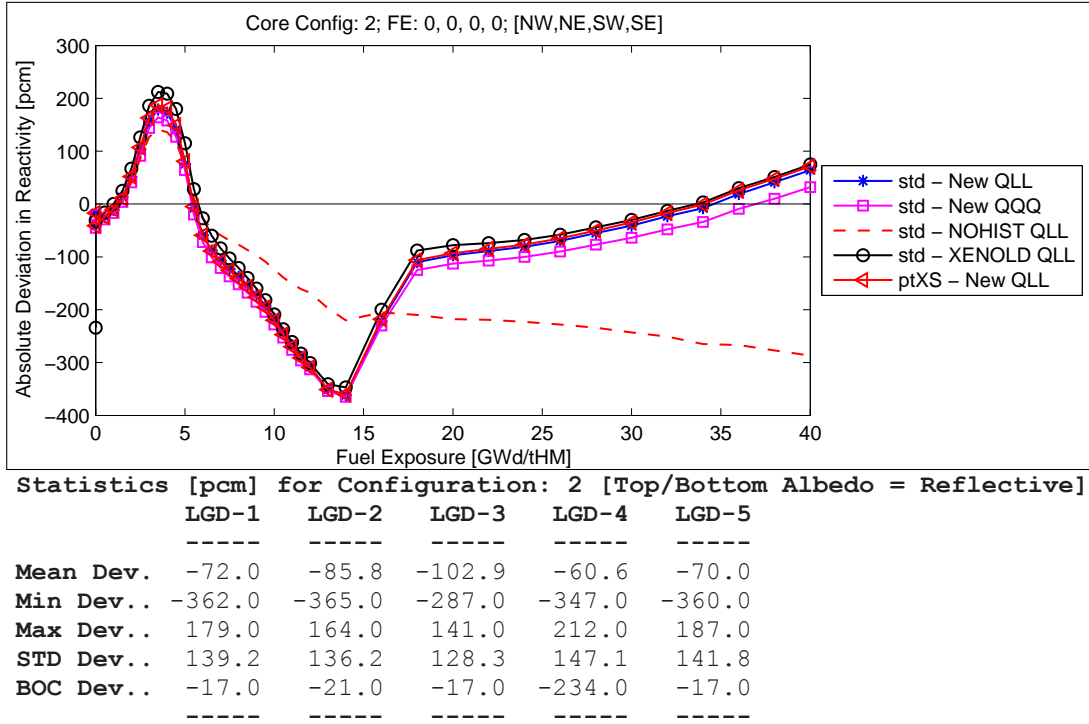


Figure 7.3: Deviation in k-infinity for Configuration 2 (reflective axial boundary conditions).

fraction while nodes 8 and 7 are at 70% void fraction (see Section 4.3.1) thereby resulting in the distinctive jumps in the predicted deviation profiles (i.e. the extrapolation error becomes larger at a higher void fraction). This results in a harder spectrum at the top of the core at BOC compared to the fine-mesh reference solution (i.e. spectrum index (Φ_2/Φ_1) is underestimated for the nodes subject to extrapolation, see Appendix C.2).

The thermal absorption (fission) cross section deviation profile in Figure 7.5 (Figure 7.7) shows a sudden drop (rise) in the magnitude of error in the burn-up interval of 15 – 20 MWd/kgHM (for the nodes subject to extrapolation) due to an incorrect depletion of BA (mainly caused by an imbalance in the complex interplay between spectrum variations i.e. spectrum softening in the fresh bundle and BA depletion). A support for this hypothesis will be given in Section 7.1.3.2, in conjunction with the evaluation of configurations with different BA concentration.

The use of QQQ has no notable improvements on the accuracy of cross section (plots for these cases are not presented in this report due to this reason) and concur with the results in Figure 7.3 (i.e. reactivity deviation profiles for both QQQ and QLL are identical and only diverge (slightly) after the burn-up point of 15 MWd/kgHM). This is because QLL (i.e. a linear extrapolation scheme for coolant density and coolant density history) is enforced for the high void nodes.

The relative node power density profile in Appendix C.3 illustrates that the top of the core is producing less power at BOC compared to the bottom of the core due to the higher void fraction at the top of the core (to encourage plutonium build-up). However, in due time and with irradiation of the fuel, power at the top of the core increases successively due to depletion of BA and an increased buildup of Pu-239 (as a consequence of increased void which encourages

plutonium build-up and slows down the depletion of BA in the upper part of the core).

The relative node power density deviation profile in Figure 7.8 shows that starting at BOC and during the BA depletion regime, the power at the top of the core is being underestimated compared to the reference solution due to extrapolation errors which makes the spectrum too hard compared to the reference solution and the depletion of BA slows down. As a consequence, the bottom of the core has to provide more power to compensate for this error thereby leading to a tilt in the power distribution. This also leads successively to increased build-up of Pu-239 causing the power to be overestimated at the top edge of the core once BA has been depleted out after 20 MWd/kgHM.

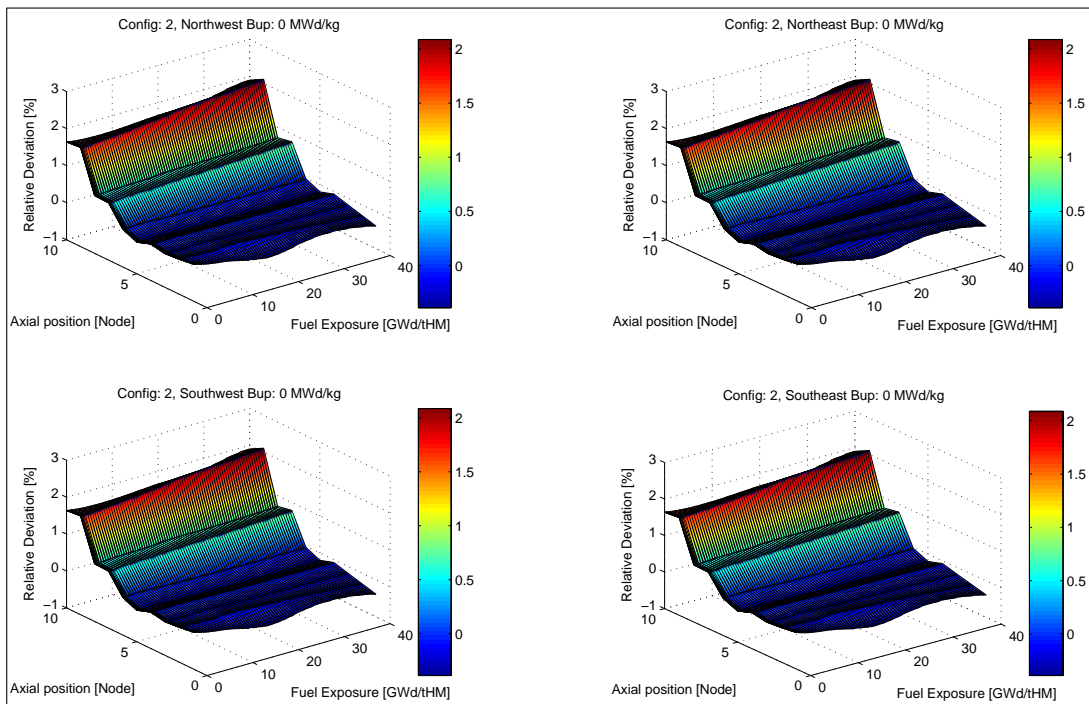


Figure 7.4: Assembly wise deviation in Σ_{a1} for Configuration 2 (reflective axial boundary conditions).

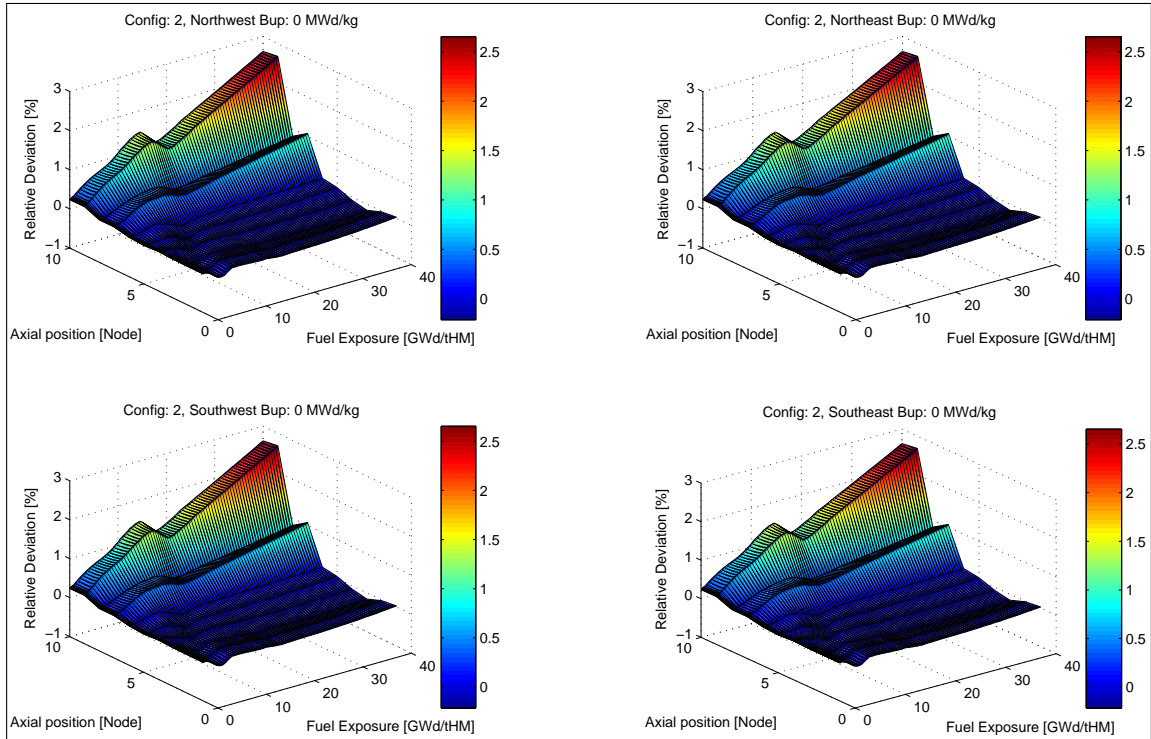


Figure 7.5: Assembly wise deviation in Σ_{a2} for Configuration 2 (reflective axial boundary conditions).

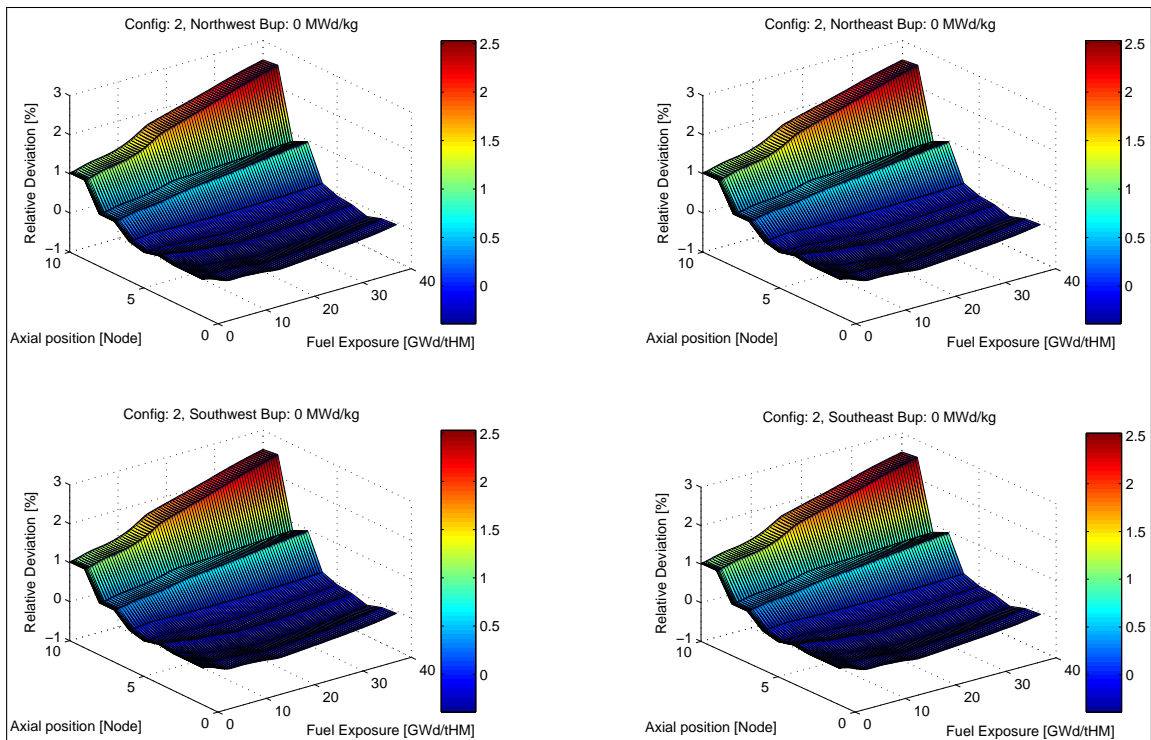


Figure 7.6: Assembly wise deviation in Σ_{f1} for Configuration 2 (reflective axial boundary conditions).

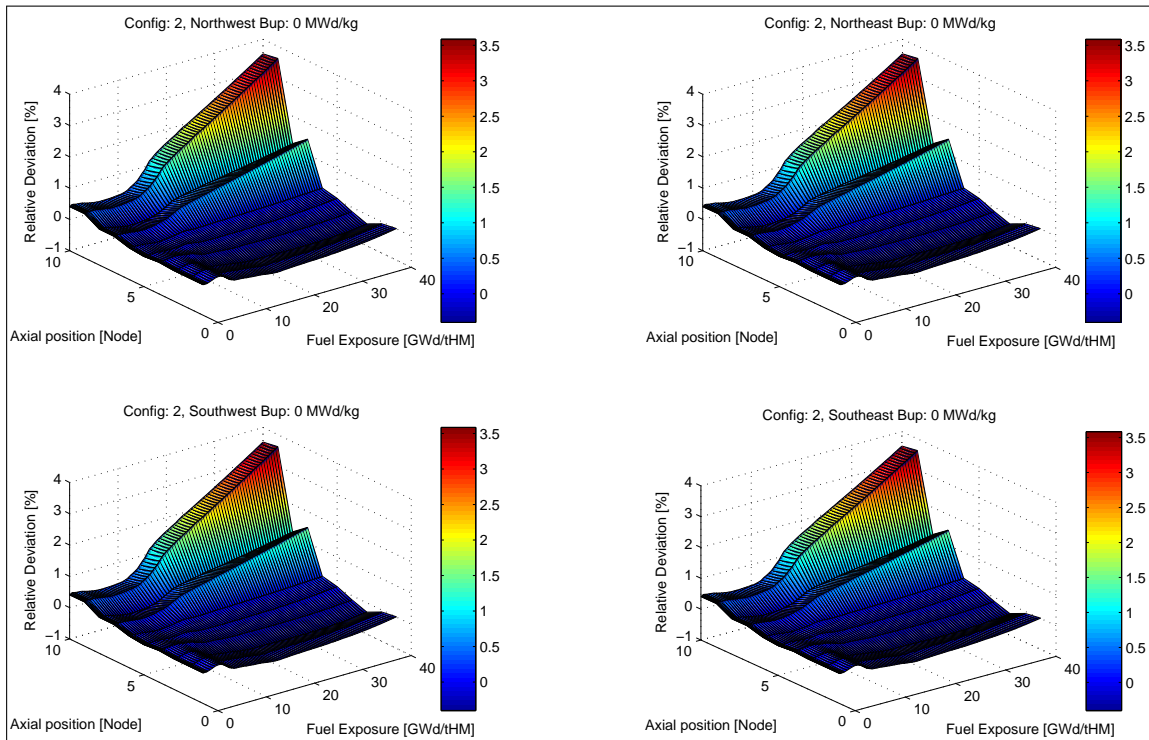


Figure 7.7: Assembly wise deviation in Σ_{f2} for Configuration 2 (reflective axial boundary conditions).

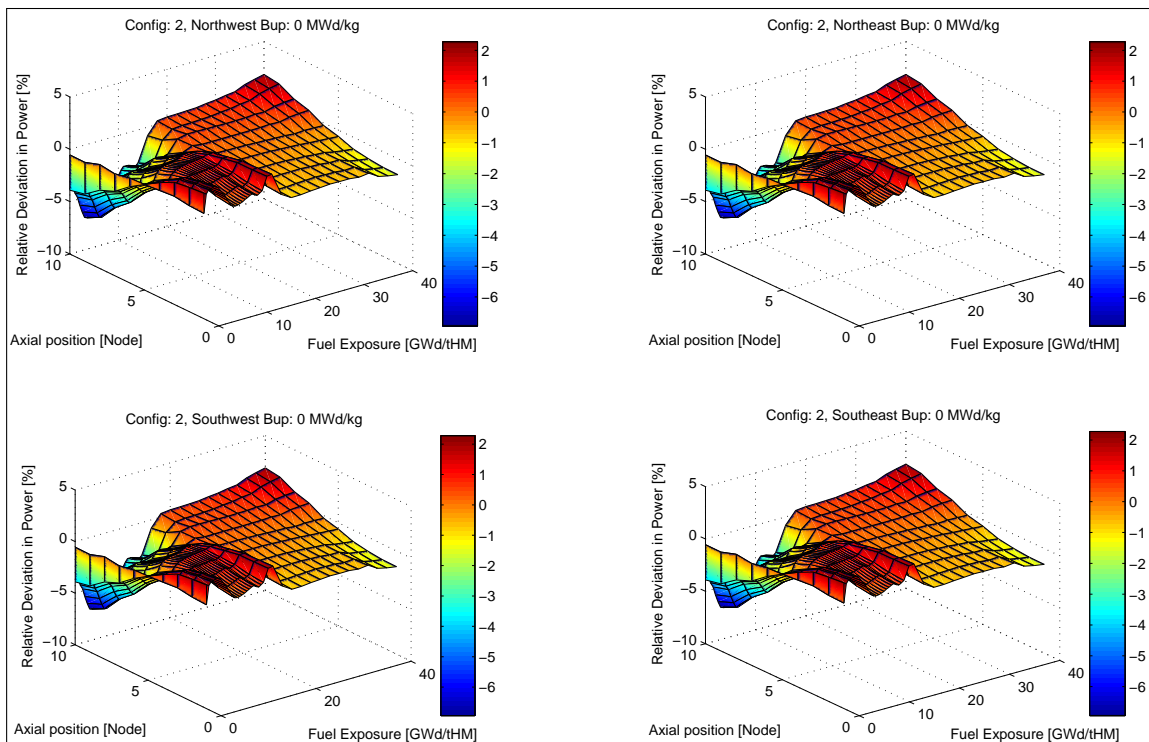


Figure 7.8: Assembly wise deviation in relative nodal power density profile for Configuration 2 (reflective axial boundary conditions).

7.1.3.2 Configuration 4

Likewise observed for the previous configurations, superior performance is obtained with the current xenon feedback model (Equation 2.3) at BOC compared to the old xenon implementation (compare BOC deviation for “std – NEW QLL” and “std – XENOLD QLL” in the table associated with Figure 7.9). In addition, for reasons mentioned in Section 7.1.2, the isotopic history model plays an important role in providing accurate results at the BOC, as is evident from the large under-prediction in the reactivity by the case utilizing NOHIST (see the table associated with Figure 7.9).

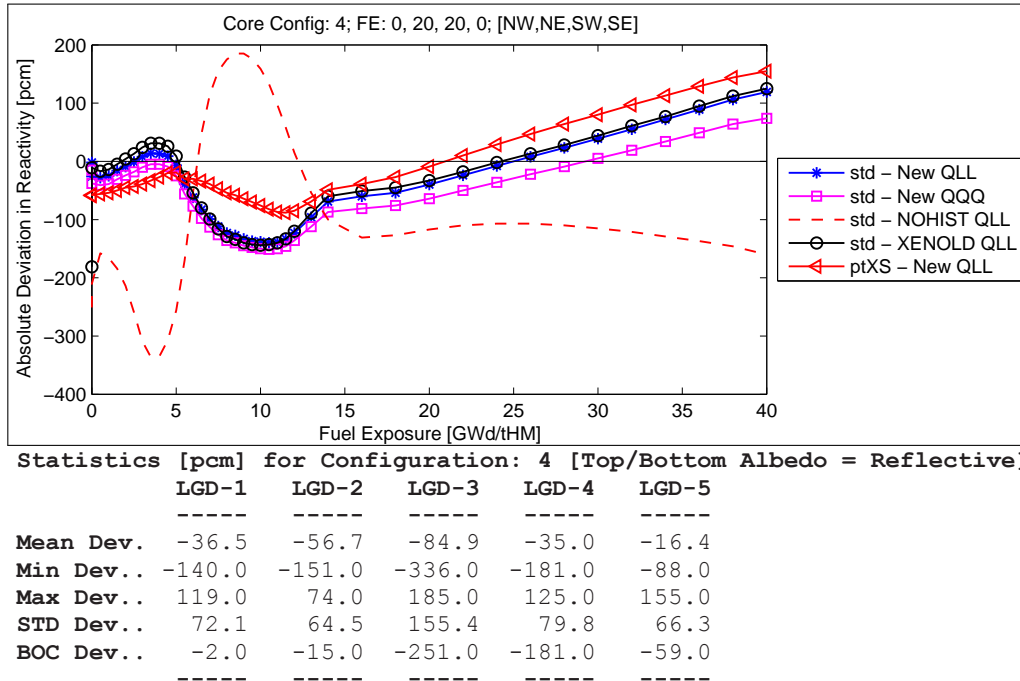


Figure 7.9: Deviation in k-infinity for Configuration 4 (reflective axial boundary conditions).

A similar oscillation that was seen for Configuration 2 may also be observed in the reactivity deviation profiles for Configuration 4, but with a smaller peak-to-peak amplitude around 180 pcm. This is due to the following reasons,

1. The magnitude of the extrapolation error in the cross sections for the already depleted assemblies in Configuration 4 is much more subtle compared to Configuration 3 at BOC or otherwise, as seen⁵ in Figure 7.11 and 7.12 (i.e. NE and SW shows smaller deviation in cross sections compared to Configuration 2 as seen in Figure 7.4-7.7). This is due to the fact that the top nodes of the already depleted assemblies in Configuration 4 (node 10, 9 and 8) are at 70% void fraction whereas the fresh assemblies have 80% void fraction for node 10 and 9. This means that in total, four nodes are subject to 8% void fraction while ten nodes are subject to 70% void fraction in Configuration 4. In contrast, Configuration 2 has eight nodes at 80% void fraction while eight nodes at 70% void fraction. Hence, compared to Configuration 2, the error in the cross sections due to extrapolation is considerably less.
2. Only two out of four assemblies have BA. Hence the oscillation in the thermal cross section deviation profiles observed in Section 7.1.3.1 is only present in the two fresh assemblies in

⁵Plots for epithermal cross sections is located in Appendix C.5 and C.6.

Configuration 4 (see Figure 7.11 and 7.12).

In order to provide support for the hypothesis that an incorrect depletion of BA is the main cause of the observed oscillation in thermal cross section deviation profiles, Configuration 4 was executed using a specially built CD-file which had no BA pins. The results, as shown in Figure 7.10, show no oscillation in the reactivity deviation profiles, thereby confirming the hypothesis. Furthermore, it may be observed that the core-wise worth of the extrapolation is -20 pcm at BOC with an average worth of -36 pcm using the current best-estimate cross section model during the cycle depletion range of 0-40 MWd/kgHM. In contrast, Configuration 2 records -60 pcm of worth at BOC with an average worth of -91 pcm due to increased void fraction. This implies that the extrapolation error is problematic only when BA is present in the core due to its sensitivity to local spectrum conditions.

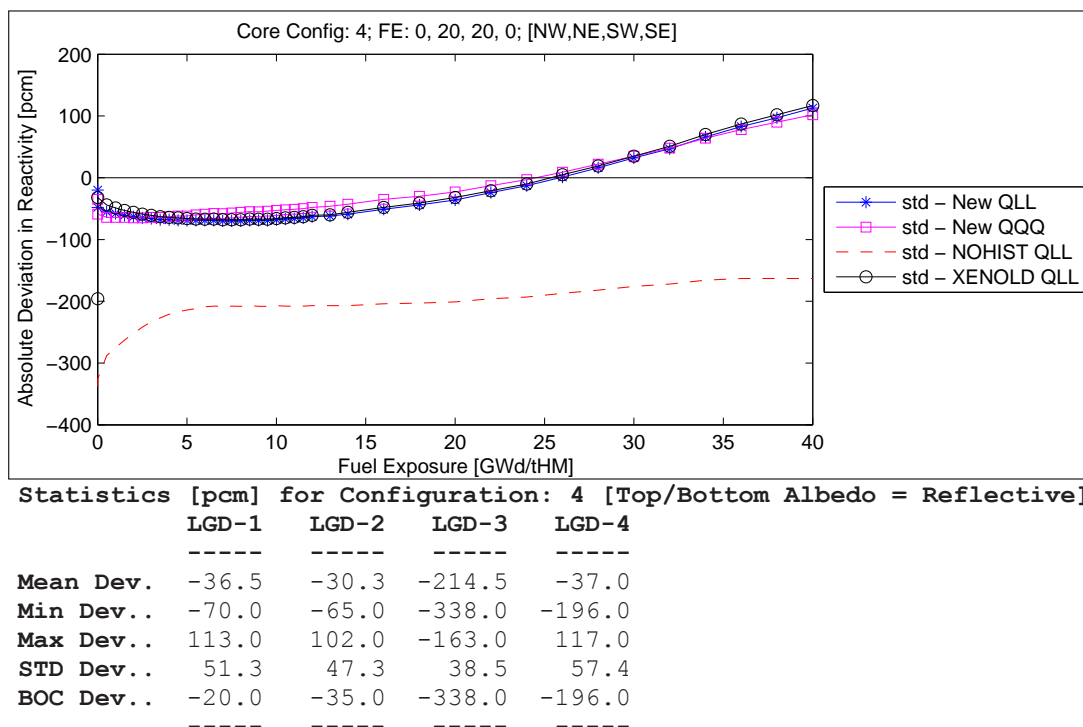


Figure 7.10: Deviation in k-infinity for Configuration 4 (reflective axial boundary conditions **without gadolinium**).

Appendix C.7 shows the relative nodal power density profile, while the deviation in relative nodal power density profile is presented in Appendix C.8. Both trends are similar to that seen for Configuration 2 but with lower magnitude of oscillation due to the reasons mentioned in the previous paragraphs.

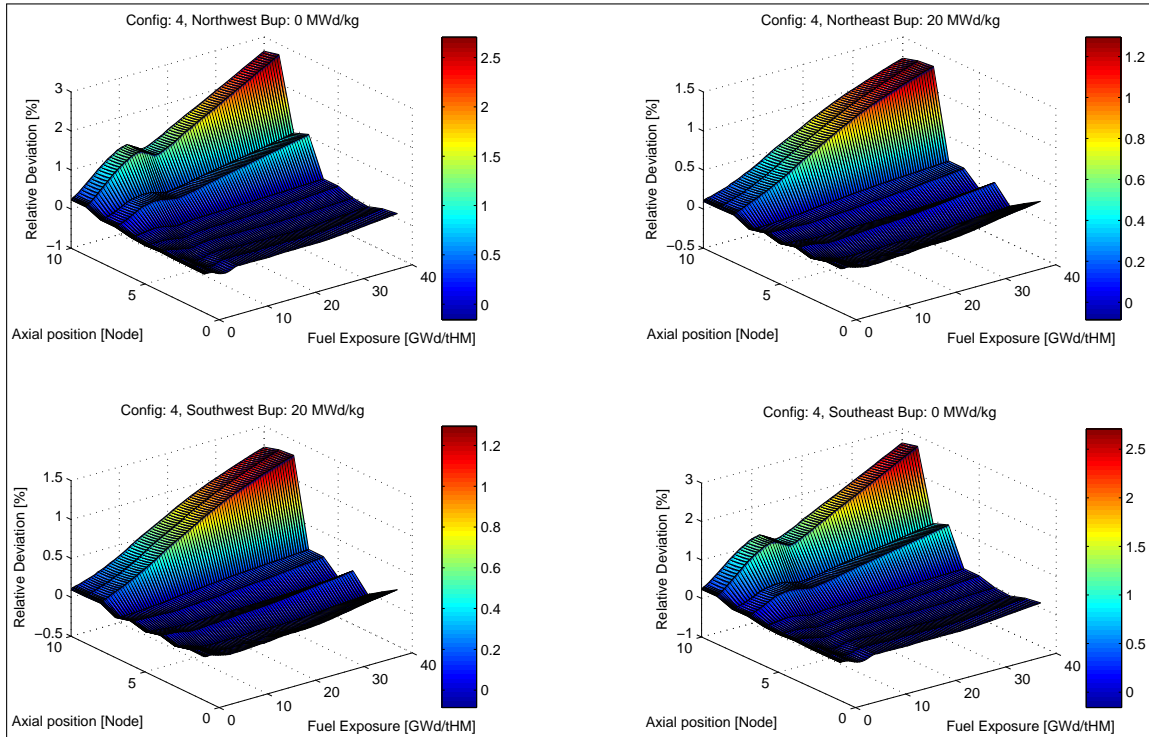


Figure 7.11: Assembly wise deviation in Σ_{a2} for Configuration 3 (reflective axial boundary conditions).

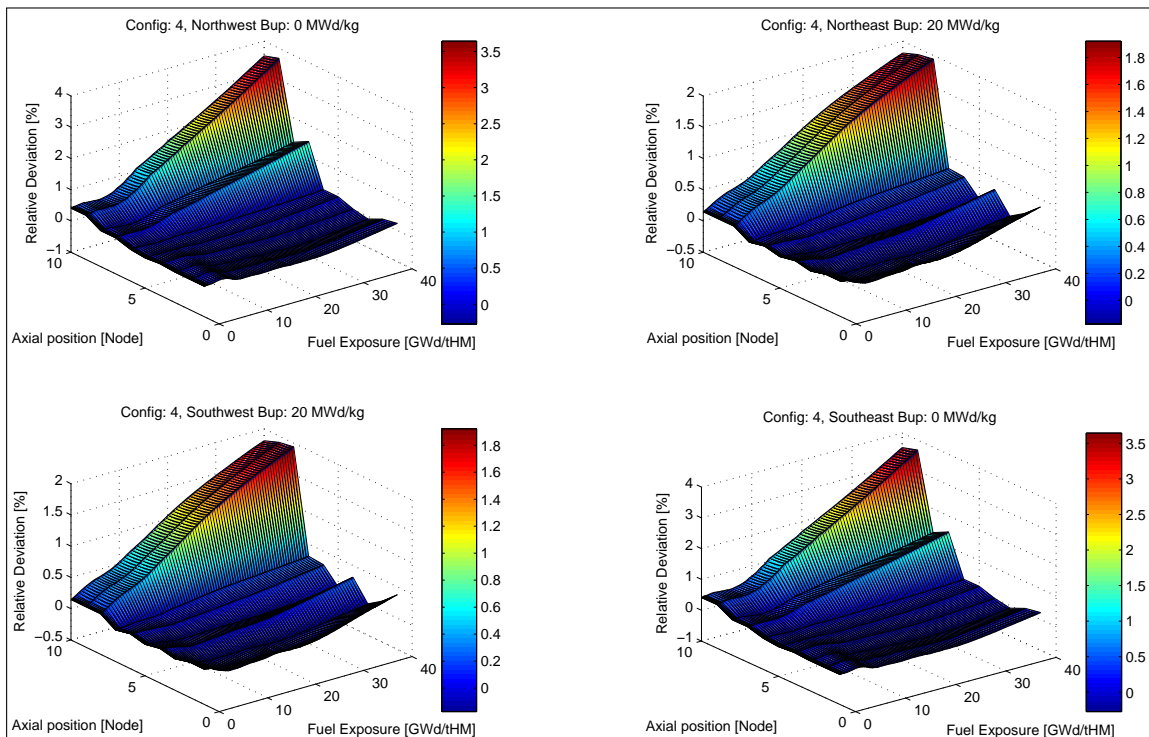


Figure 7.12: Assembly wise deviation in Σ_{f2} for Configuration 4 (reflective axial boundary conditions).

7.1.3.3 Configuration 5

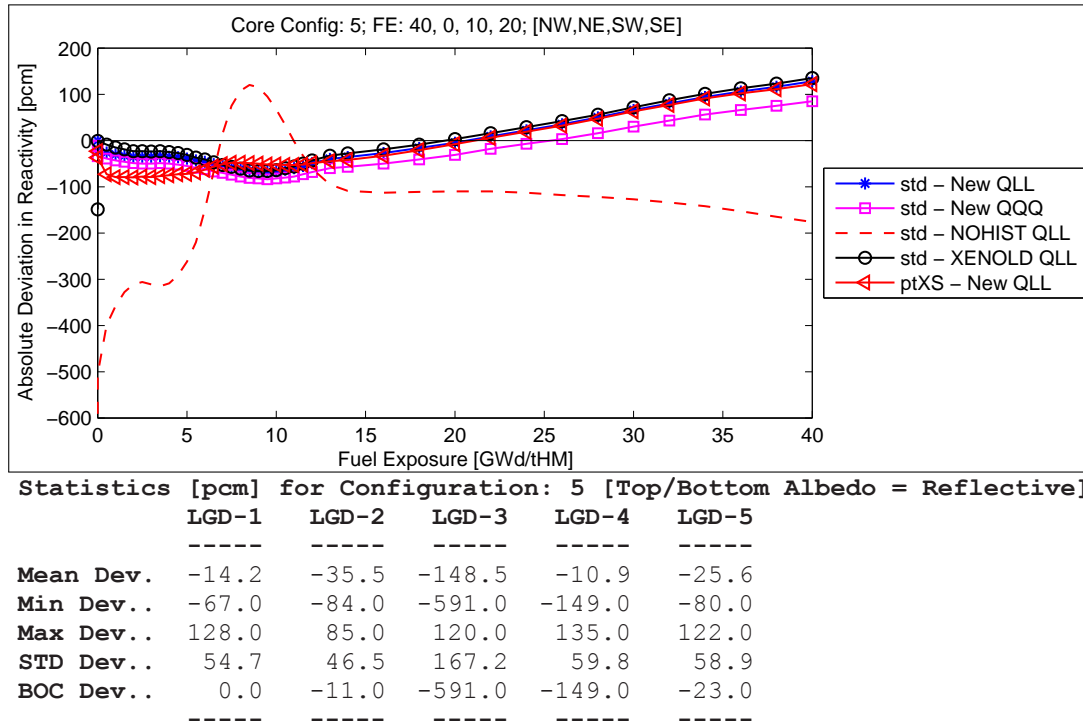


Figure 7.13: Deviation in k-infinity for Configuration 5 (reflective axial boundary conditions).

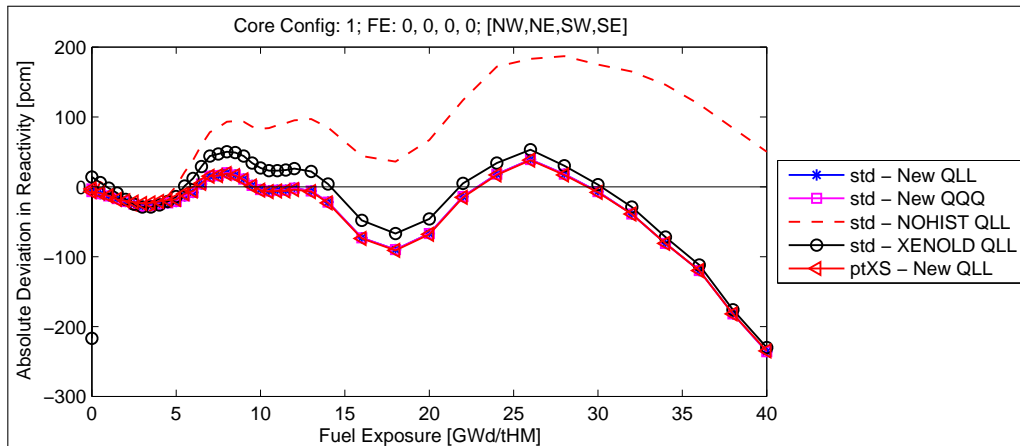
In accordance with the conclusions made for Configuration 4, the oscillation in reactivity is almost non-existent due to the fact that there is only one assembly with full inventory of BA and also because less nodes are subjected to extrapolation errors (i.e. only three nodes are subjected to 80% void while nine nodes are subjected to 70% void conditions).

These results are consistent with the conclusions drawn at the end of Section 7.1.3.2 as the error in k-effective seems also to approach asymptotically the error behavior obtained for the BA-free core presented in Figure 7.10, thereby confirming the previous statement that the presence of BA is the main cause of deviation in reactivity profile.

7.2 Black boundary conditions

In this section the absolute deviations in k -effective and relative node power density of the different mini-core configurations specified in Section 4.3 are presented using black boundary conditions at the top and bottom edge of the core by setting the albedo to zero.

7.2.1 Clean Configuration 1



Statistics [pcm] for Configuration: 1 [Top/Bottom Albedo = Zero]

	LGD-1	LGD-2	LGD-3	LGD-4	LGD-5
Mean Dev.	-25.4	-25.4	63.9	-13.8	-25.1
Min Dev..	-236.0	-236.0	-37.0	-230.0	-235.0
Max Dev..	39.0	39.0	187.0	53.0	38.0
STD Dev..	53.0	53.0	65.2	66.4	52.8
BOC Dev..	-3.0	-3.0	-3.0	-217.0	-3.0

Figure 7.14: Deviation in k -infinity for Configuration 1 (black boundary conditions).

Setting the top and bottom boundary albedo to zero for Configuration 1 results in oscillations in the reactivity deviation profiles as observed in Figure 7.14 due to the truncation errors of using a coarse mesh. Consequently, the nodes at the top and bottom will obtain a harder local spectrum compared to the fine-mesh reference solutions during the depletion of BA. After BA has been depleted out, the local spectrum at the top/bottom of the core becomes increasingly softer (see Figure 7.15).

The reason for this shift in the spectrum at the top and the bottom nodes (nodes 10 and 1 respectively) is that when a coarse mesh is used, the flux gradient at the top and bottom of the core is incorrectly predicted compared to the fine-mesh reference solution at BOC (i.e. incorrect axial leakage is computed due to truncation from the use of the coarse mesh) leading to a harder spectrum compared to the fine-mesh solution during the depletion of BA. This hardening of the spectrum causes the epithermal (thermal) reaction rate to increase (decrease) slightly at BOC since less migration increases the resonance absorption and Pu-239 build-up. As a consequence, a dip in reactivity deviation profile during the depletion range of 2-5 MWd/kgHM is observed after which the increased production of Pu-239 and fast depletion of U-235 (due to rapid removal of BA contents) cause the reactivity to increase again.

Once BA is depleted out, the spectrum becomes increasingly softer compared to the reference

solution due to the incorrect axial leakage, thereby causing a rapid depletion of U-235 and Pu-239 at the top/bottom of the core compared to the reference solutions (i.e. recall that there is already excess Pu-239 at the top/bottom due to the spectrum hardening during the BA depletion region). This results in the second oscillation in reactivity deviation profiles during the depletion range of 15-40 MWd/kgHM seen in Figure 7.14.

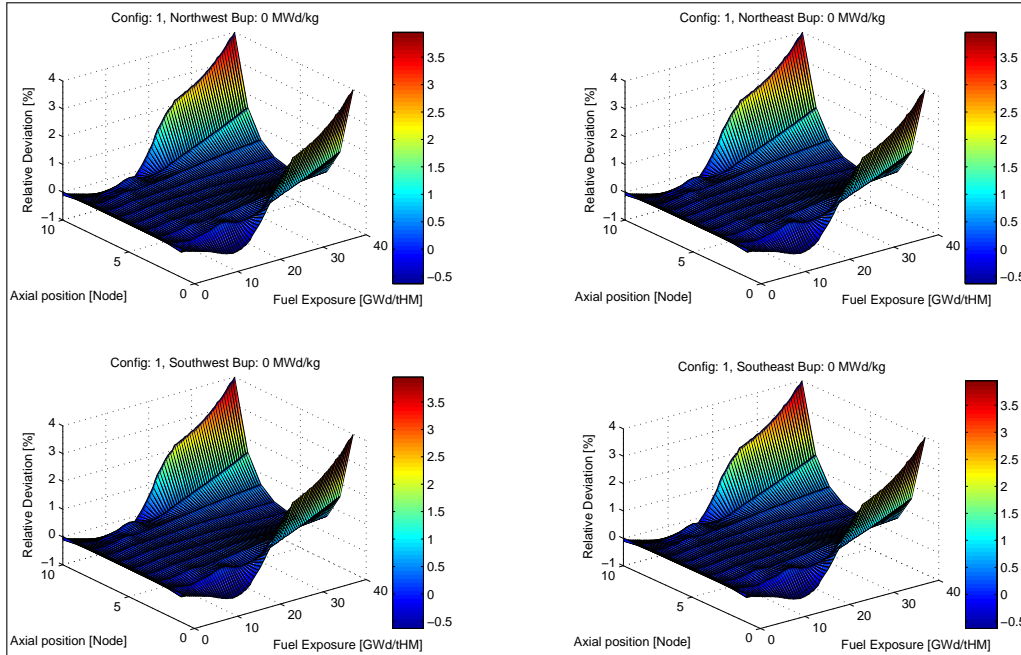


Figure 7.15: Assembly wise deviation in spectrum index for Configuration 1 (black boundary conditions).

Considering the same core without BA, like the one that was especially constructed in Section 7.1.3.2, the oscillations seen in Figure 7.15 are no longer present (see Figure 7.16) due to the fact that the local spectrum at the top/bottom edge of the core starts to become increasingly softer from BOC. This translates to a slower rate of production of Pu-239 and hence the reactivity is increasingly underestimated with burn-up (i.e. diverges from the reference solution with depletion), reaching as much as - 482 pcm of deviation at 40 MWd/kgHM. In other words, the error due to incorrect depletion of BA actually counteracts the error due to incorrect axial leakage which results in a smaller deviation at higher fuel exposure (compare Figure 7.15 with Figure 7.16). It can also be seen that deactivating the history model results in better prediction of reactivity in the BA-free case. The reason of obtaining worse results using the isotopic history model is that the spectrum-induced changes in microscopic cross sections are not accounted for in the current history model (as explained in Parts A and B), which results in an accumulation of errors with depletion.

The relative node power density profile is what one would expect from a core with the boundary albedo set to zero (i.e. the power at the top/bottom edge of the core is almost zero; see Appendix C.1). The relative node power density deviation profiles in Figure 7.17 are in accordance with the conclusions made regarding reactivity, i.e. power at the top/bottom being underestimated during the BA depletion period (0- 15 MWd/kgHM) due a too hard local spectrum at these core locations leading to an overestimated inventory of Pu-239. Once the spectrum becomes softer, an overestimation in the power output during the depletion period

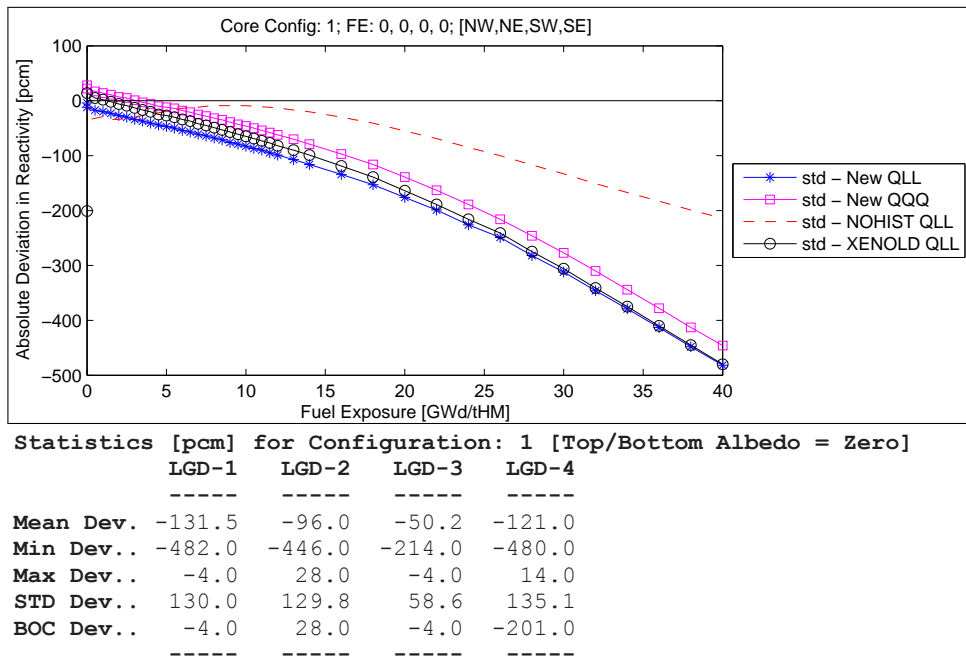


Figure 7.16: Deviation in k -infinity for Configuration 1 (black boundary conditions **without** gadolinium).

of 15-25 MWd/kgHM is observed due to a softer spectrum leading to a faster depletion of U-235 and Pu-239. As a consequence of this rapid depletion, the power production from the top/bottom of the core starts to decrease after 25 MWd/kgHM which leads to an overestimation of node power in the center of the core.

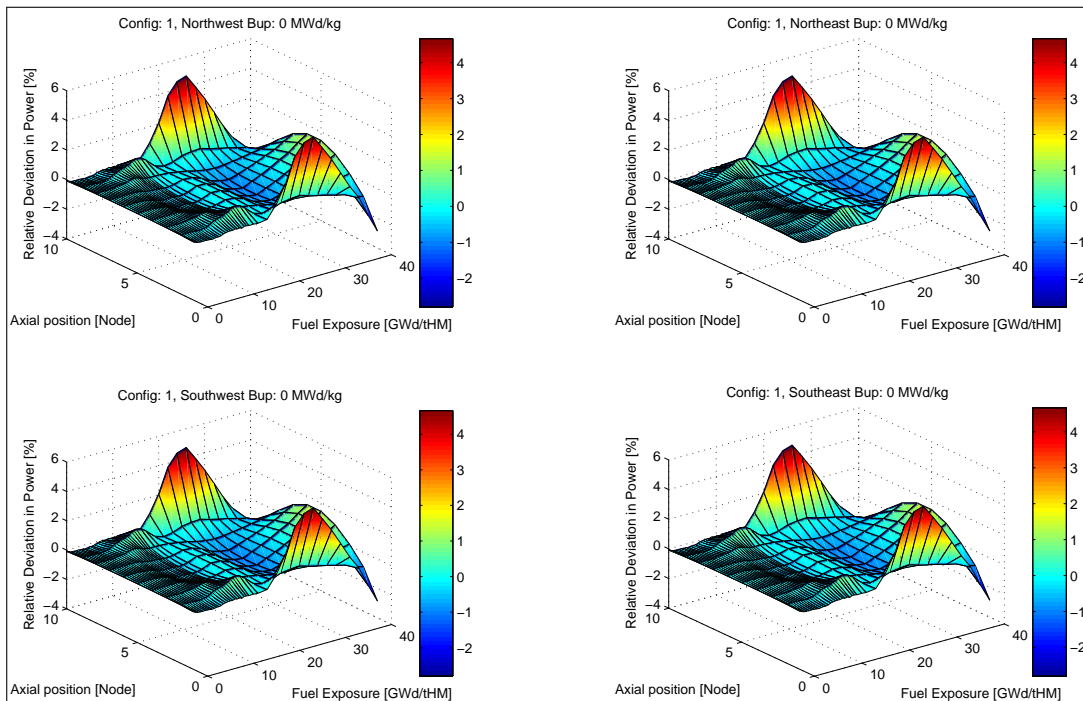


Figure 7.17: Assembly wise deviation in relative nodal power density profile for Configuration 1 (black boundary conditions).

7.2.2 Configuration 3 with assembly-wise homogeneous void distribution

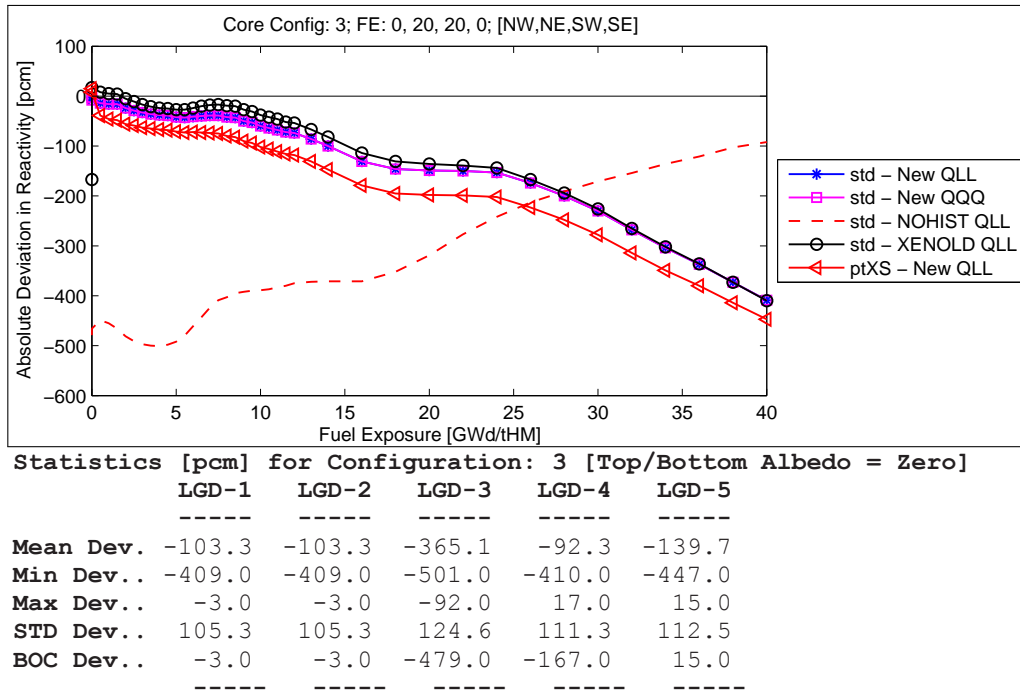


Figure 7.18: Deviation in k -infinity for Configuration 3 (black boundary conditions).

Setting the top and bottom albedo at zero (black boundary flux condition) in Configuration 3 results in more subtle oscillations in the reactivity deviation profiles (see Figure 7.18) compared to Configuration 1 in Figure 7.14. Instead, the deviation profiles bear more resemblance to BA-free core implementation of Configuration 1 in Figure 7.14. This is due to the fact that the amount of BA in the core has been halved in Configuration 3 (i.e. two out of four assemblies are fresh and have BA) compared to Configuration 1. Hence, the local spectrum at the top/bottom of the core for the depleted assemblies does not oscillate⁶ for the NE and SW assemblies (compare the NW assembly with the NE in Figure 7.19). These results are consistent with the results of the previous section and are further confirmed by comparing the deviation in relative node power distribution as presented in Figure 7.20, which shows that the power from the top/bottom of the already depleted assemblies is increasingly underestimated with depletion instead of oscillating. This is also in accordance with the conclusion drawn in Section 7.2.1.

⁶Recall that this oscillation is inducing the oscillation in the reactivity deviation profile.

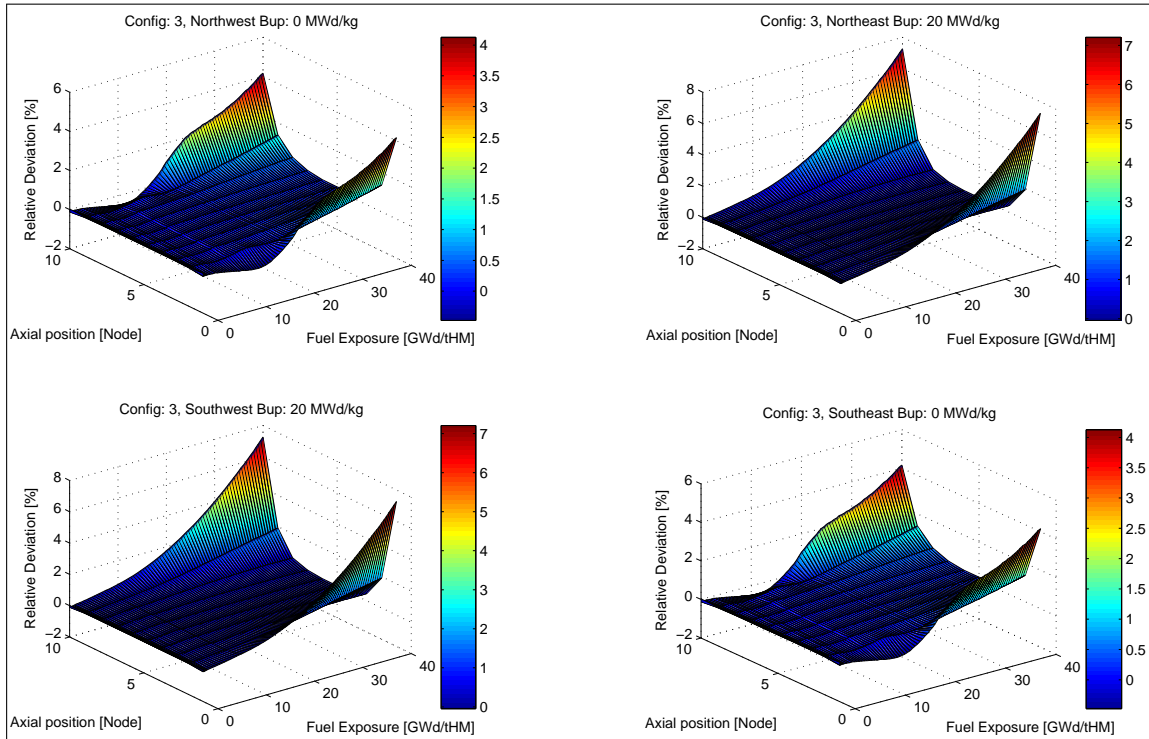


Figure 7.19: Assembly wise deviation in spectrum index for Configuration 3 (black boundary conditions).

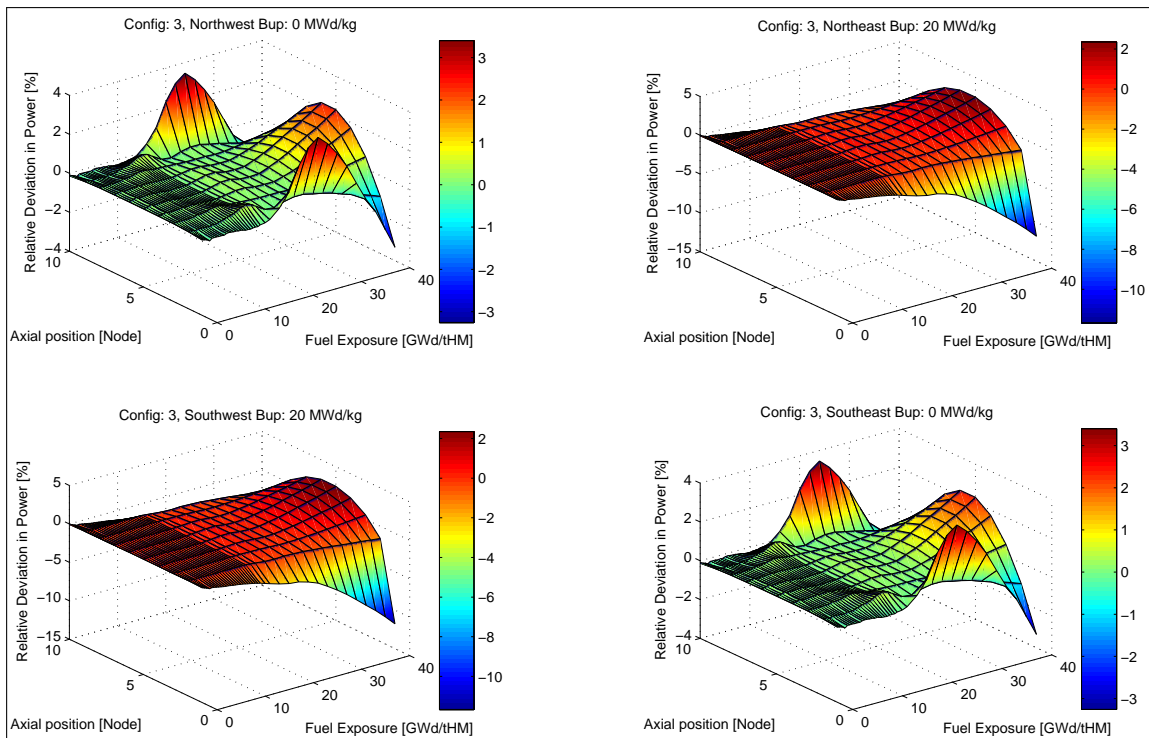
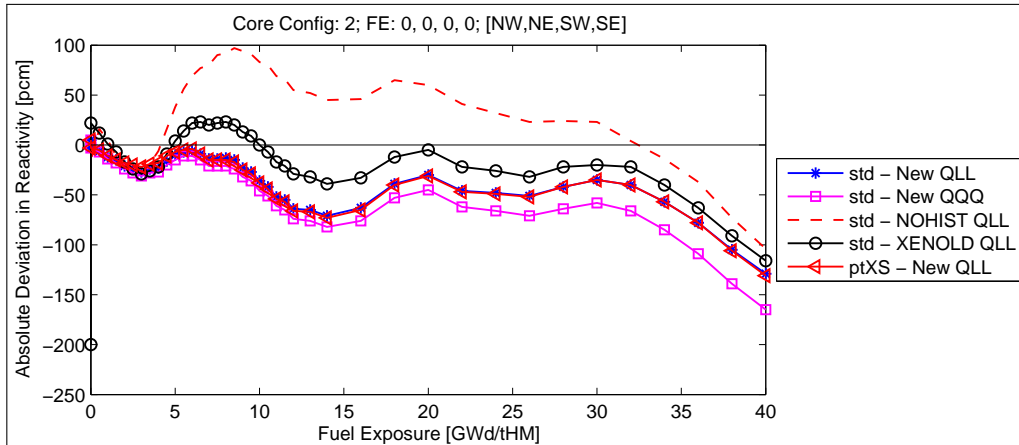


Figure 7.20: Assembly wise deviation in relative nodal power density profile for Configuration 3 (black boundary conditions).

7.2.3 Configuration 2, 4 & 5 with axially heterogeneous of void distribution

Configuration 2, 4 and 5 constitute cases with axial void profiles imposed (see Section 4.3.1) for each individual assembly (see Section 4.3) using black boundary conditions at the top/bottom edges of the core.

7.2.3.1 Configuration 2



Statistics [pcm] for Configuration: 2 [Top/Bottom Albedo = Zero]

	LGD-1	LGD-2	LGD-3	LGD-4	LGD-5
Mean Dev.	-35.4	-46.7	30.2	-19.0	-35.4
Min Dev..	-129.0	-165.0	-104.0	-200.0	-131.0
Max Dev..	5.0	5.0	97.0	23.0	5.0
STD Dev..	28.1	36.1	48.2	41.4	29.1
BOC Dev..	5.0	5.0	5.0	-200.0	5.0

Figure 7.21: Deviation in k-infinity for Configuration 2 (black boundary conditions).

When comparing reactivity deviation profiles for Configuration 2 (Figure 7.21) to Configuration 1 (Figure 7.14), similar configuration but with homogeneous axial void profile, one will notice that the differences between these plots are very small (i.e. differences only seen at high fuel exposure after BA has depleted out). This is in contrast to what was seen in Section 7.1.1 and 7.1.3 (i.e. reflective boundary conditions at the top/bottom edge of the core) where a large oscillation was observed during the BA depletion. Recall from Section 7.1.3 that the predicted spectrum was seen to be too hard compared to the reference values due to the extrapolation error in the cross sections, and that the opposite was observed in Section 7.2.1 where the spectrum was too soft compared to the reference solution (after BA was depleted out) with depletion due to an incorrect axial leakage in the coarse mesh solution. Since the underlining cause of both these errors exist in this configuration (i.e. conditions instigating the two errors are present in this configuration, namely extrapolation at the top of the core and black boundary conditions), an error amplification occurs during the BA depletion burn-up regime followed by an error cancellation after the BA was depleted out. However, it is evident from the similarities in the reactivity deviation profiles during the BA burn-up regime between Configuration 1 and 2 (Figure 7.14 and 7.21, both having black boundary conditions) that the impact of an incorrect axial flux leakage profile is the dominating error out of the two. However, since the two errors are opposite to each other after the BA depletion burn-up regime, an error cancellation occurs, thereby minimizing the error in the predicted reactivity for high fuel exposure. Hence, due

to this error cancellation, the minimum deviation in reactivity reached for Configuration 2 is -129 pcm as opposed to -239 pcm for Configuration 1 (see in the tables associated with Figure 7.14 and 7.21, respectively). The relative node power density deviation profile in Figure 7.23 is in accordance with these conclusions (i.e. the error at high fuel exposures is subject to small oscillations compared to Configuration 1 in Section 7.2.1).

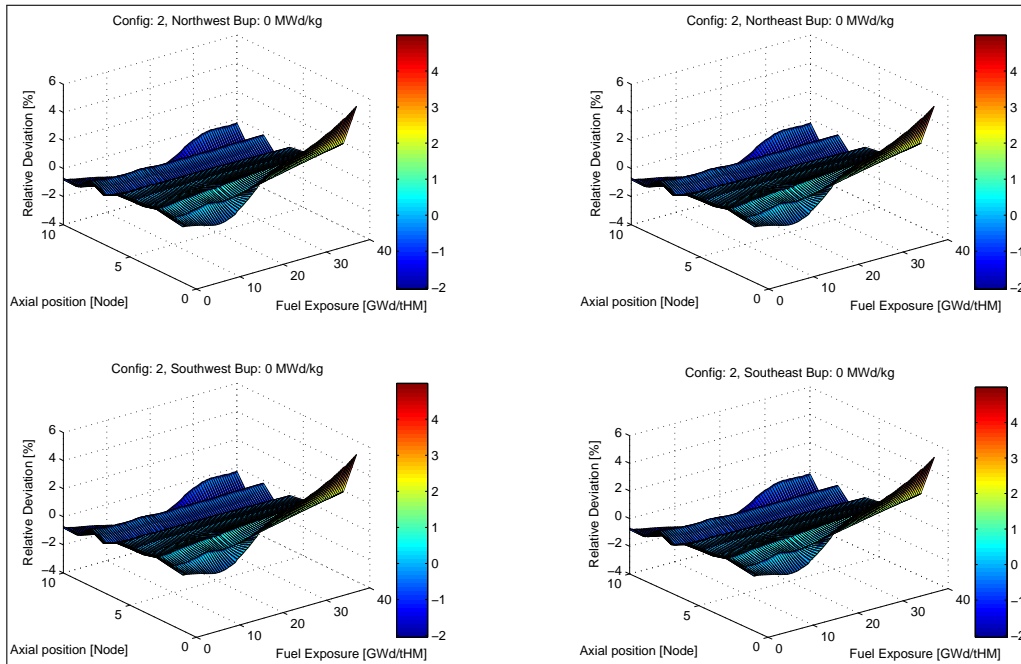


Figure 7.22: Assembly wise deviation in spectrum index for Configuration 2 (black boundary conditions).

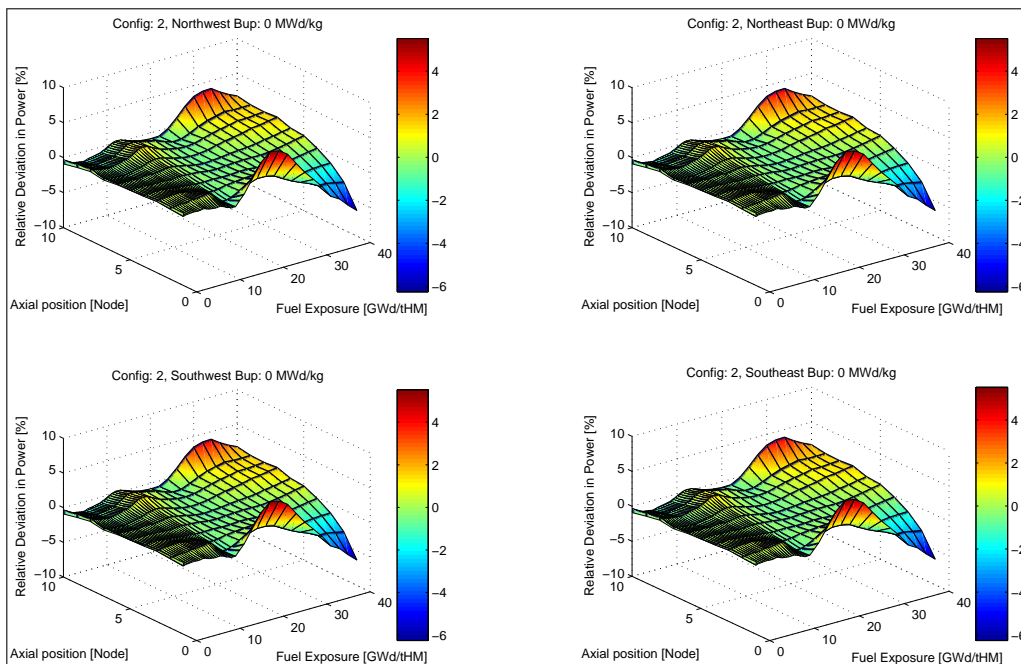
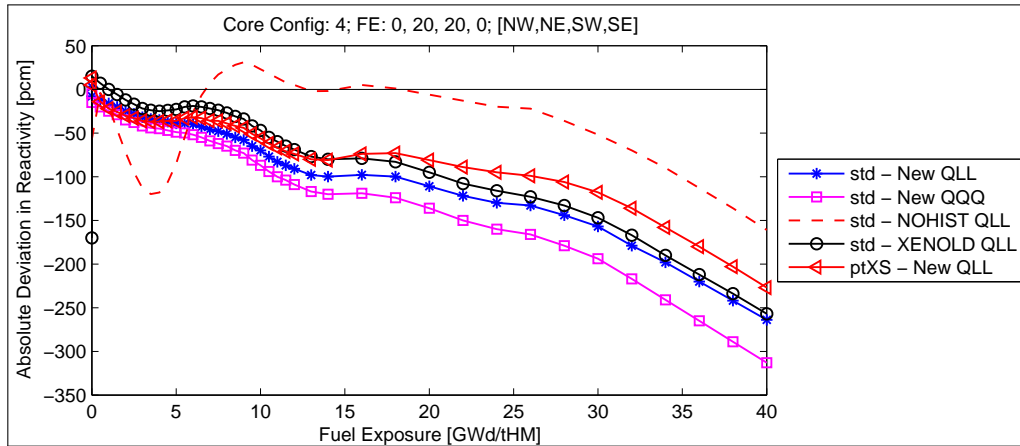


Figure 7.23: Assembly wise deviation in relative nodal power density profile for Configuration 2 (black boundary conditions).

7.2.3.2 Configuration 4 & 5



Statistics [pcm] for Configuration: 4 [Top/Bottom Albedo = Zero]

	LGD-1	LGD-2	LGD-3	LGD-4	LGD-5
Mean Dev.	-83.7	-103.5	-36.5	-71.6	-67.4
Min Dev..	-264.0	-313.0	-161.0	-257.0	-227.0
Max Dev..	3.0	-5.0	31.0	15.0	13.0
STD Dev..	65.5	77.4	52.8	69.0	52.5
BOC Dev..	3.0	-5.0	-57.0	-170.0	13.0

Figure 7.24: Deviation in k-infinity for Configuration 4 (black boundary conditions).

Comparing the reactivity deviation profiles for Configuration 4 applying black boundary conditions (Figure 7.24) with the results employing reflective boundary conditions (Figure 7.9), one will observe that the large oscillation due to extrapolation error at the top of the core (i.e. when the boundary conditions at the top/bottom is set to reflective) is no longer present. Instead, the reactivity deviation profiles in Figure 7.24 have a much closer resemblance with the profiles seen for Configuration 3 in Figure 7.18, which has a similar layout as Configuration 4 but with axially homogeneous void profile. The minimum deviation (which is at the EOL) is less severe compared to Configuration 3. These observations are in accordance with conclusions drawn for Configuration 2 using black boundary conditions (Section 7.2.3.1). Additionally, it may be seen that the use of the history model results in worse results at high fuel exposure for the reasons mentioned in Section 7.1.1.

The relative node power density deviation profiles in Appendix C.10 show a behavior consistent with these conclusions. It can be observed that there is no oscillation in the nodal power distribution at the top/bottom of the nodes from the already depleted assemblies, thereby confirming that the incorrect depletion of BA is the main cause of the oscillation seen in the fresh assemblies. The reactivity deviation profiles and the relative node power density deviation profile for Configuration 5 are presented in Appendix C.12 and C.13 respectively, which confirms findings in this section.

This page was left blank intentionally.

8

Conclusion

IN this analysis, various 2D single-node, 2D mini-core and 3D mini-core depletion test problems have been evaluated. Different fuel assembly depletion conditions have been considered in these simulations, such as different power levels, fuel temperature values, coolant void fractions, and their various combinations. In addition, an assessment of the capability of the POLCA7 cross section model, the sensitivity of the cross section model to the choice of depletion step sizes, the effect of cross section interpolation/extrapolation and the effect of axial leakage were made. Based on the results presented in this report, the following overall conclusions can be drawn:

- Having an isotopic cross section history model with detailed tracking of important nuclides and a xenon spectrum correction model is crucial to accurately handle conditions with off-reference power and fuel temperature variations as well as to account for the impact of shutdown cooling. Otherwise, errors in k -infinity up to 1600 pcm can be obtained in single-node studies (i.e. with the NOHIST option).
- The reactivity worth of SDC on a single-node basis is approximately around 200-250 pcm at 100% power (i.e. dependent on the irradiation power level) and rather independent of the outage time.
- The importance of having a 3D table representation for the microscopic cross sections is more pronounced for mixed operation conditions with a more irregular regulation of both power levels (i.e. xenon) and fuel temperatures. However, it was observed that having a burn-up dependence of microscopic cross section data seemed to be of less importance than having a coolant density dependence.
- The errors in microscopic cross sections are seen to be small for most evaluated nuclides. However, for low power cases they are systematically underestimated in the epithermal group with, in an absolute sense, increasing trend with burn-up (from -0.5% up to -1.5% for U-235 fission cross section). The epithermal absorption cross section of Pu-240 and the thermal absorption cross section of Xe-135 seem to be most sensitive to power and fuel temperature variations having largest errors for such conditions, up to 2.0% for Pu-240 and down to -4.0% for Xe-135. Only the thermal cross section of Sm-149 is sensitive to SDC at 100% or higher irradiation power.
- There are clear indications that the various Doppler correction terms currently applied on nodal cross section data are not sufficient enough to fully account for the combined effect

of both power and fuel temperature variation conditions. In this regard, it is suspected that the assumption of a linear first order Doppler correction model in combination with missing cross-coupling correction terms between off-reference xenon concentration and fuel Doppler temperature (i.e. truncated Taylor series) are the main contributors to the observed errors in both k-infinity and some microscopic cross sections.

- The spectrum interaction models are not able to properly compensate leakage induced change in spectrum (i.e. brought on by the use of fuel having different compositions) due to ad-hoc formulation of its sensitivity coefficients, which are computed within POLCA7 without actually simulating leakage in the lattice code.
- The cross section model works with negligible errors in configurations applying reflective boundary conditions. Only a small error of 100 pcm is observed due to extrapolation of cross section at high void fraction is very small. However, presence of BA leads to incorrect inventory of Pu-239 due to extrapolation which leads an oscillation in the reactivity deviation profile (with a peak-to-peak amplitude of 600 pcm in the worst case scenario) and the node power density deviation profile. Nonetheless, in a more realistic scenario where black boundary condition (i.e. albedo set to zero) is used at the top and bottom of the core, this extrapolation error due to presence of BA is of no significance.
- Employing black boundary conditions in combination with BA presence leads to oscillation of reactivity deviation profiles due to truncation error from using a coarse mesh which currently results in an intra-cycle drop in reactivity by up to approx. 400 pcm (at EOL) in the most severely affected scenarios. Further improvements in these results are expected (may be obtained) by enhanced modeling of the axial leakage, i.e. replacing albedo with appropriate reflection data.

Overall, the current cross section representation model of POLCA7 in combination with standard 3D tabulation of microscopic cross section data performs well with an acceptable accuracy for the depletion history cases considered in this analysis. Nonetheless, further studies should be carried out with the aim of investigating methods for improving the spectrum interaction model and study the cause of the reported cycle-wise drop in reactivity in a full core scenario involving thermal hydraulic feedback.

Bibliography

- [1] K.S. Smith *An Analytic Nodal Method for Solving the Two-Group Multidimensional, Static and Transient Neutron Diffusion Equation* MSc thesis, Dept Nucl. Eng., Mass Inst. of Tech., USA (1979).
- [2] F. Bennewitz et al. *Solution of the Multidimensional Neutron Diffusion Equation by Nodal Expansion* CONF-750413, Proc. Conf. on Comput. Methods in Nucl. Eng., Vol 1, p.99, Charleston, South Carolina (1975).
- [3] Petri Forslund Guimarães *Meeting on POLCA7 eigenvalue behavior between Vattenfall and Westinghouse* Westinghouse Electric Sweden, MoM BTD 11-0924, rev 0 (2012).
- [4] Sten-Örjan Lindahl *POLCA7 - Cross Section Model* Westinghouse Electric Sweden Report BR 94-712, rev 9 (2012).
- [5] Sten-Örjan Lindahl *POLCA7 - Nuclide Concentration Tracking* Westinghouse Electric Sweden Report BR 94-710, rev 4 (2012).
- [6] Erwin Müller *CoreLink Methodology* Westinghouse Electric Sweden, BCM 98-040 (2011).
- [7] Sten-Örjan Lindahl *POLCA7 - The NEU3 Neutronics Model* Westinghouse Electric Sweden, BR 94-702, rev 2 (2000).
- [8] Petri F. Guimarães *Specification of simulation cases for studying the observed cycle-wise drop in POLCA7 core eigenvalue predictions* Westinghouse Electric Sweden (2013).
- [9] Rudi Stamm'ler *PHOENIX4-User's Guide* Westinghouse Electric Sweden, UR 85-194 (2006).
- [10] Magnus Norlén *Standardization of the IFIGEN matrix* Westinghouse Electric Sweden, BTF 06-1023, rev 4 (2006).
- [11] Weronica Linderöth *Standardized BWR cell data generation for CM2* Westinghouse Electric Sweden Report BTF 01-157, rev 3 (2002)
- [12] Kalev Tammemäe *POLCA7 - Calculation options* Westinghouse Electric Sweden, BTU 03-022, rev 6 (2012).
- [13] Eva Bäckström, Petri Forslund *Study of Spatially Homogenized & Energy Collapsed Microscopic Cross Sections for Fission Products* Westinghouse Electric Report, BTU 00-029 (2000).
- [14] Erwin Müller *POLCA7 Version 4.0.0 - Verification report* Westinghouse Electric Sweden Report BTF 02-054, rev 0 (2002).

A

2D Single-Node Studies

Deviation in reactivity

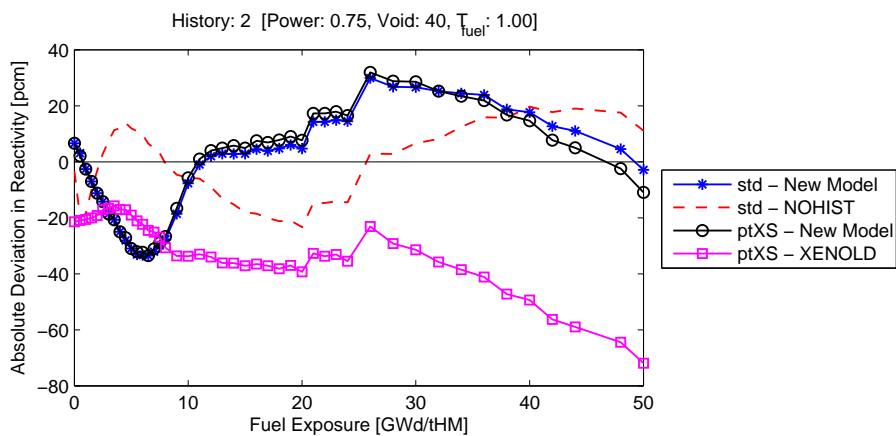


Figure A.1: Deviation in k-infinity for History 2 without SDC, CROSS vs. PHOENIX4.

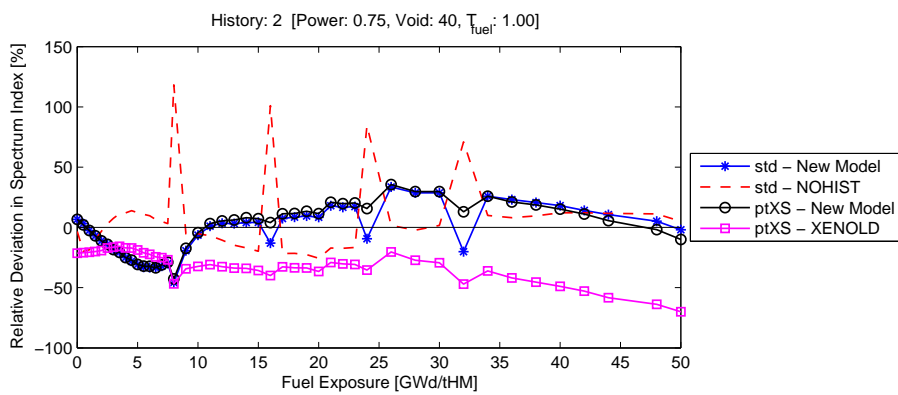


Figure A.2: Deviation in k-infinity for History 2 with SDC, CROSS vs. PHOENIX4.

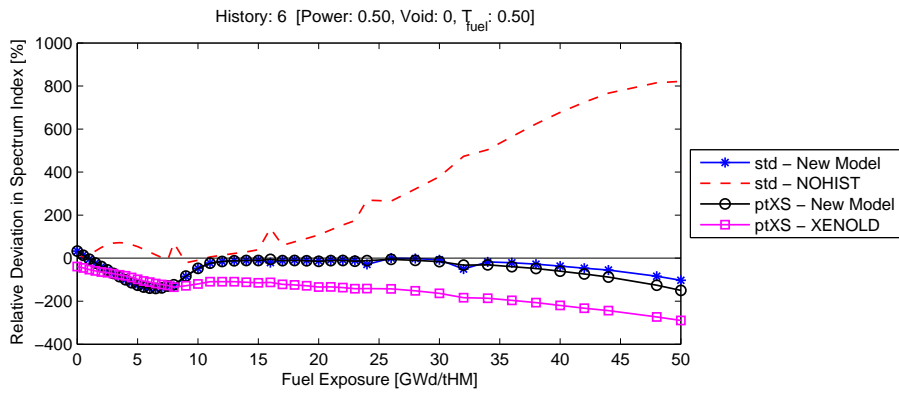


Figure A.3: Deviation in k-infinity for History 6 with SDC, CROSS vs. PHOENIX4.

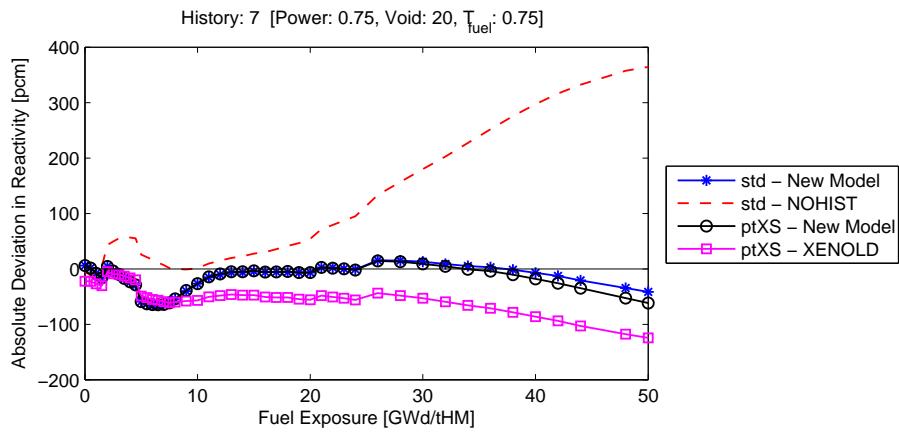


Figure A.4: Deviation in k-infinity for History 7 without SDC, CROSS vs. PHOENIX4.

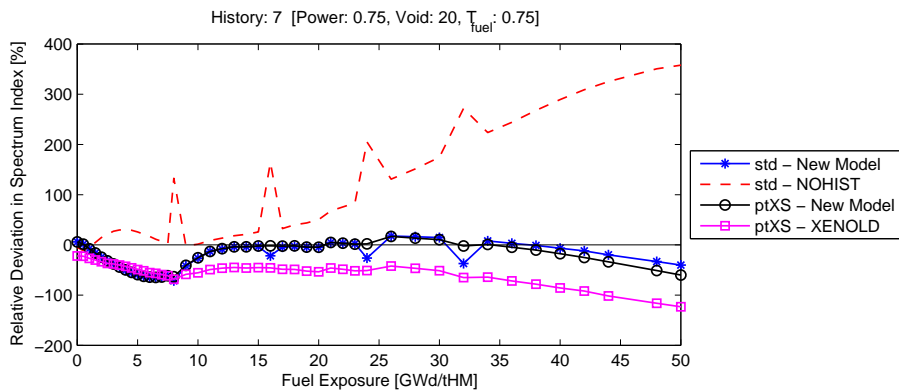


Figure A.5: Deviation in k-infinity for History 7 with SDC, CROSS vs. PHOENIX4.

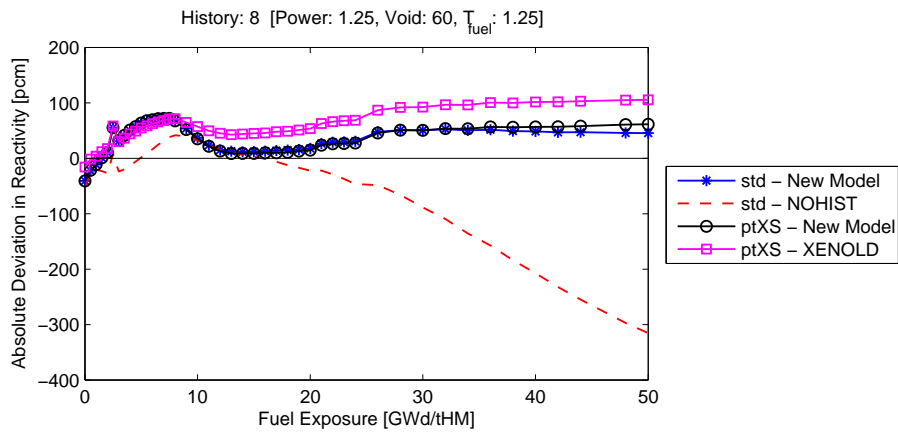


Figure A.6: Deviation in k-infinity for History 8 without SDC, CROSS vs. PHOENIX4.

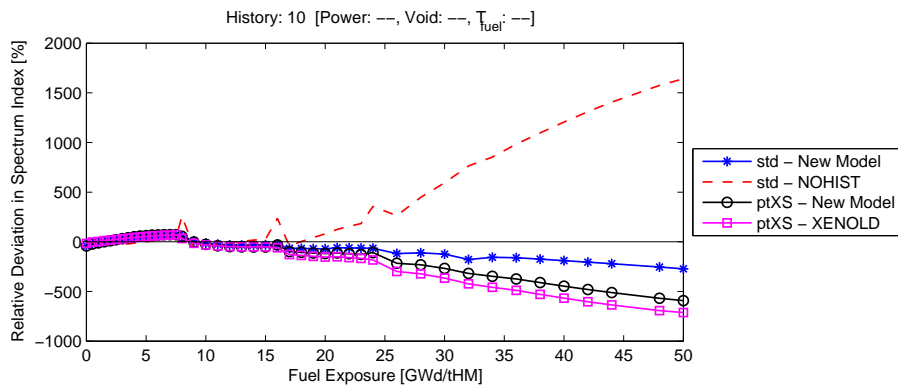


Figure A.7: Deviation in k-infinity for History 10 with SDC, CROSS vs. PHOENIX4.

Deviation in microscopic cross sections

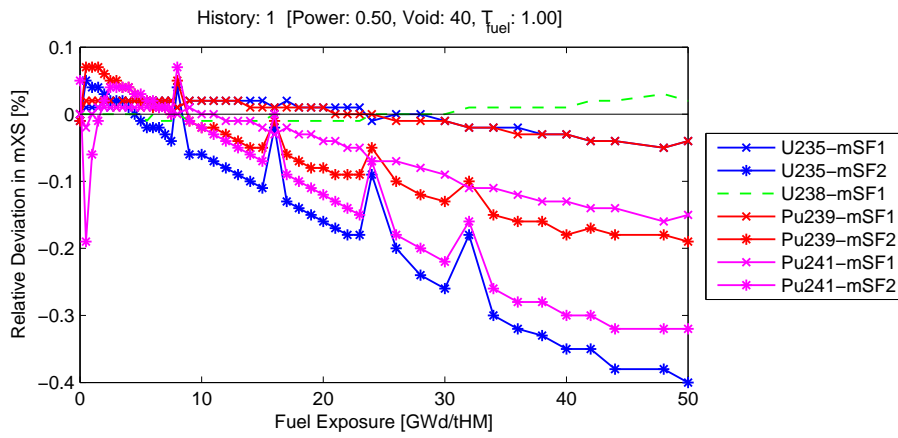


Figure A.8: Deviation in actinide $\sigma_{f,g}$ for History 1 with SDC.

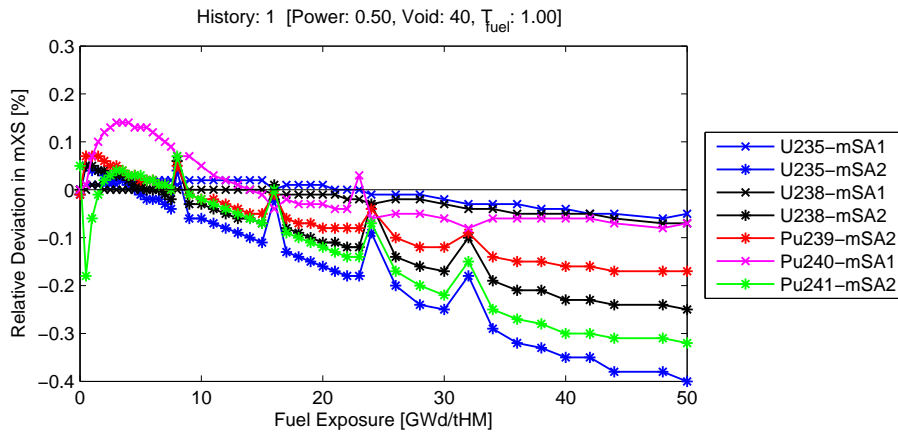


Figure A.9: Deviation in actinide $\sigma_{a,g}$ for History 1 with SDC.

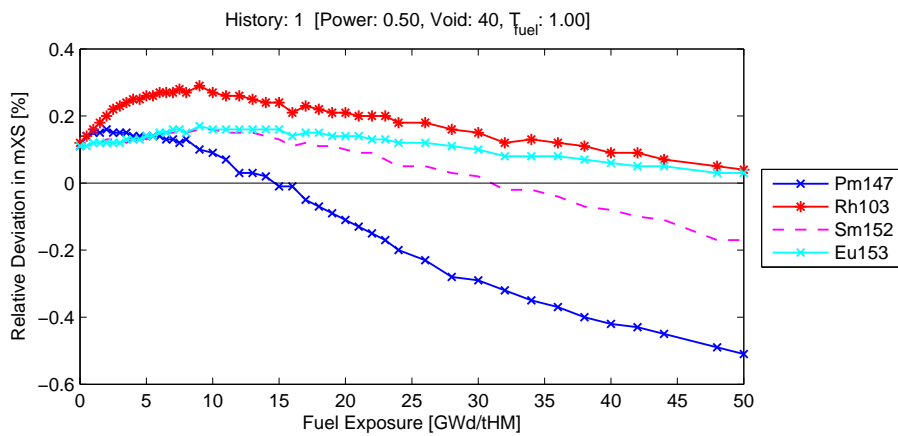


Figure A.10: Deviation in fission product $\sigma_{a,1}$ for History 1 with SDC.

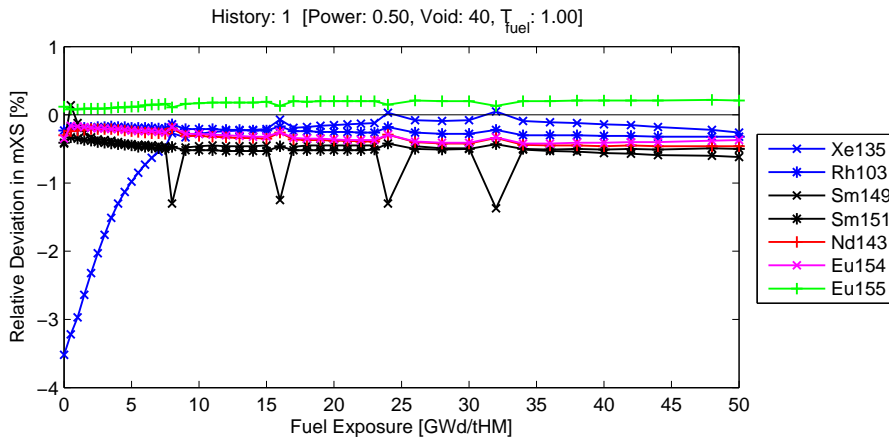


Figure A.11: Deviation in fission product $\sigma_{a,2}$ for History 1 with SDC.

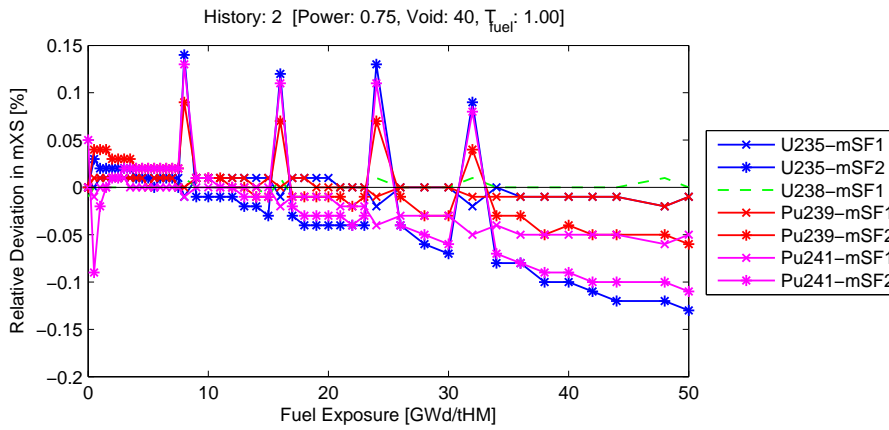


Figure A.12: Deviation in actinide $\sigma_{f,g}$ for History 2 with SDC.

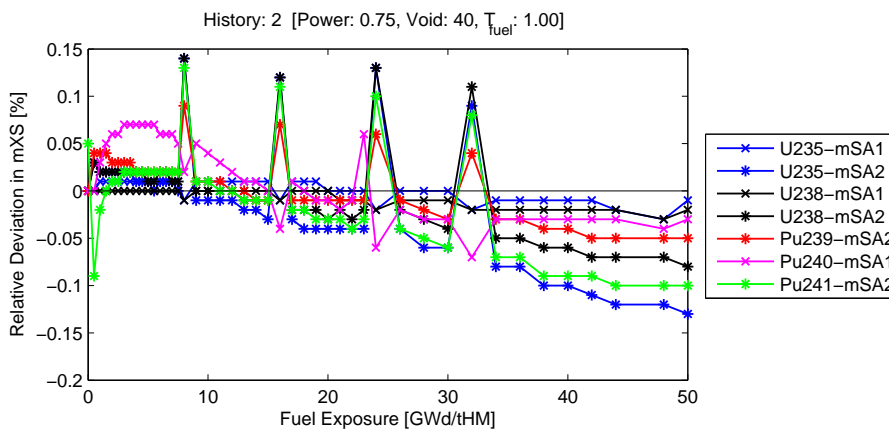


Figure A.13: Deviation in actinide $\sigma_{a,g}$ for History 2 with SDC.

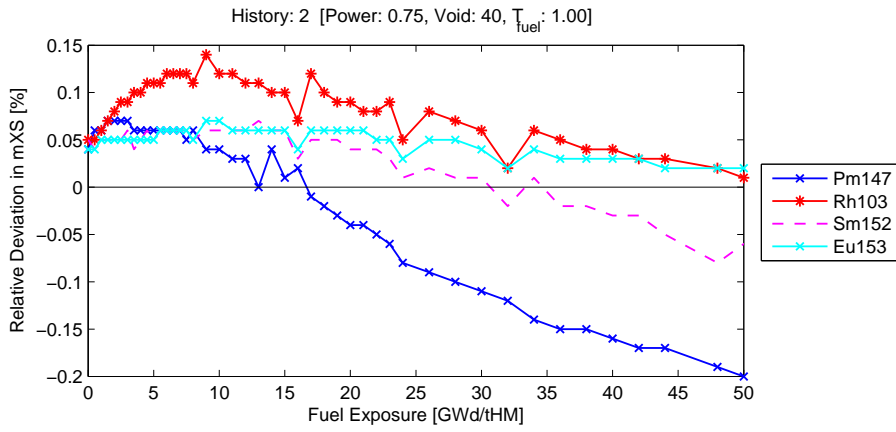


Figure A.14: Deviation in fission product $\sigma_{a,1}$ for History 2 with SDC.

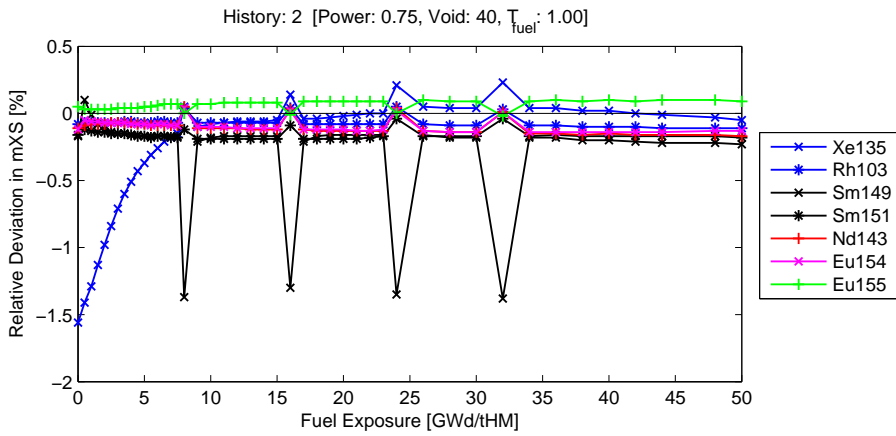


Figure A.15: Deviation in fission product $\sigma_{a,2}$ for History 2 with SDC.

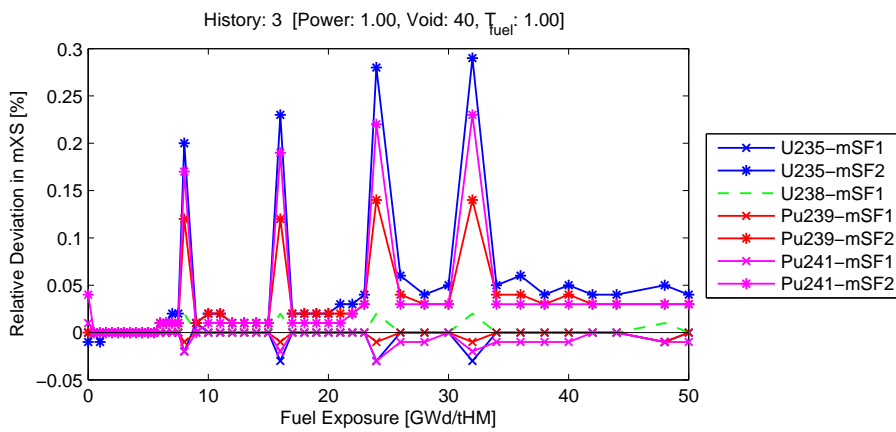


Figure A.16: Deviation in actinide $\sigma_{f,g}$ for History 3 with SDC.

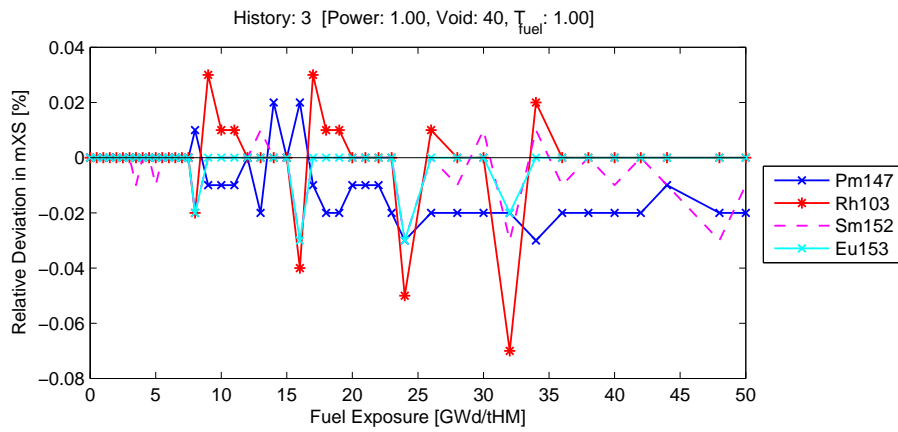


Figure A.17: Deviation in fission product $\sigma_{a,1}$ for History 3 with SDC.

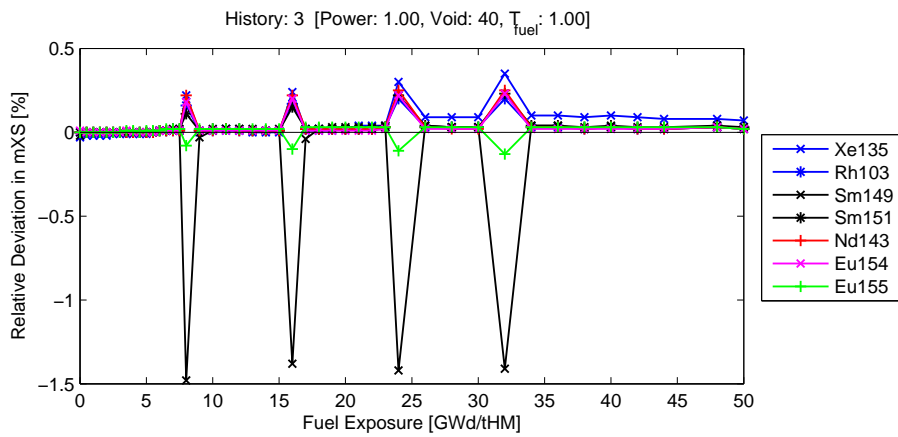


Figure A.18: Deviation in fission product $\sigma_{a,2}$ for History 3 with SDC.

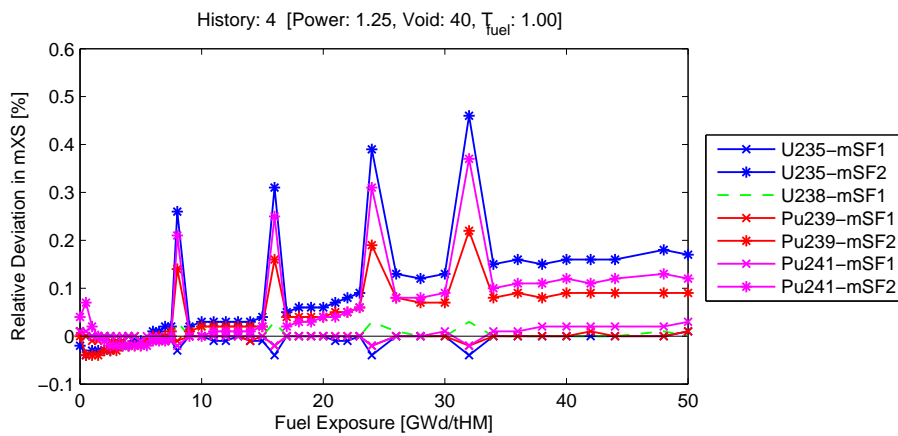


Figure A.19: Deviation in actinide $\sigma_{f,g}$ for History 4 with SDC.

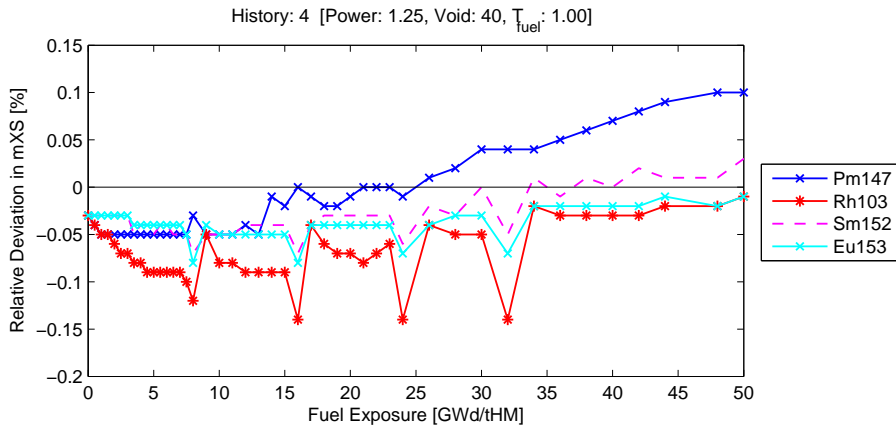


Figure A.20: Deviation in fission product $\sigma_{a,1}$ for History 4 with SDC.

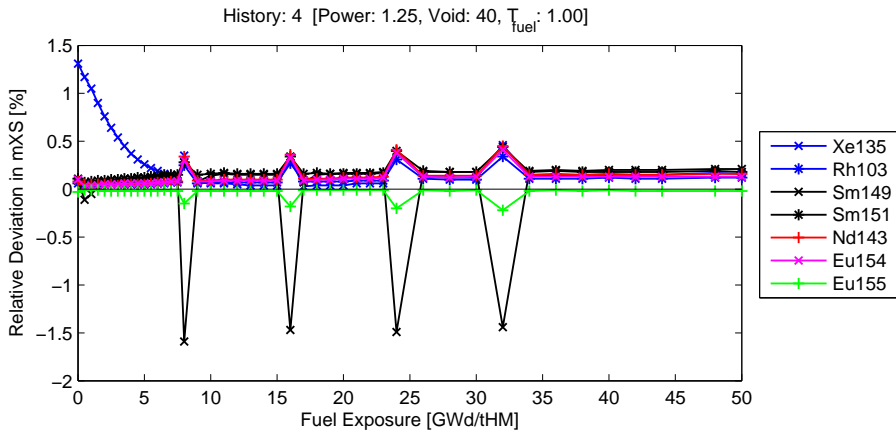


Figure A.21: Deviation in fission product $\sigma_{a,2}$ for History 4 with SDC.

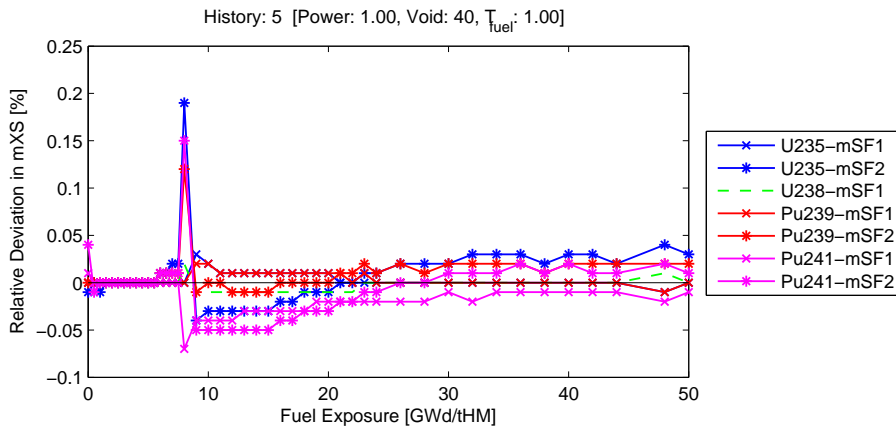


Figure A.22: Deviation in actinide $\sigma_{f,g}$ for History 5 with SDC.

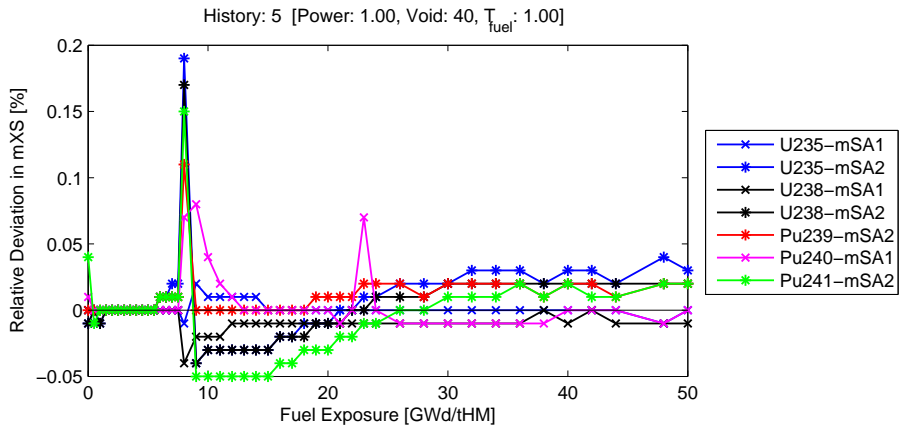


Figure A.23: Deviation in actinide $\sigma_{a,g}$ for History 5 with SDC.

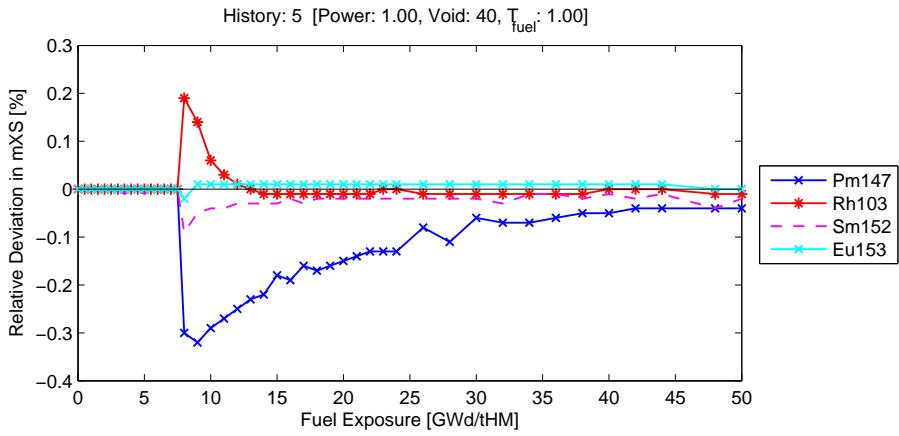


Figure A.24: Deviation in fission product $\sigma_{a,1}$ for History 5 with SDC.

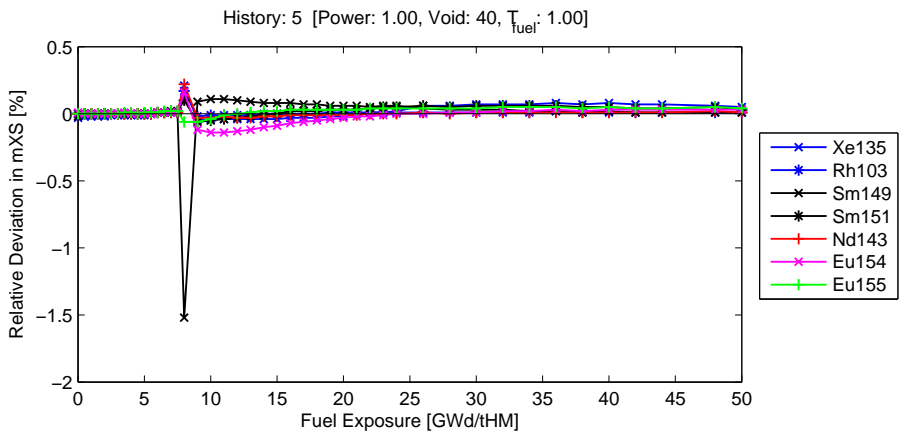


Figure A.25: Deviation in fission product $\sigma_{a,2}$ for History 5 with SDC.

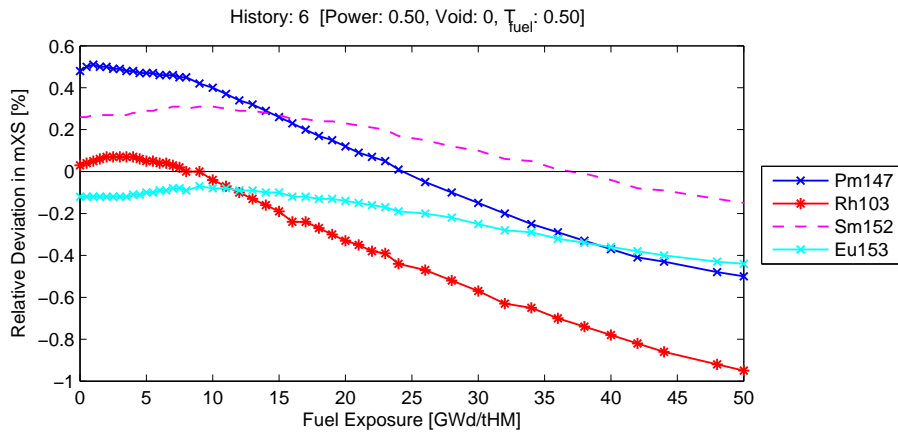


Figure A.26: Deviation in fission product $\sigma_{a,1}$ for History 6 with SDC.

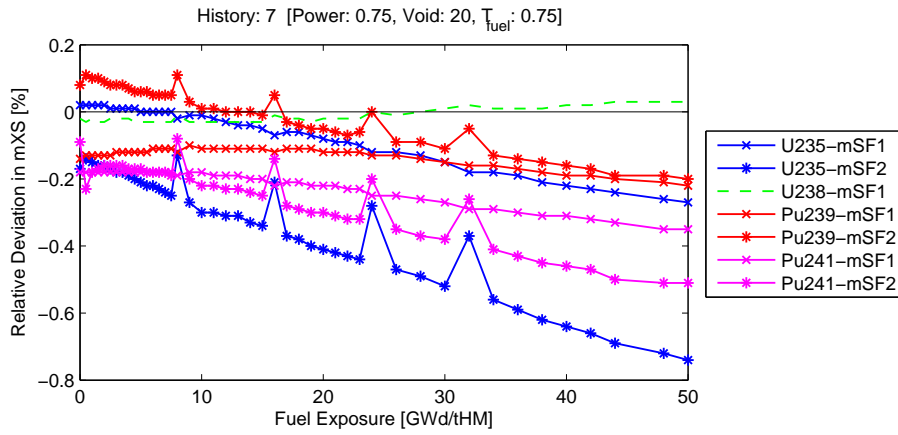


Figure A.27: Deviation in actinide $\sigma_{f,g}$ for History 7 with SDC.

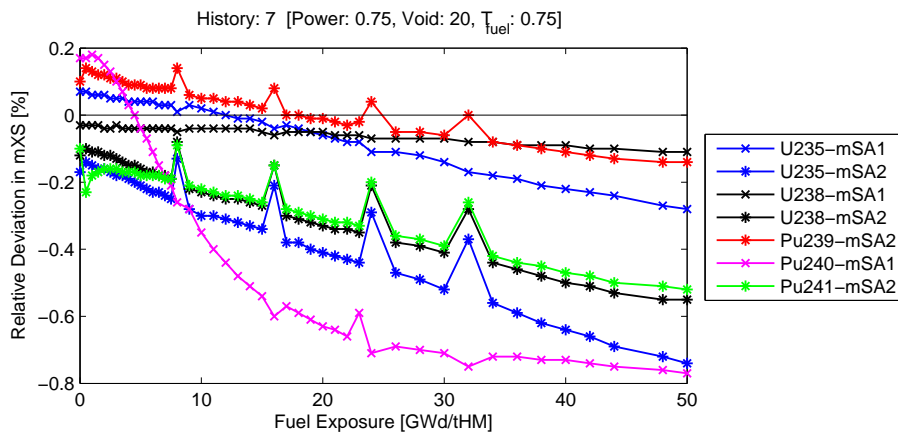


Figure A.28: Deviation in actinide $\sigma_{a,g}$ for History 7 with SDC.

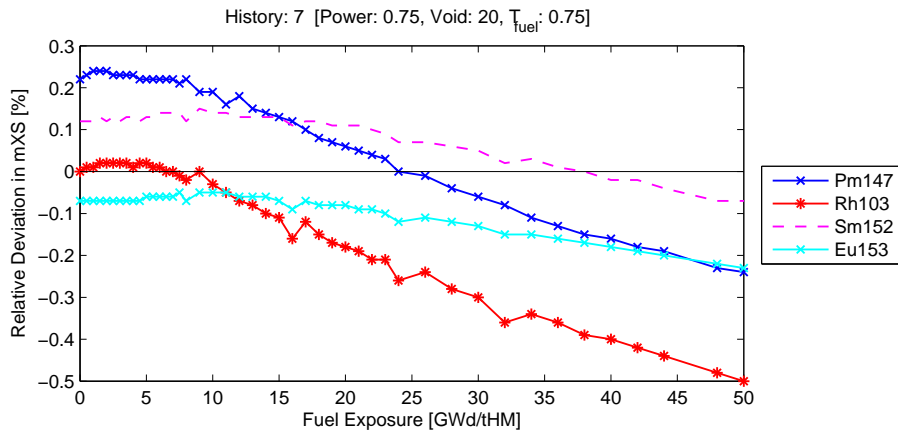


Figure A.29: Deviation in fission product $\sigma_{a,1}$ for History 7 with SDC.

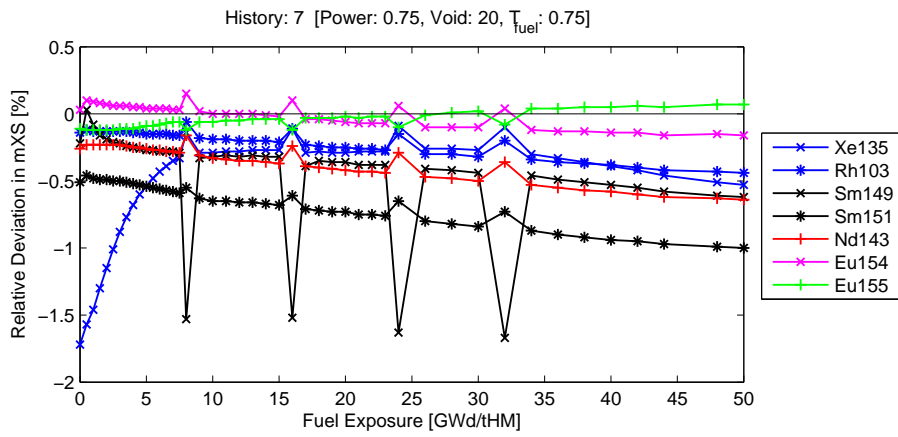


Figure A.30: Deviation in fission product $\sigma_{a,2}$ for History 7 with SDC.

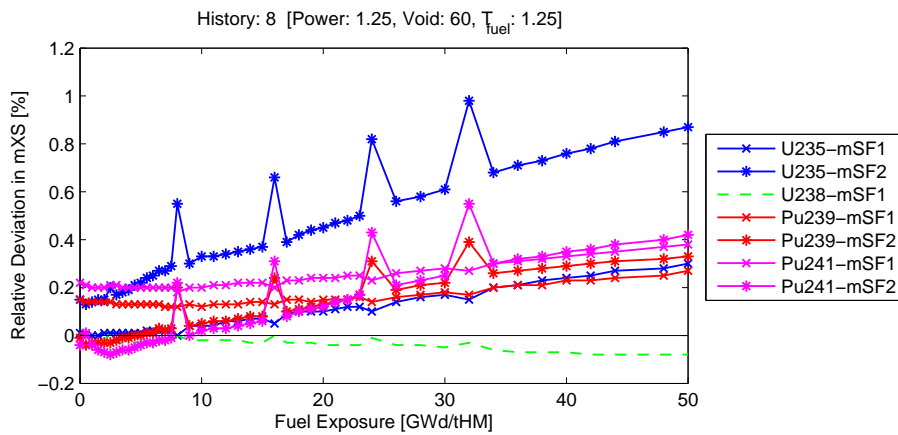


Figure A.31: Deviation in actinide $\sigma_{f,g}$ for History 8 with SDC.

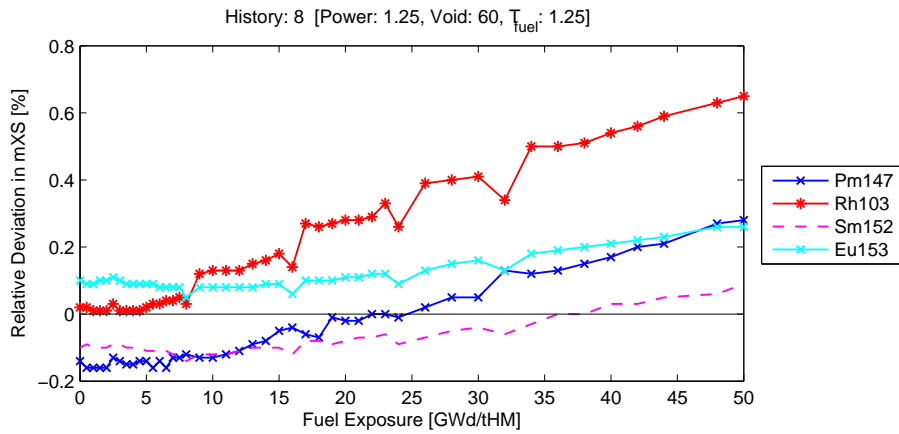


Figure A.32: Deviation in fission product $\sigma_{a,1}$ for History 8 with SDC.

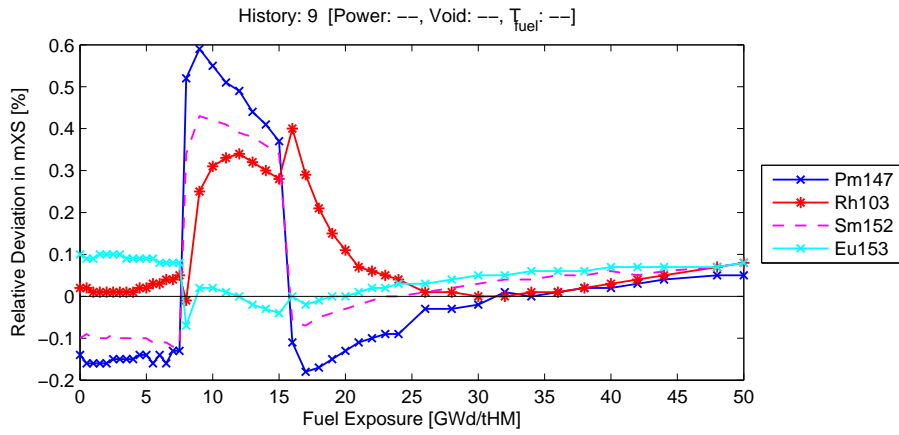


Figure A.33: Deviation in fission product $\sigma_{a,1}$ for History 9 with SDC.

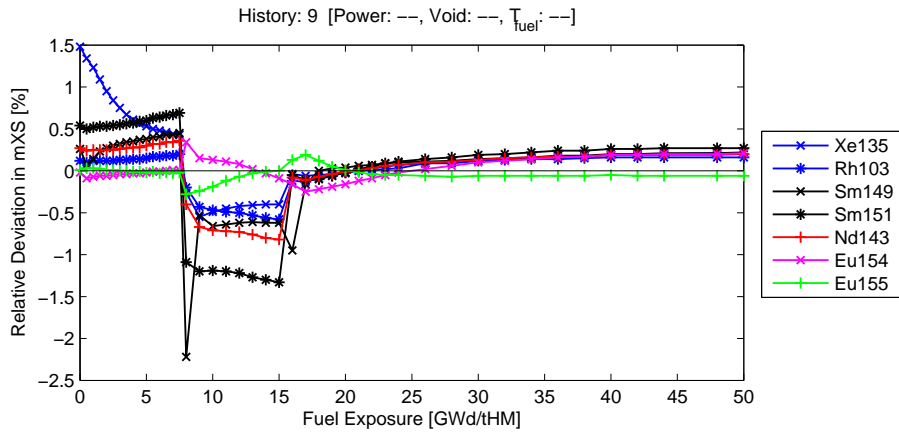


Figure A.34: Deviation in fission product $\sigma_{a,2}$ for History 9 with SDC.

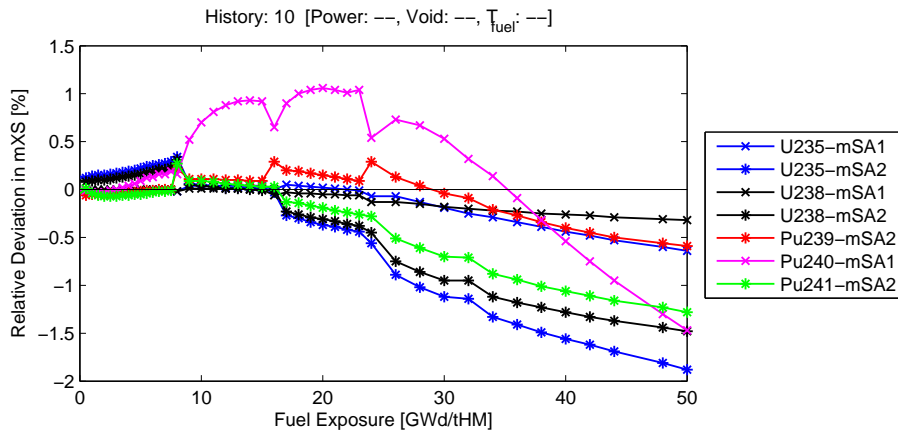


Figure A.35: Deviation in actinide $\sigma_{a,g}$ for History 10 with SDC.

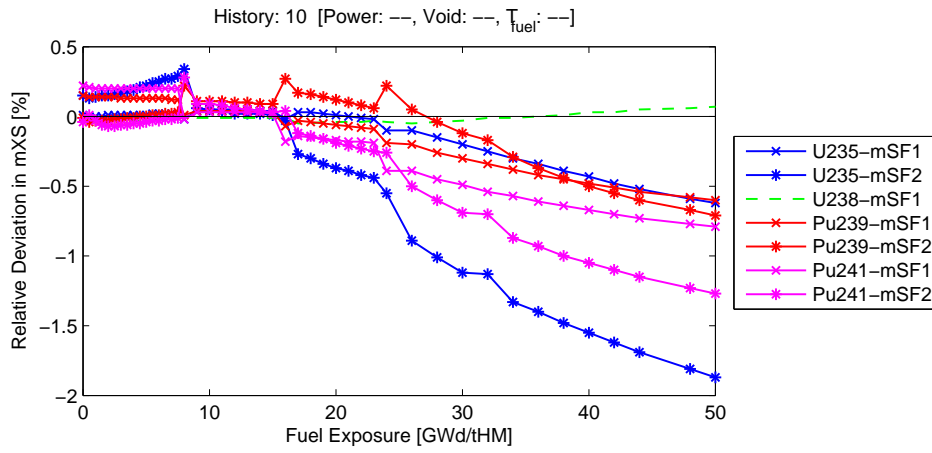


Figure A.36: Deviation in microscopic fission cross section for History 10 with SDC.

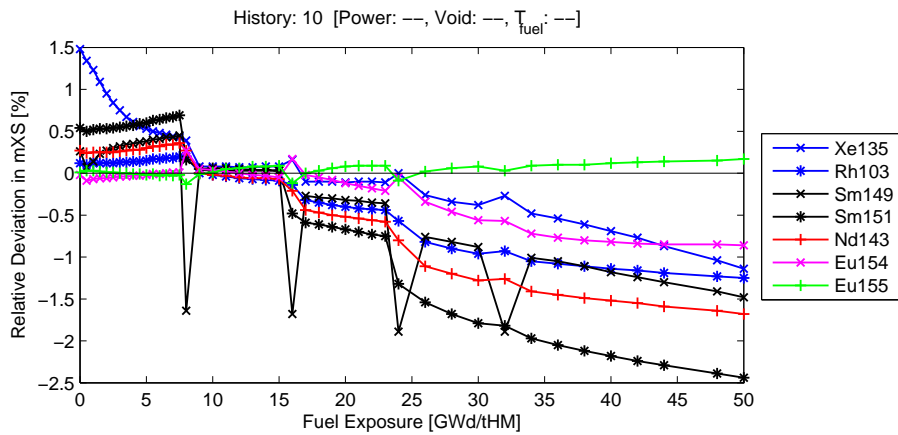


Figure A.37: Deviation in fission product $\sigma_{a,2}$ for History 10 with SDC.

B

2D Mini-Core Studies

Configuration 4

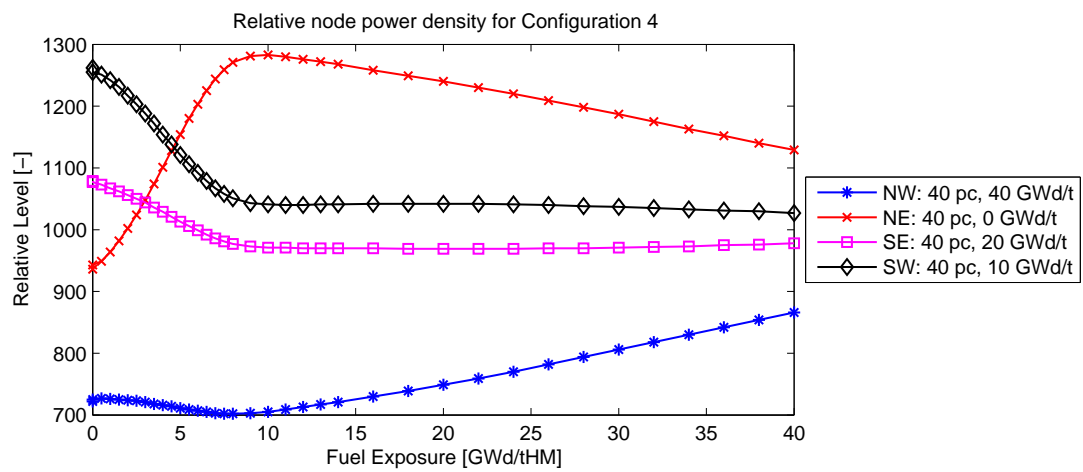


Figure B.1: Relative node power density profile for Configuration 4.

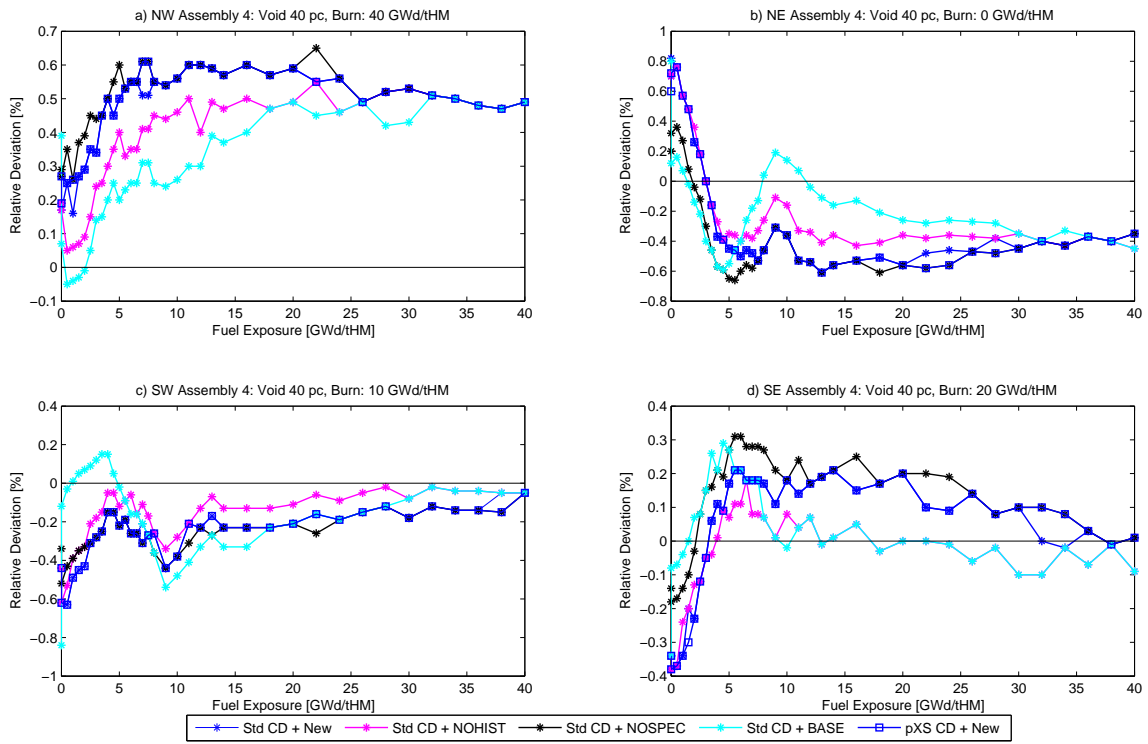


Figure B.2: Assembly wise deviation in relative node power density for Configuration 4.

Configuration 5

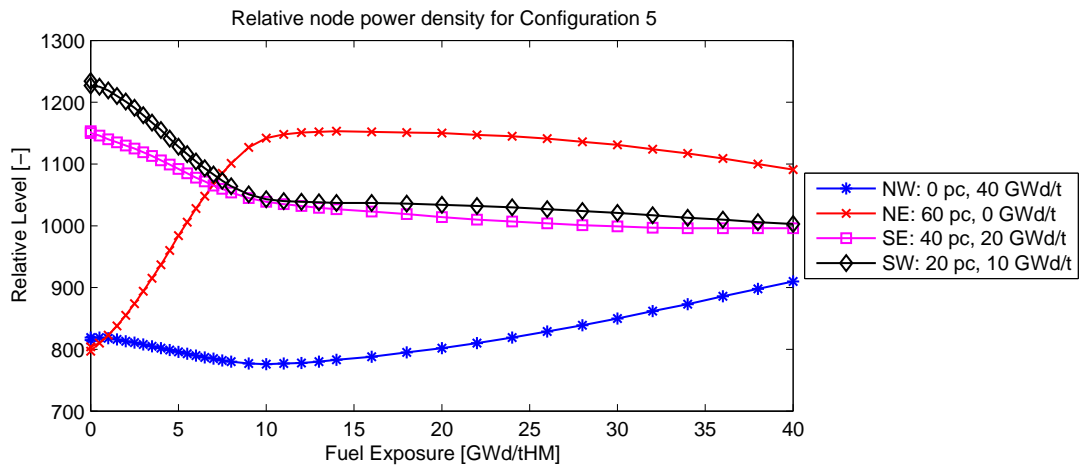


Figure B.3: Relative node power density profile for Configuration 4.

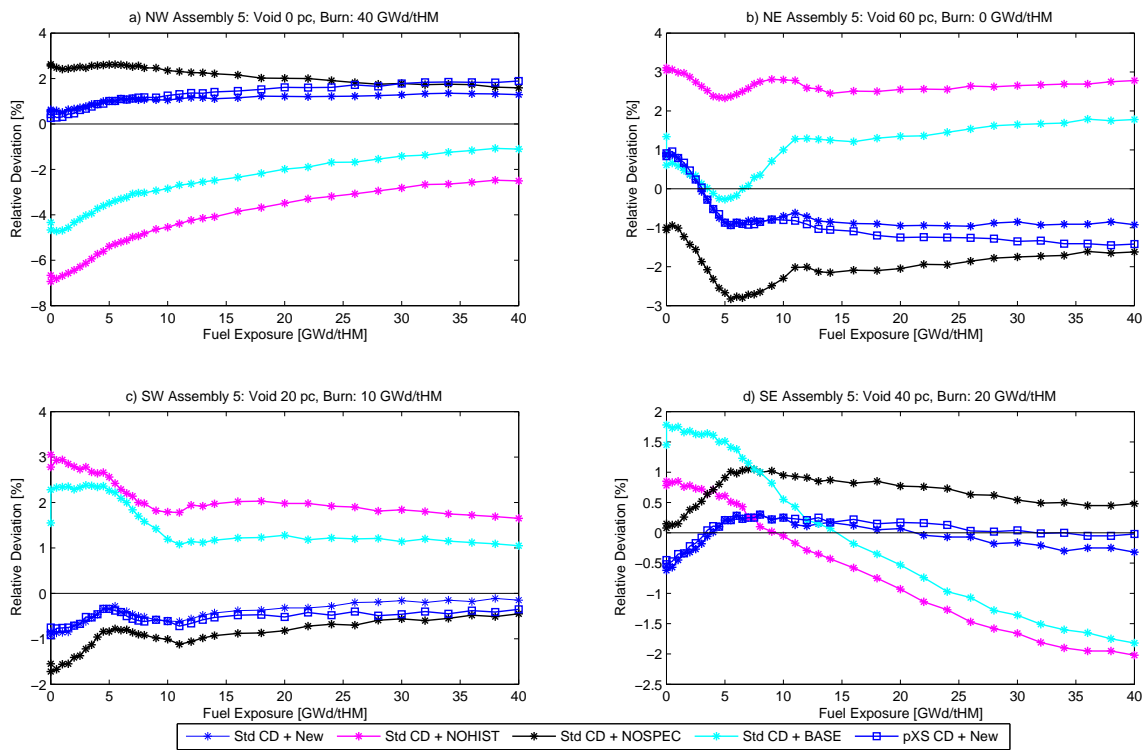


Figure B.4: Deviation in relative node power density for Configuration 4.

C

3D Mini-Core Studies

Configuration 1

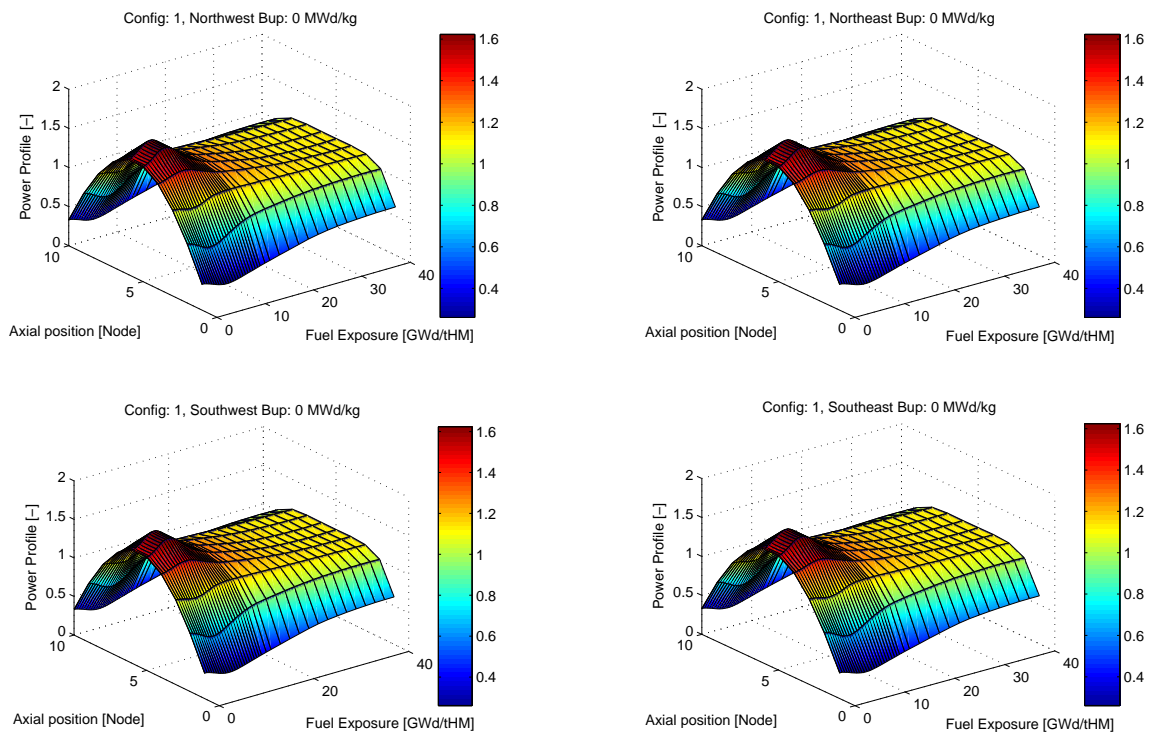


Figure C.1: Assembly wise relative nodal power density profile for Configuration 1 (black boundary conditions).

Configuration 2

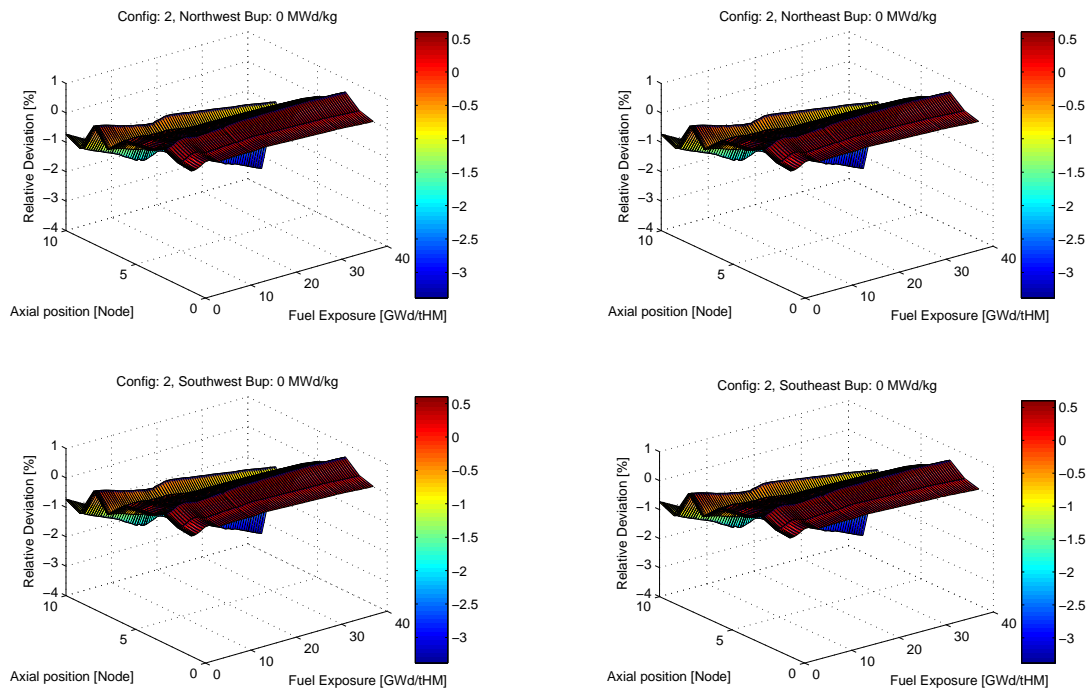


Figure C.2: Assembly wise deviation in spectrum index for Configuration 2 (reflective axial boundary conditions).

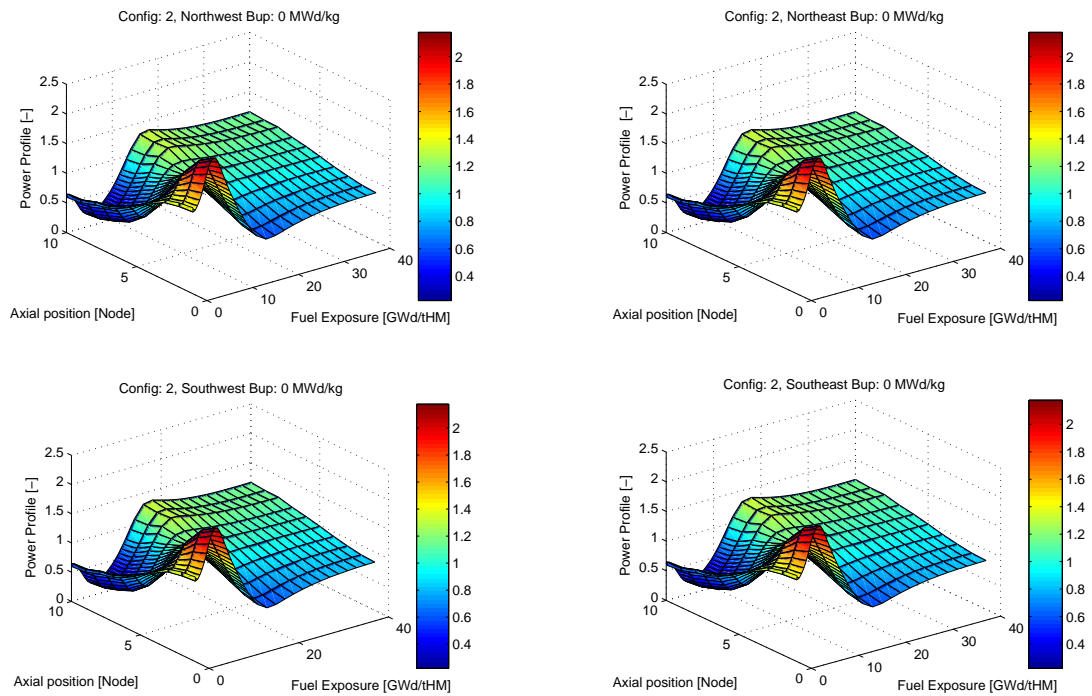


Figure C.3: Assembly wise relative nodal power density profile for Configuration 2 (reflective axial boundary conditions).

Configuration 3

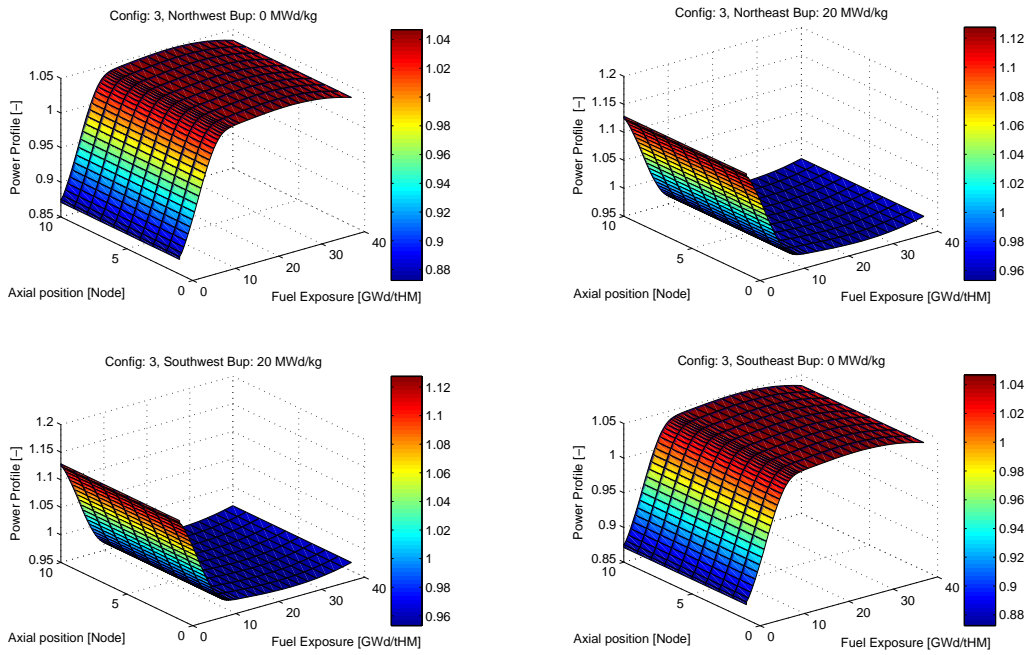


Figure C.4: Assembly wise relative nodal power density for Configuration 3 with reflective boundary condition at the top/bottom.

Configuration 4

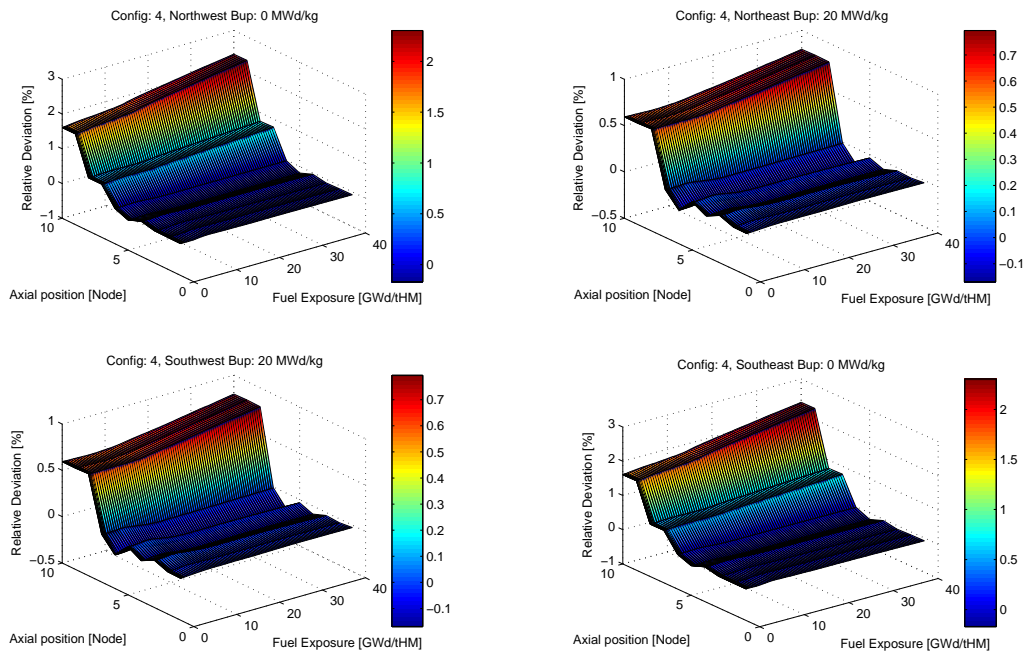


Figure C.5: Assembly wise deviation in Σ_{a1} for Configuration 4 (reflective axial boundary conditions).

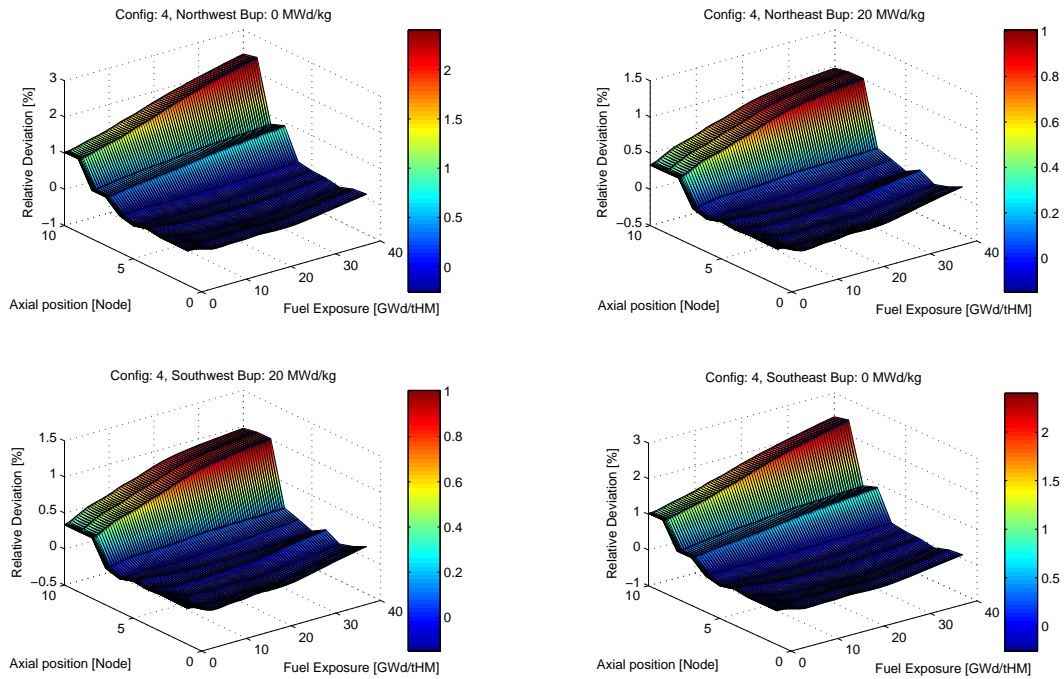


Figure C.6: Assembly wise deviation in Σ_{f1} for Configuration 4 (reflective axial boundary conditions).

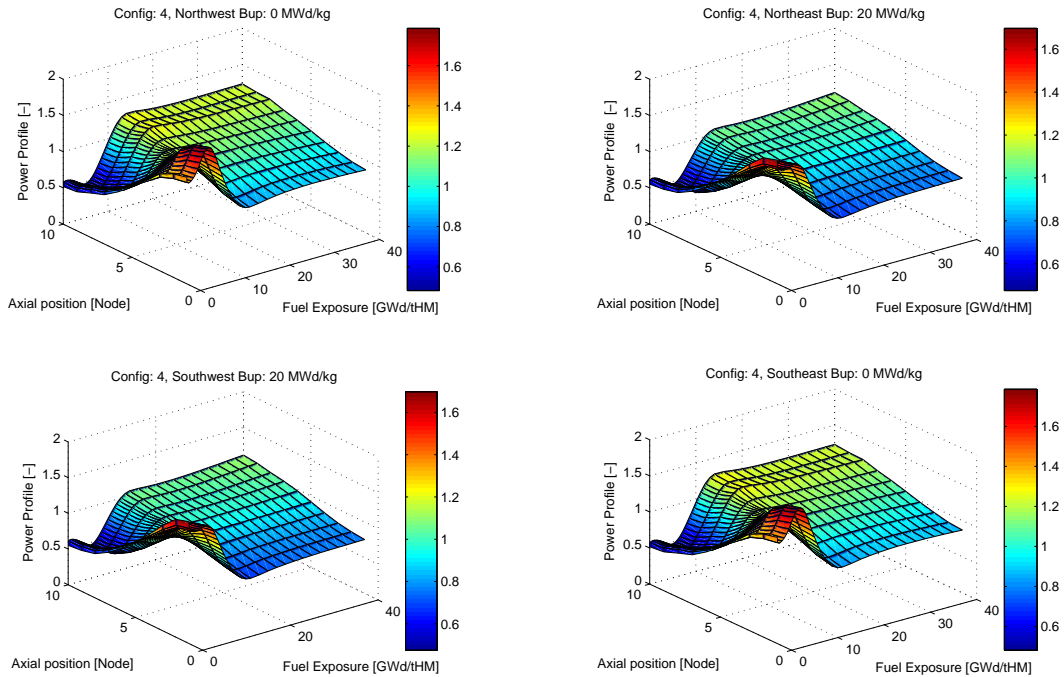


Figure C.7: Assembly wise relative nodal power density profile for Configuration 4 (reflective axial boundary conditions).

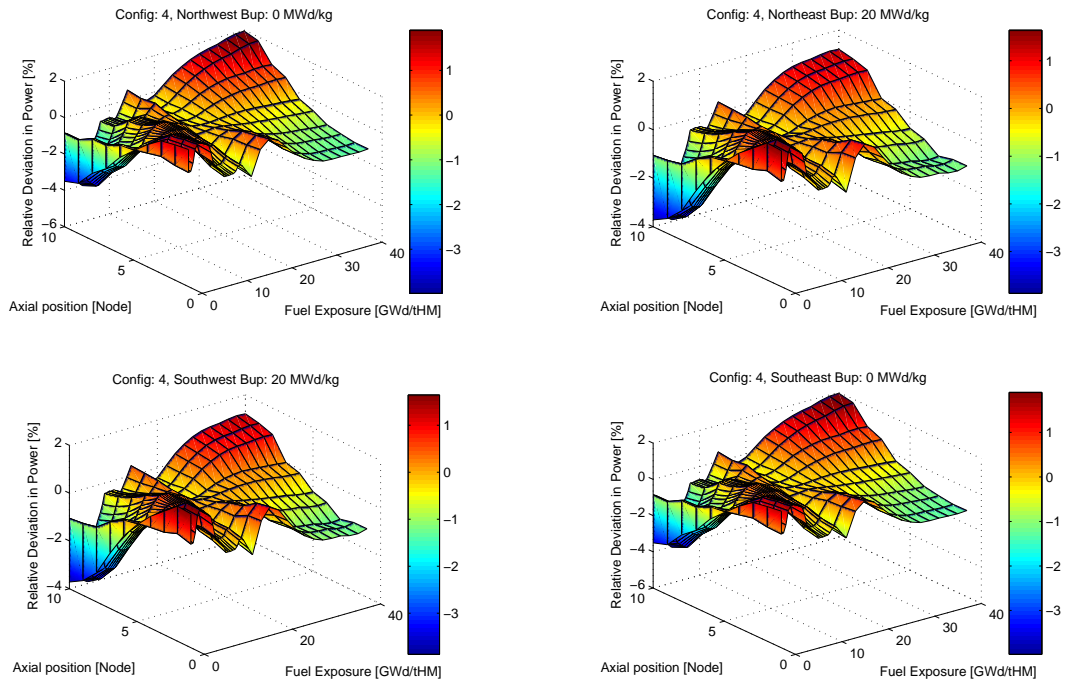


Figure C.8: Assembly wise deviation in relative nodal power density profile for Configuration 4 (reflective axial boundary conditions).

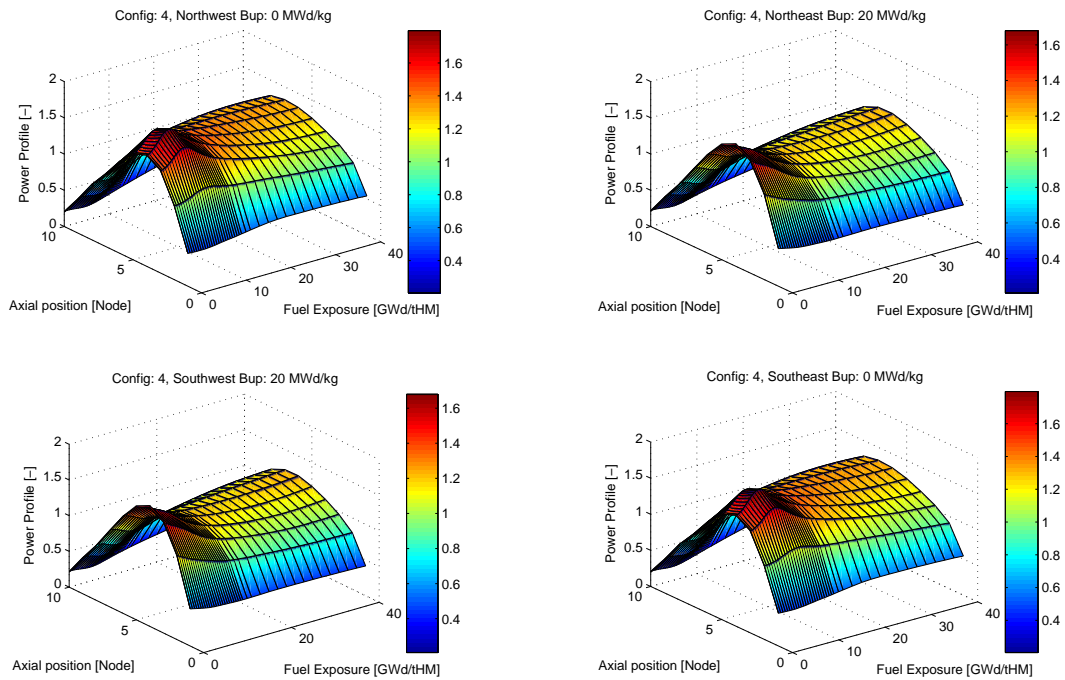


Figure C.9: Assembly wise relative nodal power density profile for Configuration 4 (black boundary conditions).

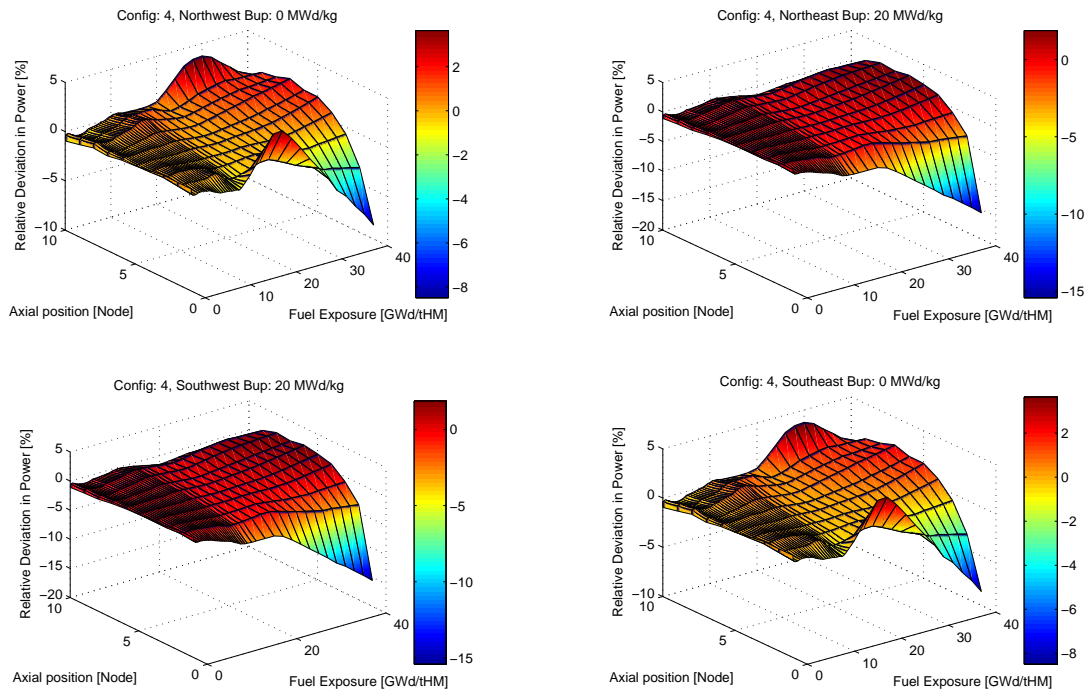


Figure C.10: Assembly wise deviation in relative nodal power density for Configuration 4 (black boundary conditions).

Configuration 5

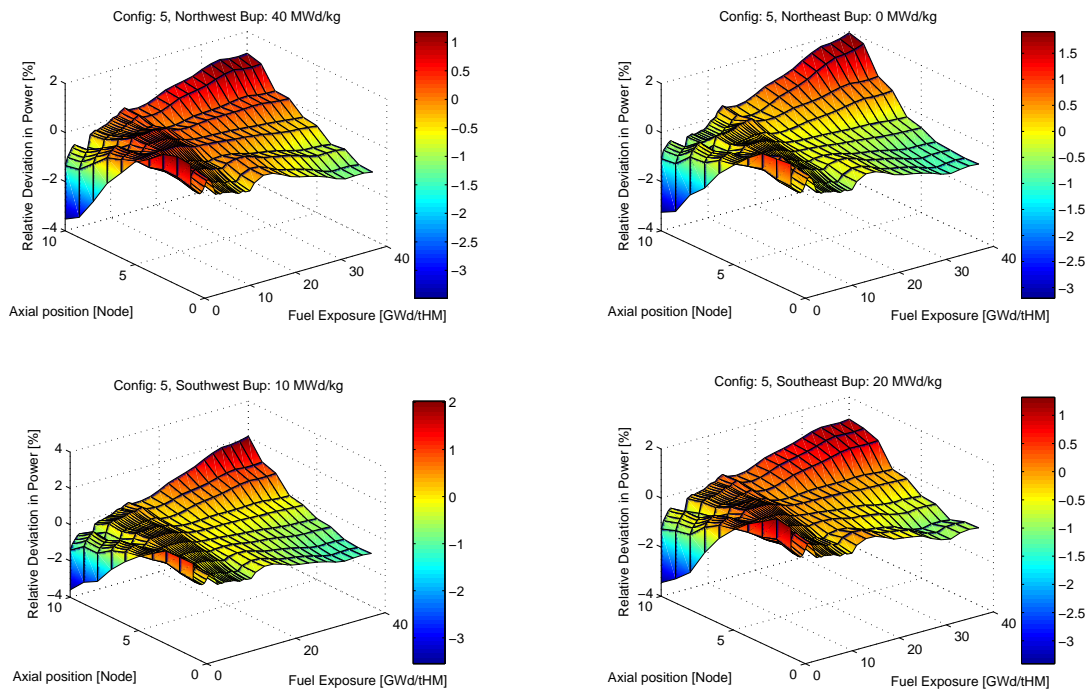
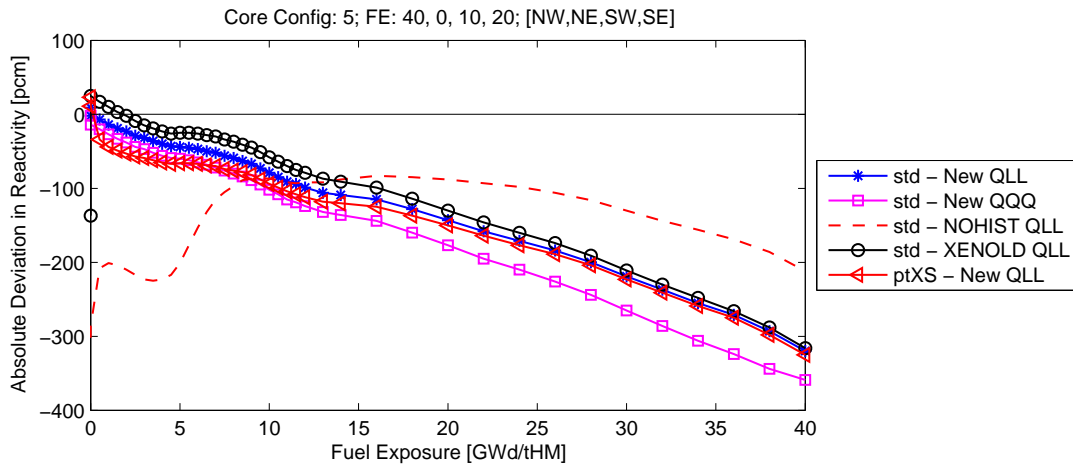


Figure C.11: Assembly wise deviation in relative nodal power density for Configuration 5 (reflective axial boundary conditions).



Statistics [pcm] for Configuration: 5 [Top/Bottom Albedo = Zero]

	LGD-1	LGD-2	LGD-3	LGD-4	LGD-5
Mean Dev.	-101.2	-127.3	-147.7	-88.2	-115.0
Min Dev..	-320.0	-359.0	-302.0	-316.0	-325.0
Max Dev..	9.0	-2.0	-83.0	25.0	23.0
STD Dev..	85.5	97.4	61.9	89.6	80.7
BOC Dev..	9.0	-2.0	-302.0	-137.0	23.0

Figure C.12: Deviation in k-infinity for Configuration 5 (black boundary conditions).

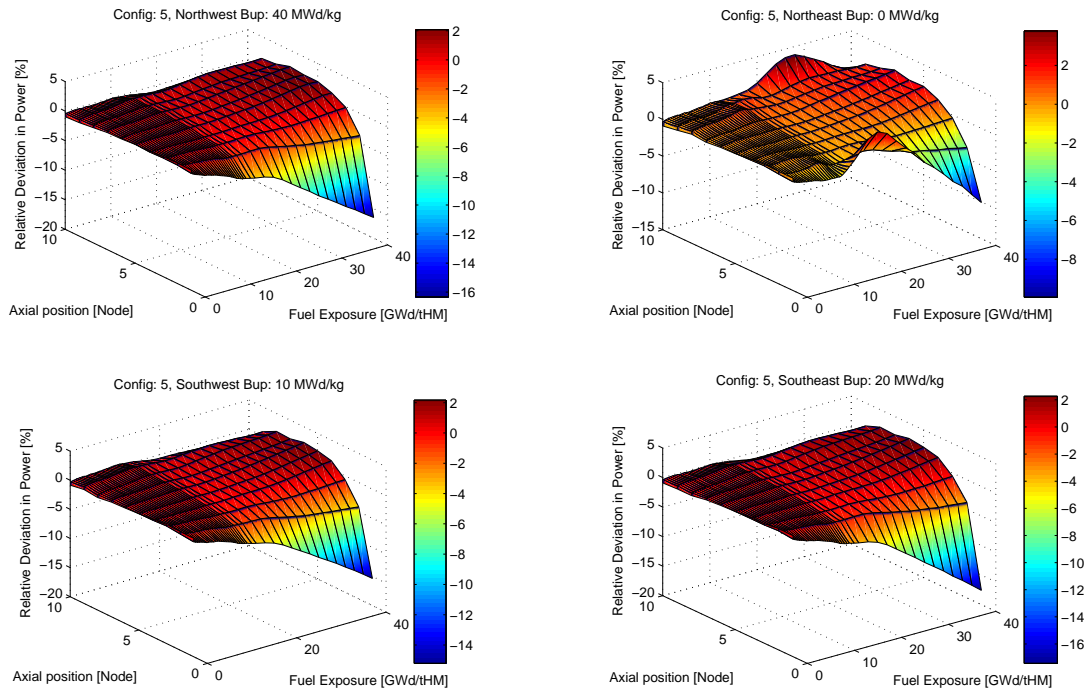


Figure C.13: Assembly wise deviation in relative nodal power density for Configuration 5 (black boundary conditions).